

ASSESSMENT OF THE META-GGA SCAN AND SELF-INTERACTION CORRECTED SCAN DENSITY FUNCTIONAL

A Dissertation
Submitted to
The Temple University Graduate Board

in Partial Fulfillment
of the Requirements for the Degree of
DOCTOR OF PHILOSOPHY IN PHYSICS

by
Chandra Shahi
December, 2019

Examining Committee Members:

John P. Perdew, Advisory Committee Chair, Dept. of Physics
Adrienn Ruzsinszky, Examining Committee Chair, Dept. of Physics
Qimin Yan, Examining Committee member, Dept. of Physics
Vincenzo Carnevale, External member of Examining Committee, Dept. of
Biology

ABSTRACT

by

Chandra Shahi

Kohn-Sham density functional theory is a widely-used method to predict the ground-state total energies and densities of interacting correlated electrons in atoms, molecules, clusters, solids, and liquids. In principle, exact results for these properties can be found by solving self-consistent one-electron Schrödinger equations based upon density functionals for the energy. In practice, the density functional for the exchange-correlation contribution to the energy must be approximated for the sake of computational efficiency. More accurate but still computationally efficient approximations are being developed by the satisfaction of exact constraints. These include the SCAN (strongly constrained and appropriately normed) semi-local density functional.

We used the pressure induced structural phase transition of solids to validate SCAN. To predict an accurate critical pressure, a method must account for a small energy difference between close-lying phases which have very different electronic structures. We computed the critical pressure for the structural phase transition of 25 group IV, III-V, and II-VI compounds using the local density approximation (LDA), Perdew-Burke-Ernzerhof (PBE), and SCAN. LDA systematically underestimates the critical pressures as reported in a previous study. PBE which often improves upon LDA performances yields under- or overestimated pressures in many cases. SCAN, on the other hand, predicts accurate critical pressures with an accuracy comparable to the computationally expensive methods like the quantum Monte Carlo (QMC), random phase approximation (RPA), and the hybrid functional HSE06, in the cases where pressures with these methods are reported.

The impressive success of the approximate density functionals, however, comes

at a price. There is an incomplete cancellation of the hartree and approximate exchange energies for one-electron densities, giving rise to a spurious interaction of an electron with itself. This is called the self-interaction error (SIE). Perdew-Zunger self-interaction correction (PZ SIC) makes an approximate density functional SIE free for all one-electron density. The transition states, which involve stretched bonds, are poorly described by the semilocal density functionals. Thus LDA, PBE, and SCAN predict too low barrier height for a chemical reaction. We tested the Perdew-Zunger self-interaction correction (PZ SIC) for the barrier heights of the representative test set BH6. We found that the barrier heights are greatly improved when we go from LDA to PBE to SCAN. We also tested the PZ SIC for the atomization energies of the molecular test set AE6. SCAN predicts very accurate atomization energies, whereas SCAN-SIC severely worsens the atomization energies. We attribute such worsening to the noded localized orbitals, over which the PZ energy is minimized. The nodality of the orbital density is a consequence of the orthogonality criterion for overlapping real orbitals, and this nodality increases when free atoms bind to form a molecule. This explains why the error in the atomization energies is reduced when the PZ energy is minimized using complex orbitals, which yield nodeless orbital densities. The complex orbitals, however, do not completely eliminate the error. The remaining error is attributed to the fact that PZ SIC loses the exactness of LDA, PBE, or SCAN for densities that vary slowly over space, suggesting for a generalization of the PZ theory.

Dedicated to my parents, wife Priya, and daughter Prasiddhi

ACKNOWLEDGEMENTS

First of all, I would like to thank my advisor Prof. John P. Perdew for his support and guidance during my entire graduate research. Without him, this dissertation would not have been possible. I would like to extend my sincere thanks to Professor Adrienn Ruzsinszky and Professor Jianwei sun for their help. I am also grateful to Dr. Haowei Peng, Dr. Jeb Bates, Dr. Abhirup Patra, Dr. Niladri Sengupta for the helpful discussions. This dissertation contains my published works. I would like to thank all the co-authors for their contribution. I owe immense gratitude to my family members for their love and support. My dad's blessing, probably his final words have been a source of hope and motivation in my life. Thanks, dad! You would have been proud to see your son achieve a doctorate. Thanks to my mom and wife for filling me with positivity and believing in me. I would like to acknowledge Narendra Acharya, Niraj K Nepal, Puskar Bhattarai, Kamal Wagle, Santosh Adhikari, Huta Banjade, Bimal Neupane and Mukesh Pandey for being wonderful friends and making my life easier and happier in Philly.

TABLE OF CONTENTS

ABSTRACT	ii
DEDICATION	iv
ACKNOWLEDGEMENTS	v
LIST OF FIGURES	viii
LIST OF TABLES	x
CHAPTER	
1. DENSITY FUNCTIONAL THEORY	1
1.1 Basics of wavefunction theory	1
1.2 Thomas-Fermi Model	7
1.3 Hohenberg-Kohn theory	8
1.3.1 Levy constrained search method:	11
1.4 Kohn-Sham self-consistent equation:	13
1.5 Exchange-correlation functional	16
1.6 Approximate density functional:	19
1.6.1 Local spin density functional approximation:	20
1.6.2 Generalized gradient approximation:	23
1.6.3 Meta-generalized gradient approximation:	25
1.7 Self-interaction error:	27
2. ACCURATE CRITICAL PRESSURES FOR STRUCTURAL PHASE TRANSITIONS OF GROUP IV, III-V, AND II-VI COMPOUNDS FROM THE SCAN DENSITY FUNCTION- AL	29
2.1 Abstract	29
2.2 Introduction	30
2.3 Computational Method	33
2.4 Results and discussions	34
2.4.1 Si and Ge	34
2.4.2 Sn	35
2.4.3 Pb	36
2.4.4 SiC	36

2.4.5	GaP	36
2.4.6	GaAs	37
2.4.7	GaN, InN, and AlN	39
2.4.8	InP and InAs	40
2.4.9	AlP and AlAs	40
2.4.10	AlSb	41
2.4.11	ZnO	41
2.4.12	ZnS	41
2.4.13	ZnSe	42
2.4.14	ZnTe	42
2.4.15	CdS and CdSe	42
2.4.16	CdTe	43
2.4.17	HgS	43
2.4.18	HgSe and HgTe	44
2.4.19	Overall Analysis	44
2.5	Conclusions	49
2.6	Acknowledgements	49
3.	STRETCHED OR NODED ORBITAL DENSITIES AND SELF-INTERACTION CORRECTION IN DENSITY FUNC- TIONAL THEORY	55
3.1	Abstract	55
3.2	Introduction: Semilocal Approximation and Self-Interaction Correction	56
3.3	Why semilocal approximations fail for lobed (e.g., stretched or noded) one-electron densities.	62
3.4	Why complex localized orbitals work better than real ones in PZ SIC	71
3.5	Discussions and Conclusions	73
3.6	Computational details: ERKALE and PySCF/PyFLOSIC	77
3.7	Atomization energies: AE6 benchmark	79
3.8	Barrier heights: BH6 benchmark	79
3.9	Enthalpies of formation: G2-1 benchmark	80
4.	SUMMARY AND CONCLUSIONS	86
	BIBLIOGRAPHY	88
	APPENDIX	104

LIST OF FIGURES

Figure

2.1	Ratio of the calculated transition pressure P_c and the experimental pressure \bar{P}_e . \bar{P}_e is the average of all experimental forward pressures (from Tables 2.1-2.3). An accurate functional might make this ratio less than or about equal to 1, in view of hysteresis, uncertainty, and vibrational effects in the experiments. Reverse pressures have been measured for only 13 out of the 25 materials.	46
2.2	Comparison of the calculated transition pressure P_c with the RPA transition pressure P_{rpa}	47
3.1	Binding energy curves: exact (or equivalently SIC), LSDA, and SCAN total energies as functions of bond length R , for the one-electron molecular ion H_2^+ , calculated from self-consistent densities with the PySCF code[1, 2] and the cc-pVQZ [3] Gaussian basis set. Note that SCAN (as well as PBE, not shown) is accurate for the compact one-electron densities of compressed or equilibrium bond length but makes the energy increasingly too negative as the bond is stretched. (Note further that, beyond one- and two-electron densities, SCAN and SIC make greater demands on the mesh for the integral of Eq. (3.2.1) than LSDA or PBE do. For example, in the FLOSIC [4] code, the volume per mesh point is 3.7 times smaller for SCAN than for LSDA or PBE.)	61
3.2	(a) Exact (Hartree-Fock or PZ SIC) nonrelativistic electron density (in atomic units) of the one-electron molecular ion H_2^+ in its ground state at stretched bond length $R = 4$ Bohrs, computed in the complete basis-set limit using the code HeIFEM.[5, 6] A similar density with slightly lower and more rounded nuclear cusps was obtained with the FLOSIC [4] all-electron Gaussian-type-orbital code using the NRLMOL default basis set.[7] (b) Electron density (in atomic units) of He^+ in its noded $2p_z$ excited state, computed using the exact nonrelativistic analytic expression. The one-electron density of (a) is stretched and that of (b) is noded, but both are similarly lobed. . .	63

3.3 Relative error of LSDA, PBE, and SCAN for E_{xc} of H_2^+ , using exact (i.e.,SIC) electron densities from the FLOSIC code,[4] as functions of bond length R . Note that at $R = 0$, the exchange-correlation energy is that of $He^+ 1s$. The equilibrium bond length is around 2 Bohrs (Fig. 3.1). The results for the nonzero bondlengths of H_2^+ correct erroneous results from Ref.[8]. For PBE and SCAN, the self-interaction error grows as the bond is stretched, but it grows more slowly in SCAN. 65

LIST OF TABLES

Table

2.1	The calculated equilibrium transition pressure (in GPa) for the group IV materials within the LDA, PBE and SCAN XC functionals. ZPE and vibrational effects are not included in the calculated value. The experimental pressure (in GPa) to the right of the vertical bar corresponds to the forward transition and the left one to the reverse transition.	35
2.2	The calculated equilibrium transition pressure (in GPa) for the group III-IV compounds within the LDA, PBE and SCAN XC functionals. ZPE and vibrational effects are not included in the calculated value. The experimental pressure (in GPa) to the right of the vertical bar corresponds to forward transition and the left one to reverse transition.	38
2.3	The calculated equilibrium transition pressure (in GPa) for the group II-VI materials within the LDA, PBE and SCAN XC functionals. ZPE and vibrational effects are not included in the calculated value. The experimental pressure (in GPa) to the right of the vertical bar corresponds to the forward transition and the left one to the reverse transition	43
2.4	The mean percentage error (MPE) and mean absolute percentage error (MAPE) for XC functionals LDA, PBE, and SCAN. The experimental reference value is \bar{P}_e , as defined in the caption of Fig. 1.	44
2.5	The calculated equilibrium energy E_0 (in eV) and volume V_0 (in A^3) per formula unit and the bulk modulus B_0 (in GPa) and its pressure derivative B'_0 for XC functionals SCAN, PBE, and LDA. The equilibrium energy of the low-pressure phase has been set to zero and that of the high-pressure phase to the energy difference. Only the structural change in E_0 from a PAW code is physically meaningful.	51

2.6	The calculated equilibrium energy E_0 (in eV) and volume V_0 (in A^3) per formula unit and the bulk modulus B_0 (in GPa) and its pressure derivative B'_0 for XC functionals SCAN, PBE, and LDA. The equilibrium energy of the low-pressure phase has been set to zero and that of the high-pressure phase to the energy difference. Only the structural change in E_0 from a PAW code is physically meaningful.	52
2.7	The kinetic energy cutoff and the k-mesh size. The cutoffs used here for SCAN are un-necessarily large. VASP recommends setting the cutoff for the energy-volume calculation to 1.3 times the default cutoff. We have found the same SCAN transition pressure for Si with 440 eV as with 720 eV. For fine energy differences, we believe that 520 eV, as used in Ref.[9], should be safe.	53
2.8	The kinetic energy cutoff and the k-mesh size. The cutoffs used here for SCAN are un-necessarily large. VASP recommends setting the cutoff for the energy-volume calculation to 1.3 times the default cutoff. We have found the same SCAN transition pressure for InAs with 440 eV as with 700 eV. For fine energy differences, we believe that 520 eV, as used in Ref.[9], should be safe.	54
3.1	Relative errors (%) of LSDA, PBE, and SCAN for E_{xc} of H_2^+ at $R = 4$ Bohrs and $He^+ 2p_z$, both using exact densities. The H_2^+ values from PySCF[1, 2] using the cc-pVQZ[3] Gaussian basis set correct erroneous values from Ref.[8]. Exact and approximate exchange (but not correlation) energies of the He^+ canonical orbitals scale up in proportion to the nuclear charge Z . Note the similarities in the numbers between the stretched H_2^+ and the noded $He^+ 2p_z$ densities. Note further that SCAN is better than PBE for these highly stretched or strongly noded one-electron densities. The bottom row shows the exact E_{xc} of Eq. (3.3-6), in Hartrees.	66

3.2	<p>Relative errors of LSDA, PBE, and SCAN for E_{xc} of individual real Fermi-Löwdin orbitals in the Ne atom and the CH₄ molecule, calculated here using the corresponding SIC orbital densities from the FLOSIC[4] code. The exact entry $-U[n_{i\sigma}]$ is displayed for the SCAN-SIC orbital density. For the Ne atom, the core orbital is 1s and the valence orbitals are rotationally equivalent sp^3 hybrids. The purpose of this table is not to compare atoms with molecules but to show that the relative errors of PBE and SCAN for the valence orbitals are much smaller here than those in Table 3.1 because the real Fermi-Löwdin orbital densities are less severely noded than is the $2p_z$ orbital density. (As usual, PBE and SCAN are much more accurate than LSDA for the compact 1s core orbital densities.) The bottom row shows the exact E_{xc} of Eq. (3.3-6), in Hartrees. For CH₄, we have employed the QCISD/MG3 equilibrium geometry[10] from the HTBH38/08 database.</p>	66
3.3	<p>Mean error (ME) and mean absolute error (MAE) (kcal/mol) for LSDA, PBE, SCAN, LSDA-RSIC, PBE-RSIC, SCAN-RSIC, LSDA-CSIC, PBE-CSIC, and SCAN-CSIC for the molecular atomization energies of the small representative AE6 set. RSIC is SIC with real localized orbitals, and CSIC is SIC with complex localized orbitals. The AE6[10] set comprises the six molecules SiH₄, S₂, SiO, C₃H₄ (propyne), HCOCOH (glyoxal), and C₄H₈ (cyclobutane). All densities are self-consistent. We have used the Gaussian-type-orbital ERKALE code of Lehtola et al.[11, 2] with the cc-pVQZ[3] basis set, using fixed nuclear geometries at the QCISD/MG3 level (see https://comp.chem.umn.edu/db/index.html). A Lebedev grid of 50 radial and 194 angular points delivered good agreement with reference values.[12] See the supplementary material for further details. (1 Hartree = 627.5 kcal/mol = 27.21 eV.) Note that here PZ SIC worsens the atomization energies of SCAN, but less severely in CSIC than in RSIC.</p>	68
3.4	<p>Same as Table 3.3, but for the barrier heights of the small representative BH6[10] set. There are forward and backward barriers for each of three reactions: (1) OH + CH₄ → CH₃ + H₂O, (2) OH + H → O + H₂, and (3) H + H₂S → HS + H₂. Note that PZ SIC improves the barrier heights for all the semilocal functionals</p>	69

3.5	Same as Table 3.3, but for the 55 molecular formation energies of the G2-1 data set,[13] using SCAN, SCAN-RSIC, and SCAN-CSIC. The formation energies are constructed in such a way that their MAEs are essentially those of the molecular atomization energies, and their MEs are essentially minus those of the atomization energies. We have used B3LYP geometries with zero-point expansion. Note that the FLOSIC method implemented in the PySCF code [1, 2] (PyFLOSIC[14]) agrees within 0.6 kcal/mol with these RSIC results from the ERKALE code.[11, 2] (See the supplementary material for details.) For LSDA, LSDA-RSIC, PBE, and PBE-RSIC, see Ref.[15].	70
3.6	Total PZ self-interaction corrections to the exchange-correlation energies of rare-gas atoms, in Hartrees. Shown is the orbital-density-dependent correction of Eq. (3.2-3) to the exchange-correlation energy in an energy-minimized SIC calculation, with real (RSIC) or complex (CSIC) orbitals, using the ERKALE code[11, 2] and the standard NRLMOL basis set.[7] Note that the CSIC values are lower than the RSIC values, as expected, and that the difference increases from LSDA to PBE to SCAN. The CSIC correction to PBE is relatively small, consistent with Ref.[16]. To set a scale, the last rows show the accurate total exchange-correlation energy from a self-consistent SCAN calculation and a nearly exact exchange-correlation energy (exchange from Ref.[17] and correlation from Ref. [18]). . . .	74
3.7	Total energies (in Hartree) using ERKALE[11] and the cc-pVQZ basis set. A Lebedev-Lakov grid of 50 radial and 194 angular points was used.	78
3.8	BH6: Total energies (in Hartree) using ERKALE[11] and the cc-pVQZ basis set. A Lebedev-Lakov grid of 50 radial and 194 angular points was used.	81
3.9	ERKALE G2-1 (atoms): Total energies (in Hartree) using ERKALE [11] and the cc-pVQZ basis set. A Lebedev-Lakov grid of 50 radial and 194 angular points was used.	82
3.10	ERKALE G2-1 (molecules): Total energies (in Hartree) using ERKALE[11] and the cc-pVQZ basis set. A Lebedev-Lakov grid of 50 radial and 194 angular points was used.	82
3.11	pyFLOSIC G2-1 (atoms): Total energies (in Hartree) using PyFLOSIC [14] and the DFO [7] basis set. A PySCF/PyFLOSIC grid level of 7 was used (e.g. corresponds for the H atom to Lebedev-Lakov grid of 90 radial and 974 angular points)[19].	83

3.12	pyFLOSIC G2-1 (molecules): Total energies (in Hartree) using PyFLOSIC[14] and theDFO[7] basis set. A PySCF/PyFLOSIC grid level of 7 was used (e.g. corresponds for the H atom to Lebedev-Lakov grid of 90 radial and 974 angular points)[19].	84
3.13	Errors of enthalpies of formation with respect to reference values [20] in kcal/mol for FLOSIC and DFT with the SCAN functional for the full G2-1 set calculated with PyFLOSIC [14] using the DFO [7] basis set. A PySCF/PyFLOSIC grid level of 7 was used (e.g. corresponds for the H atom to Lebedev-Lakov grid of 90 radial and 974 angular points)[19]	85

CHAPTER 1

DENSITY FUNCTIONAL THEORY

1.1 Basics of wavefunction theory

A wealth of information can be extracted by solving the non-relativistic time-independent Schrödinger equation [21]

$$\hat{H}\Psi = E\Psi, \quad (1.1-1)$$

with the Hamiltonian \hat{H} for a system of M nuclei and N electrons represented respectively by set of position vectors $\{\vec{R}_\alpha, \alpha = 1, \dots, M\}$ and $\{\vec{r}_i, i = 1, 2, \dots, N\}$ interacting through Coulomb interaction in atomic units ($m_e = c = \hbar = 1$)

$$\hat{H} = -\frac{1}{2} \sum_{\alpha=1}^M \frac{\nabla_R^2}{M_\alpha} - \frac{1}{2} \sum_{i=1}^N \nabla_r^2 + \frac{1}{2} \sum_{\alpha=1}^M \sum_{\beta \neq \alpha}^M \frac{Z_\alpha Z_\beta}{|\vec{R}_\alpha - \vec{R}_\beta|} + \frac{1}{2} \sum_{i=1}^N \sum_{j \neq i}^N \frac{1}{|\vec{r}_i - \vec{r}_j|} - \sum_{\alpha=1}^M \sum_{i=1}^N \frac{Z_\alpha}{|\vec{r}_i - \vec{R}_\alpha|} \quad (1.1-2)$$

It is often written as

$$\hat{H} = \hat{T}_n + \hat{T}_e + \hat{V}_{nn} + \hat{V}_{ee} + \hat{V}_{ne} \quad (1.1-3)$$

where

$$\hat{T}_n = -\frac{1}{2} \sum_{\alpha=1}^M \frac{\nabla_R^2}{M_\alpha} \quad (1.1-4)$$

is the nuclear kinetic energy operator. M_α is the ratio of the mass of the α th nucleus to the mass of an electron.

$$\hat{T}_e = -\frac{1}{2} \sum_{i=1}^N \nabla_r^2 \quad (1.1-5)$$

is the electronic kinetic energy operator.

$$\hat{V}_{nn} = \frac{1}{2} \sum_{\alpha=1}^M \sum_{\beta \neq \alpha}^M \frac{Z_\alpha Z_\beta}{|\vec{R}_\alpha - \vec{R}_\beta|} \quad (1.1-6)$$

is the nucleus-nucleus interaction energy operator.

$$\hat{V}_{ne} = \sum_{\alpha=1}^M \sum_{i=1}^N \frac{Z_\alpha}{|\vec{r}_i - \vec{R}_\alpha|} \quad (1.1-7)$$

is the nucleus-electron interaction energy operator, also called the external potential \hat{V}_{ext} . And

$$\hat{V}_{ee} = \frac{1}{2} \sum_{i=1}^N \sum_{j \neq i}^N \frac{1}{|\vec{r}_i - \vec{r}_j|} \quad (1.1-8)$$

represents the electron-electron interaction energy. Unfortunately, Eq. (1.1-1) can be solved exactly only for hydrogen-like ($M = 1, N = 1$) systems. Even $M = 2, N = 1$ (i.e. the H_2^+ molecule) case is not possible to solve analytically without an approximation. A reasonable approximation can be made by using the fact that a proton is much heavier than an electron. Born and Oppenheimer[22] showed that to good accuracy the motion of nuclei does not affect the electronic wavefunction. As a result, if electrons are in the ground state of the electronic Hamiltonian they remain locked into the ground state for each set of nuclear positions. This allows us to write

$$\Psi(\vec{R}, \vec{r}) = \Phi(\vec{R})\Psi(\vec{R}, \vec{r}) \quad (1.1-9)$$

where $\Phi(\vec{R})$ is the nuclear wavefunction and $\Psi(\vec{R}, \vec{r})$ is the electronic wavefunction which satisfies

$$\hat{H}_e \Psi(\vec{R}, \vec{r}) = E(\vec{R})\Psi(\vec{R}, \vec{r}) \quad (1.1-10)$$

where $\hat{H}_e = \hat{T}_e + \hat{V}_{ne} + \hat{V}_{ee}$ is the electronic Hamiltonian. Some also include \hat{V}_{nn} . If we further assume the nuclei are at rest, the problem boils down to solving the Schrödinger equation for the electronic wavefunction. Here \vec{R} enters just like a parameter. By solving the above equation for a set of \vec{R} and minimizing the energy one can calculate the equilibrium bond length of a molecule. However, solving the equation for the system having many electrons ($N > 1$) is a very challenging task because of the correlated motion of electrons. We must resort to some approximation to decouple the correlated motion.

One popular approach is the wavefunction theory (WFT). Hartree[23] introduced a self-consistent field (SCF) method to deal with the many-body problems by assuming that an electron moves in the field of nuclei and the average field of $N - 1$ electrons. This allows us to express the wavefunction as a product of N one-electron orbitals. Later, Fock[24] modified it to incorporate the antisymmetry property of the many electron wavefunctions. In the Hartree-Fock SCF theory, a single Slater determinant of the spin-orbitals represents the many-electron wavefunction. The Hartree-Fock theory misses the important correlation effect. Many subsequent efforts [25, 26, 27, 28] have been made to incorporate this effect. They give very accurate results for atoms and small molecules but their computational cost scales up ($N^4 - N^6$) rapidly with the number of electrons. The difficulty with WFT can also be realized by an argument from Walter Kohns Nobel lecture[29]. For a N -electron wavefunction $\Psi(\vec{r}_1, \vec{r}_2, \dots, \vec{r}_N)$, if we take the number of grid points along one axis to be M , there are M^{3N} values of the wavefunction to be computed and stored. For a system $N = 1$ electron this is manageable M^3 , but for a system with $N = 10$ electrons it is an unmanageable M^{30} . This considerations makes WFT an inefficient tool for studying systems with many electrons: big molecules and solids.

An alternative approach to solving the many-body Schrödinger equation is the density functional theory (DFT)[30, 31, 32], in which the complicated wavefunction

is replaced by the electron density. Let us first define the electron density. The total electronic density of a system of N electrons can be defined as follows-

$$n(\vec{r}) = N \sum_{\sigma} \sum_{\sigma_2} \dots \sum_{\sigma_N} \int d^3r_2 \int d^3r_3 \dots \int d^3r_N |\Psi(\vec{r}, \sigma, \vec{r}_2, \sigma_2, \dots, \vec{r}_N, \sigma_N)|^2 \quad (1.1-11)$$

where $N! |\Psi(\vec{r}_1, \sigma_1, \vec{r}_2, \sigma_2, \dots, \vec{r}_N, \sigma_N)|^2$ represents the probability of finding any electron in d^3r_1 with z-spin σ_1 , and any electron in d^3r_2 with z-spin σ_2 , ... and any electron in d^3r_N with z-spin σ_N . And the spin density is

$$n_{\sigma}(\vec{r}) = N \sum_{\sigma_2} \dots \sum_{\sigma_N} \int d^3r_2 \int d^3r_3 \dots \int d^3r_N |\Psi(\vec{r}, \sigma, \vec{r}_2, \sigma_2, \dots, \vec{r}_N, \sigma_N)|^2 \quad (1.1-12)$$

Similarly, we can define more general objects: one-body and two-body density matrices as following

$$\begin{aligned} \rho_1(\vec{r}', \sigma', \vec{r}, \sigma) &= N \sum_{\sigma_2} \dots \sum_{\sigma_N} \int d^3r_2 \int d^3r_3 \dots \int d^3r_N * \\ &\Psi^*(\vec{r}', \sigma', \vec{r}_2, \sigma_2, \dots, \vec{r}_N, \sigma_N) \Psi(\vec{r}, \sigma, \vec{r}_2, \sigma_2, \dots, \vec{r}_N, \sigma_N) \end{aligned} \quad (1.1-13)$$

and

$$\rho_2(\vec{r}', \sigma', \vec{r}, \sigma) = N(N-1) \sum_{\sigma_3} \dots \sum_{\sigma_N} \int d^3r_3 \int d^3r_4 \dots \int d^3r_N |\Psi(\vec{r}', \sigma', \vec{r}, \sigma, \dots, \vec{r}_N, \sigma_N)|^2 \quad (1.1-14)$$

The two-body density matrix has simple probabilistic interpretation: $\rho_2(\vec{r}, \sigma, \vec{r}', \sigma')$ represents the joint probability of finding a particle of spin σ' in d^3r' at \vec{r}' and another particle of spin σ in d^3r at \vec{r} . Clearly

$$\rho_1(\vec{r}, \vec{r}') = \sum_{\sigma, \sigma'} \rho_1(\vec{r}, \sigma, \vec{r}', \sigma') \quad (1.1-15)$$

$$n_\sigma(\vec{r}) = \rho_1(\vec{r}, \sigma, \vec{r}, \sigma) \quad (1.1-16)$$

$$n(\vec{r}) = \rho_1(\vec{r}, \vec{r}) \quad (1.1-17)$$

The total energy is the expectation value of the Hamiltonian

$$E = \langle \Psi | \hat{T} + \hat{V}_{ext} + \hat{V}_{ee} | \Psi \rangle \quad (1.1-18)$$

We can evaluate the expectation values in right hand side of above equation in terms of the one- and two-body density matrices. The external potential energy is

$$\langle \hat{V}_{ext} \rangle = \left\langle \Psi \left| \sum_i v(\vec{r}_i) \right| \Psi \right\rangle \quad (1.1-19)$$

Using

$$v(\vec{r}_i) = \int d^3r v(\vec{r}) \delta(\vec{r} - \vec{r}_i) \quad (1.1-20)$$

$$n_\sigma(\vec{r}) = \left\langle \Psi \left| \sum_i^N \delta(\vec{r} - \vec{r}_i) \delta_{z_i \sigma} \right| \Psi \right\rangle \quad (1.1-21)$$

we get

$$\langle \hat{V}_{ext} \rangle = \int d^3r v(\vec{r}) n(\vec{r}) \quad (1.1-22)$$

The kinetic energy is

$$\begin{aligned} \langle \hat{T} \rangle &= -\frac{1}{2} \left\langle \Psi \left| \sum_i^N \nabla_i^2 \right| \Psi \right\rangle = -\frac{1}{2} \sum_{\sigma_1} \dots \sum_{\sigma_N} \int d^3r_1 \dots \int d^3r_N \Psi^*(\vec{r}_1, \sigma_1, \dots, \vec{r}_N, \sigma_N) * \\ &\quad \sum_i \nabla_i^2 \Psi(\vec{r}_1, \sigma_1, \dots, \vec{r}_N, \sigma_N) \end{aligned} \quad (1.1-23)$$

Using similar trick as in Eq. (1.1-19) and (1.1-20) we can easily prove

$$\langle \hat{T} \rangle = -\frac{1}{2} \int d^3r \nabla_r^2 \rho_1(\vec{r}, \vec{r}')|_{\vec{r}'=\vec{r}} \quad (1.1-24)$$

Likewise, the electron-electron repulsion energy

$$\langle \hat{V}_{ee} \rangle = \left\langle \Psi \left| \frac{1}{2} \sum_i^N \sum_j^N \frac{1}{|\vec{r}_i - \vec{r}_j|} \right| \Psi \right\rangle \quad (1.1-25)$$

can be shown to be

$$\langle \hat{V}_{ee} \rangle = \frac{1}{2} \int d^3r \int d^3r' \frac{\rho_2(\vec{r}, \vec{r}')}{|\vec{r} - \vec{r}'|} \quad (1.1-26)$$

with

$$\rho_2(\vec{r}, \vec{r}') = \sum_{\sigma} \sum_{\sigma'} \rho_2(\vec{r}', \sigma', \vec{r}, \sigma) \quad (1.1-27)$$

Here if the electrons were independent, the probability of finding a particle of spin σ' in d^3r' at \vec{r}' would be independent of whether there is a particle of spin σ at \vec{r} , i.e.

$$\rho_2(\vec{r}', \sigma', \vec{r}, \sigma) = n_{\sigma'}(\vec{r}') n_{\sigma}(\vec{r}) \quad (1.1-28)$$

But, for the real system of interacting electrons, we modify above equation as

$$\rho_2(\vec{r}', \sigma', \vec{r}, \sigma) = n_{\sigma}(\vec{r}) n_{\sigma'}(\vec{r}') + n_{xc}(\vec{r}', \sigma', \vec{r}, \sigma) \quad (1.1-29)$$

where $n_{xc}(\vec{r}, \sigma, \vec{r}', \sigma')$ is the exchange-correlation hole spin density at \vec{r}' around an electron of spin σ at \vec{r} . Eq. (1.1-26) reads

$$\langle \hat{V}_{ee} \rangle = \frac{1}{2} \int d^3r \int d^3r' \frac{n(\vec{r}) n(\vec{r}')}{|\vec{r} - \vec{r}'|} + \frac{1}{2} \sum_{\sigma} \sum_{\sigma'} \int d^3r \int d^3r' \frac{n_{\sigma}(\vec{r}) n_{xc}(\vec{r}', \sigma', \vec{r}, \sigma)}{|\vec{r} - \vec{r}'|} \quad (1.1-30)$$

The first is the coulomb repulsion energy or the Hartree energy and the second term

is the exchange-correlation energy.

1.2 Thomas-Fermi Model

The total energy is functional of the wavefunction

$$E[\Psi] = \langle \hat{T} \rangle + \langle \hat{V}_{ext} \rangle + \langle \hat{V}_{ee} \rangle \quad (1.2-31)$$

Thomas[33] and Fermi[34] sought to use the electron density as a basic variable instead of a wavefunction. But, from Eq. (1.1-24) and (1.1-29) we noticed that expressing the total energy as a functional of the electron density is not an easy task. However, making some simpler approximation we can achieve the goal. First, let us assume that electrons interact with each other via the classical Coulomb interaction of the density with itself. Then

$$\langle \hat{V}_{ee} \rangle \approx U[n] = \frac{1}{2} \int d^3r \int d^3r' \frac{n(\vec{r})n(\vec{r}')}{|\vec{r} - \vec{r}'|} \quad (1.2-32)$$

Thomas Fermi (TF) theory further assumes that the electron density is locally homogeneous,

$$\langle \hat{T} \rangle \approx T[n] = A \int d^3r n^{5/3}(\vec{r}) \quad (1.2-33)$$

where $A = \frac{3}{5}(3\pi^2)^{5/3}$. Thus using Eq. (1.1-22), the Thomas Fermi energy functional can be written as

$$E_{TF}[n] = A \int d^3r n^{5/3}(\vec{r}) + \int d^3r n(\vec{r})v(\vec{r}) + \frac{1}{2} \int d^3r \int d^3r' \frac{n(\vec{r})n(\vec{r}')}{|\vec{r} - \vec{r}'|} \quad (1.2-34)$$

The total energy can be minimized with respect to the density under the constraint

$$\delta N = \delta \int d^3r n(\vec{r}) = 0$$

$$\delta(E_{TF} - \mu \int d^3r n(\vec{r})) = 0 \quad (1.2-35)$$

where the Lagrange multiplier is the chemical potential. Using properties of the functional derivative

$$\frac{5}{3}An^{2/3}(\vec{r}) + v(\vec{r}) + \int d^3r \frac{n(\vec{r}')}{|\vec{r} - \vec{r}'|} = \mu \quad (1.2-36)$$

The TF model is size consistent (Eq. (1.2-34)). When applied to atoms it gives qualitatively correct energy ($\pm 10\%$) for heavy atoms but, it fails to account for the shell structure effect. Atoms do not bind to form molecules in the Thomas-Fermi model: Teller's theorem[35]. It is not hard to see that the TF model is a crude approximation of a real picture. It misses the important exchange and correlation effect. The kinetic energy density is solely determined by the density at a point whereas the Laplacian is not a local object. Attempts[32, 36] have been made to improve the TF model by including the exchange energy[37], correlation energy[38] and gradient correction for the kinetic energy[39], but that does not make it a good theory. However, it has played an important role in the development of the modern density functional theory; it hints at the one-to-one mapping[29] of the electron density and the external potential.

1.3 Hohenberg-Kohn theory

The TF model uses approximations to express the total energy as a functional of the electron density. In 1964, Hohenberg and Kohn[30] formally proved that such an exact energy functional does indeed exist by showing the one-to-one mapping between the external potential and the ground state electron density, and also proposed the variational principle for the energy functional and the density. The following are two Hohenberg-Kohn (HK) theorems.

Theorem 1: For a system of interacting electrons in an external potential, the ground state electron density uniquely determines the external potential.

It can be easily proven by the *reductio ad absurdum* method. Let us suppose that there exist two Hamiltonians \hat{H} and \hat{H}' differing in their external potentials by more than a trivial additive constant but corresponding to the same electronic ground state $n(\vec{r})$. Let their respective ground state wavefunctions are Ψ and Ψ' and the ground state energies are E_0 and E'_0 . Now applying the Rayleigh-Ritz variational principle for Hamiltonian \hat{H} with Ψ' as trial wavefunction. We get

$$E_0 < \langle \Psi' | \hat{H} | \Psi' \rangle = \langle \Psi' | \hat{H}' | \Psi' \rangle + \langle \Psi' | \hat{H} - \hat{H}' | \Psi' \rangle \quad (1.3-37)$$

$$E_0 < E'_0 + \int d^3r n(\vec{r})(v(\vec{r}) - v'(\vec{r})) \quad (1.3-38)$$

Similarly, for \hat{H}' with as trial wavefunction Ψ , we get

$$E'_0 < E_0 - \int d^3r n(\vec{r})(v(\vec{r}) - v'(\vec{r})) \quad (1.3-39)$$

upon adding Eq. (1.3-38) and (1.3-39)

$$E_0 + E'_0 < E'_0 + E_0 \quad (1.3-40)$$

This contradicts our assumption proving that the external potentials corresponding to the same ground state density can not differ by more than an additive constant. Thus the ground state density uniquely determines the external potential. Since the number of electrons ($\int d^3r n(\vec{r}) = N$) and the external potential determine the Hamiltonian of the system, with the knowledge of the electron density we can find everything else including the ground state and excited state wavefunctions. This theorem enables us to write the energy as a functional of the density

$$E[n] = T[n] + V_{ee}[n] + \int d^3r n(\vec{r})v(\vec{r}) \quad (1.3-41)$$

Here $T[n] + V_{ee}[n]$ is independent of the external potential, so we define a universal functional $Q[n]$ that is true for all electron systems

$$Q_{HK}[n] = T[n] + V_{ee}[n] \quad (1.3-42)$$

Theorem 2: For a non-negative trial density $n'(\vec{r})$ with $\int d^3r n(\vec{r}) = N$, $E[n'] \geq E_0$. Where E_0 is the ground state energy.

Proof: Theorem 1 tells us that $n'(\vec{r})$ determine its Hamiltonian \hat{H}' and hence the wavefunction Ψ' . Using Ψ' as a trial wavefunction for Hamiltonian \hat{H} we can define the energy functional

$$\langle \Psi' | \hat{H} | \Psi' \rangle = Q_{HK}[n'] + \int d^3r n'(\vec{r}) v'(\vec{r}) = E[n'] \quad (1.3-43)$$

But, the Rayleigh-Ritz variational principle says

$$\langle \Psi' | \hat{H} | \Psi' \rangle \geq E_0 \quad (1.3-44)$$

Hence

$$E[n'] \geq E_0 \quad (1.3-45)$$

These two mathematically simple theorems formed the basis of modern density functional theory. However, there are some caveats in the HK theorems. First, proof of theorem 1 does not hold if the ground state wavefunction is degenerate, which is often the case in many-electron systems. Second, the proof of theorem 2 is only true for V-representable density. A V-representable density is the one that comes from the wavefunction of the Schrödinger equation with the external potential $v(\vec{r})$. But, there are densities that are not V-representable[40, 41, 42]. In the next section, we will resolve these issues by using a weaker condition- N-representability.

1.3.1 Levy constrained search method:

Levi[43] and Lieb[44] introduced the constrained search method that eliminates the issues of HK theorems, in which the density is N -representable. A density is said to be N -representable if following conditions hold[45]:

$$n(\vec{r}) \geq 0 \quad (1.3-46)$$

$$\int d^3r n(\vec{r}) = N \quad (1.3-47)$$

$$\frac{1}{2} \int d^3r |\nabla n^{1/2}(\vec{r})|^2 < \infty \quad (1.3-48)$$

Let Ψ_n be any normalized antisymmetric wavefunction that gives the N -representable ground state density $n_g(\vec{r})$; it may not necessarily be the ground state wavefunction of Hamiltonian $\hat{H} = \hat{T} + \hat{V}_{ee} + \sum_i^N v(\vec{r}_i)$. If Ψ_g is the ground state wavefunction, the Rayleigh-Ritz principle gives

$$\langle \Psi_n | \hat{H} | \Psi_n \rangle \geq \langle \Psi_g | \hat{H} | \Psi_g \rangle \quad (1.3-49)$$

This simplifies to

$$\langle \Psi_n | \hat{T} + \hat{V}_{ee} | \Psi_n \rangle \geq \langle \Psi_g | \hat{T} + \hat{V}_{ee} | \Psi_g \rangle \quad (1.3-50)$$

Here, the right-hand side of is Hohenberg-Kohn universal density functional (Eq. (1.3-42))

$$Q_{HK}[n] = \langle \Psi_g | \hat{T} + \hat{V}_{ee} | \Psi_g \rangle \quad (1.3-51)$$

Thus the ground-state wavefunction is the one that minimizes the expectation value of $\hat{T} + \hat{V}_{ee}$. This prompts us to define a functional for any N -representable density $n(\vec{r})$

$$Q[n] = \min_{\Psi} \langle \Psi | \hat{T} + \hat{V}_{ee} | \Psi \rangle \quad (1.3-52)$$

Here the minimization is over all the normalized antisymmetric wavefunctions that give the density $n(\vec{r})$ and we pick one that minimizes $\langle \hat{T} + \hat{V}_{ee} \rangle$. This definition does not require the knowledge of external potential $v(\vec{r})$, also, the degeneracy of the ground state is not an issue as the wavefunction is constrained to yield the given density. Clearly,

$$Q[n] + \int d^3r n(\vec{r})v(\vec{r}) \geq E_0 \quad (1.3-53)$$

The ground state energy can be obtained by minimizing the left-hand side of Eq. (1.3-53) over all N -representable densities $n(\vec{r})$

$$E_0 = \underset{n}{\min} [Q[n] + \int d^3r v(\vec{r})n(\vec{r})] \quad (1.3-54)$$

Here the minimization is over 3-dimensional density, which is computationally much easier to do than the minimization over $3N$ -dimensional wavefunction.

Assuming the differentiability of $Q[n]$, we can apply the variational principle to obtain the Euler-Lagrange equation for the ground state density.

$$\delta(E[n] - \mu \int d^3r n(\vec{r})) = 0 \quad (1.3-55)$$

$$\mu = v(\vec{r}) + \frac{\delta Q[n]}{\delta n} \quad (1.3-56)$$

where $\mu = \frac{\delta E}{\delta n}$ is the chemical potential, and is a constant for ground state density. Thus, if we know the explicit form of the universal functional $Q[n]$, we can find the ground-state energy and density of the many-body Schrödinger equation. The HK theorem only tells that it exists, but does not give any recipe to find it. Finding it with the Levy constrained search is like finding the correlated wavefunction in the wavefunction theory.

1.4 Kohn-Sham self-consistent equation:

Kohn and Sham[31] in 1965 devised an ingenious idea to reduce the many-body problem to an effective one-body problem as in the Hartree-Fock theory. However, unlike the Hartree-Fock theory, the Kohn-Sham (KS) theory is not a mean field theory, as it explicitly considers all many-body effects. To demonstrate the Kohn-Sham scheme, let us consider a system of interacting electrons having ground state density $n(\vec{r})$ in an external field $v(\vec{r})$. The energy functional is

$$E[n] = T[n] + V_{ee}[n] + \int d^3r n(\vec{r})v(\vec{r}) \quad (1.4-57)$$

Now, we assume that there exists a fictitious system of non-interacting electrons that has the same ground state density $n(\vec{r})$ in some reference potential $v^s(\vec{r})$. Thus the Kohn-Sham theory will work if $n(\vec{r})$ is non-interacting V -representable. We can modify the above equation as follows

$$E[n] = T_s[n] + \int d^3r n(\vec{r})v(\vec{r}) + U_{ee}[n] + E_{xc}[n] \quad (1.4-58)$$

where $E_{xc} = T[n] - T_s[n] + V_{ee}[n] + U_{ee}[n]$ is the exchange-correlation energy; this is different than the exchange-correlation energy term in Eq. (1.1-30), for it contains the kinetic correlation energy. T_s is the kinetic energy of the non-interacting electrons, which can be evaluated exactly using the spin-orbitals. The Hamiltonian of this fictitious system can be decoupled into one-electron Hamiltonians as

$$\hat{H} = \sum_i^N \left(\frac{1}{2} \nabla_i^2 + v^s(\vec{r}_i) \right) \quad (1.4-59)$$

and the wavefunction is represented by the single Slater determinant of spin-orbitals

$$\Psi = \frac{1}{\sqrt{N!}} \det[\psi_1, \psi_2, \dots, \psi_N] \quad (1.4-60)$$

where the spin-orbitals are the solution of one-electron Schrödinger equation (or KS equation)

$$\left(-\frac{1}{2}\nabla^2 + v^s(\vec{r})\right)\psi_i = \epsilon_i\psi_i \quad (1.4-61)$$

ψ_i is called Kohn-Sham orbital and the eigenvalue ϵ_i the Kohn-Sham orbital energy. The non-interacting kinetic energy

$$T_s = \langle \Psi | \hat{T}_s | \Psi \rangle = -\frac{1}{2} \sum_{i=1}^N \langle \psi_i | \nabla^2 | \psi_i \rangle \quad (1.4-62)$$

and the ground state density is

$$n(\vec{r}) = \sum_{i=1}^N |\psi_i|^2 \quad (1.4-63)$$

Here the non-interacting kinetic energy is an implicit functional of density via the spin-orbital which is a functional of the density. Now applying the variational principle under the constraint of a fixed number of electrons Eq. (1.3-55) yields

$$\frac{\delta T_s}{\delta n} + v(\vec{r}) + \int d^3r' \frac{n(\vec{r}')}{|\vec{r} - \vec{r}'|} + v_{xc}[n] = \mu \quad (1.4-64)$$

Where $v_{xc}[n] = \frac{\delta E_{xc}[n]}{\delta n}$. We can find similar Euler-Lagrange equation for the system of the non-interacting electron whose total energy is $E[n] = T_s[n] + \int d^3r n(\vec{r})v^s(\vec{r})$

$$\frac{\delta T_s}{\delta n} + v^s(\vec{r}) = \mu \quad (1.4-65)$$

Here the chemical potentials for the real interacting and fictitious non-interacting systems are the same, as their densities are the same. From Eq. (1.4-64) and (1.4-65)

$$v^s(\vec{r}) = v(\vec{r}) + \int d^3r' \frac{n(\vec{r}')}{|\vec{r} - \vec{r}'|} + v_{xc}(\vec{r}) \quad (1.4-66)$$

The effective potential depends upon the density, suggesting that we need to solve the KS equation self-consistently. So the recipe to find the ground state energy of the interacting electrons is to start with a guess for the density which determines the effective potential; then solve the KS Eq. (1.4-61) for the Kohn-Sham orbitals which determine the density. We repeat this process until the density stops changing.

For the spin polarized cases, such as open-shell atoms, we need to consider both the up-spin and down-spin densities. We can easily generalize the Kohn-Sham theory for a system of interacting electrons of ground state spin densities n_\uparrow and n_\downarrow in a spin-dependent external potential $v_\sigma(\vec{r})$ ($\sigma = \uparrow, \downarrow$). The energy functional can be expressed as

$$E[n_\uparrow, n_\downarrow] = Q[n_\uparrow, n_\downarrow] + \sum_\sigma \int d^3r v_\sigma(\vec{r}) n_\sigma(\vec{r}) \quad (1.4-67)$$

where the universal functional

$$Q[n] = \Psi \xrightarrow{\min} n_\uparrow n_\downarrow \langle \Psi | \hat{T} + \hat{V}_{ee} | \Psi \rangle \quad (1.4-68)$$

As in the previous section, we assume that there exists a fictitious system of non-interacting electrons with the same ground state spin densities n_\uparrow and n_\downarrow in a spin dependent external potential $v_\sigma^s(\vec{r}), \sigma = \uparrow, \downarrow$. We can rewrite the equation as

$$E[n_\uparrow, n_\downarrow] = T_s[n_\uparrow, n_\downarrow] + \sum_\sigma \int d^3r n_\sigma(\vec{r}) v_\sigma(\vec{r}) + U_{ee}[n] + E_{xc}[n_\uparrow, n_\downarrow] \quad (1.4-69)$$

where the total density $n = n_\uparrow + n_\downarrow$. We can obtain the following equations that comprise the Kohn-Sham self-consistent equation.

$$n_\sigma = \sum_{i=1}^N |\psi_i|^2 \quad (1.4-70)$$

$$\left(-\frac{1}{2}\nabla^2 + v_\sigma^s(\vec{r})\right)\psi_{i\sigma} = \epsilon_i\psi_{i\sigma} \quad (1.4-71)$$

$$v_\sigma^s(\vec{r}) = v_\sigma(\vec{r}) + \int d^3r' \frac{n(r')}{|\vec{r} - \vec{r}'|} + v_{xc}^\sigma(\vec{r}) \quad (1.4-72)$$

1.5 Exchange-correlation functional

As pointed out earlier the exchange energy in the Kohn-Sham theory contains the kinetic correlation. So we need to redefine the exchange-correlation energy term in Eq. (1.1-30) in the Kohn-Sham context. This can be achieved by coupling constant integration[46, 47, 48, 49, 50] method. We start with the exchange-correlation

$$E_{xc}[n] = T[n] + V_{ee}[n] - T_s[n] - U_{ee}[n] \quad (1.5-73)$$

If Ψ_n^{min} and Φ_n^{min} are the interacting and non-interacting wavefunctions that give the density $n(\vec{r})$ and deliver the minimum value of the expectation value of $\langle \hat{T} + \hat{V}_{ee} \rangle$, then we can rewrite the above equation as

$$E_{xc}[n] = \langle \Psi_n^{min} | \hat{T} + \hat{V}_{ee} | \Psi_n^{min} \rangle - \langle \Phi_n^{min} | \hat{T} | \Phi_n^{min} \rangle - U_{ee}[n] \quad (1.5-74)$$

Here we can connect the fully interacting first term and non-interacting second term by using coupling constant integration as following

$$E_{xc}[n] = \left\langle \Psi_n^{min,\lambda} \left| \hat{T} + \lambda \hat{V}_{ee} \right| \Psi_n^{min,\lambda} \right\rangle_{\lambda=1} - \left\langle \Psi_n^{min,\lambda} \left| \hat{T} + \lambda \hat{V}_{ee} \right| \Psi_n^{min,\lambda} \right\rangle_{\lambda=0} - U_{ee}[n] \quad (1.5-75)$$

$$E_{xc}[n] = \int_0^1 d\lambda \frac{d}{d\lambda} \left\langle \Psi_n^{min,\lambda} \left| \hat{T} + \lambda \hat{V}_{ee} \right| \Psi_n^{min,\lambda} \right\rangle - U_{ee}[n] \quad (1.5-76)$$

Here λ is called the coupling constant. $\Psi_n^{min,\lambda}$ is the normalized wavefunction that gives density $n(\vec{r})$ and minimizes the expectation value of $\langle \hat{T} + \hat{V}_{ee} \rangle$. $\lambda = 0$ corresponds to the non-interacting system (i.e., $\Psi_n^{min,0} = \Phi_n^{min}$) and $\lambda = 1$ corresponds to the interacting system. As λ goes from 0 to 1 the system transitions from fully non-interacting Kohn-Sham system to fully interacting real system, keeping the same ground state density. This is called adiabatic connection. Using the Hellmann-Feynman theorem

$$E_{xc}[n] = \int_0^1 d\lambda \langle \Psi^{min,\lambda} | \hat{V}_{ee} | \Psi^{min,\lambda} \rangle - U_{ee}[n] \quad (1.5-77)$$

From Eq. (1.1-26)

$$V_{ee}[n] = \frac{1}{2} \int d^3r \int d^3r' \frac{\rho_2(\vec{r}, \vec{r}')}{|\vec{r} - \vec{r}'|} \quad (1.5-78)$$

where the two-body density matrix can be written as

$$\rho_2(\vec{r}, \vec{r}') = n(\vec{r})n_2(\vec{r}, \vec{r}') \quad (1.5-79)$$

Using the definition

$$\rho_2(\vec{r}, \vec{r}') = N(N-1) \sum_{\sigma_1} \dots \sum_{\sigma_N} \int d^3r_3 \int d^3r_4 \dots \int d^3r_N |\Psi(\vec{r}, \sigma_1, \vec{r}', \sigma_2, \dots, \vec{r}_N, \sigma_N)|^2 \quad (1.5-80)$$

Integrating over \vec{r}' we get

$$\int d^3r' \rho_2(\vec{r}, \vec{r}') = (N-1)n(\vec{r}) \quad (1.5-81)$$

Using this, Eq. (1.5-79)

$$\int d^3r' n_2(\vec{r}, \vec{r}') = N-1 \quad (1.5-82)$$

If electrons were simply classical particles, $n_2(\vec{r}, \vec{r}')$ would be simply the density $n(\vec{r}')$. So, we can write

$$n_2(\vec{r}, \vec{r}') = n(\vec{r}) + n_{xc}^\lambda(\vec{r}, \vec{r}') \quad (1.5-83)$$

where $n_{xc}^\lambda(\vec{r}, \vec{r}')$ is the density of exchange-correlation hole at \vec{r}' around an electron at \vec{r} , which satisfies (using Eq. (1.5-82) and (1.5-83))

$$\int d^3r' n_{xc}^\lambda(\vec{r}, \vec{r}') = -1 \quad (1.5-84)$$

which tells if an electron is at \vec{r} it cannot be anywhere in the rest of the space. Using Eq. (1.5-77), (1.5-78), (1.5-79), (1.5-83), and (1.2-32) we obtain

$$E_{xc}[n] = \frac{1}{2} \int d^3r \int d^3r' \frac{n(\vec{r}) \bar{n}_{xc}(\vec{r}, \vec{r}')}{|\vec{r} - \vec{r}'|} \quad (1.5-85)$$

where

$$\bar{n}_{xc}(\vec{r}, \vec{r}') = \int_0^1 d\lambda n_{xc}^\lambda(\vec{r}, \vec{r}') \quad (1.5-86)$$

Eq. (1.5-85) shows that the exchange-correlation energy can be interpreted as the electrostatic interaction between the electron density and the coupling-constant averaged density of the exchange-correlation hole. If we separate the exchange and correlation contribution

$$\int d^3r' n_x(\vec{r}, \vec{r}') = -1 \quad (1.5-87)$$

and

$$\int d^3r' n_c(\vec{r}, \vec{r}') = 0 \quad (1.5-88)$$

Some other important properties:

I) Correlation energy of one-electron system[51] $E_c[n] = 0$

II) Scaling properties[52] of the exchange and correlation energy

$$E_x[n_\lambda] = \lambda E_x[n] \quad (1.5-89)$$

$$E_c[n_\lambda] > \lambda E_c[n] \quad (1.5-90)$$

$$E_c[n_\lambda] \leq \lambda E_c[n] \quad (1.5-91)$$

III) Spin-scaling relation[53]

$$E_x[n_\uparrow, n_\downarrow] = \frac{1}{2}(E_x[2n_\uparrow] + E_x[2n_\downarrow]) \quad (1.5-92)$$

IV) Lieb-Oxford bound[54]

$$E_{xc} \geq -1.679 \int d^3r n^{4/3}(\vec{r}) \quad (1.5-93)$$

V) high-density limit under uniform scaling[55]

$$\lim_{\gamma \rightarrow \infty} E_c[n_\gamma] = c \quad (1.5-94)$$

VI) Non-positivity of the exchange hole density:

$$n_x(\vec{r}, \vec{r}') \leq 0 \quad (1.5-95)$$

1.6 Approximate density functional:

Kohn-Sham theory would be an exact theory if we knew the exact form of v_{xc}^σ and hence $E_{xc}[n_\uparrow, n_\downarrow]$. If we used the exact form, supposing we have one, it would not be computationally feasible. So, we must approximate the exchange-correlation energy. Fortunately, thanks to the exact mathematical conditions of the exchange-correlation

energy, some of them discussed in the previous section, a systematic and rigorous approximation is possible. As the mathematical conditions are universal, the resulting approximations are general-purpose, unlike the empirical ones that are fitted to molecular or solid state data sets. So, the approximation of the exchange-correlation is a central challenge in the density functional theory. The exchange and correlation energies are separately approximated. The exchange energy $E_x[n]$ can be evaluated using the Kohn-Sham orbitals but involves computationally-demanding integrals. An exact form of the correlation energy $E_c[n]$, on the other hand, is unknown and so must be approximated. However, in practice, the exchange is always also approximated. It has been found that there is a cancellation of errors when we add the approximate E_x and E_c . In the following three sections we discuss the three popular density functional approximations.

1.6.1 Local spin density functional approximation:

The TF model is, in fact, a local density approximation (LDA), in which the kinetic energy density is determined solely from the local density at a point. In this approximation, we approximate the exchange and correlation energy assuming the electron density to be locally uniform. An exact expression for the exchange energy of uniform electron gas was derived by Dirac[37]. The exchange energy per electron is

$$\epsilon_x^{unif}[n] = -\frac{3}{4\pi}(3\pi^2n)^{1/3} = -\frac{0.458}{r_s} \quad (1.6-96)$$

where $r_s = (3/4\pi n)^{1/3}$ is the average distance between electrons. So in LDA[31], the exchange energy can be expressed as

$$E_x^{LDA} = \int d^3r n(\vec{r}) \epsilon_x^{unif}(n(\vec{r})) \quad (1.6-97)$$

$$E_x^{LDA} = -A \int d^3r n^{4/3}(\vec{r}) \quad (1.6-98)$$

where $A = 3/4(3/\pi)^{1/3}$. Now if we take the spin densities into account, we obtain the local spin density approximation (LSDA). We can easily get the LSDA exchange-energy using the spin-scaling relation Eq. (1.5-92).

$$n\epsilon_x^{unif}[n_\uparrow, n_\downarrow] = A\frac{1}{2}[(2n_\uparrow)^{4/3} + (2n_\downarrow)^{4/3}] \quad (1.6-99)$$

Let us define the relative spin polarization

$$\zeta = \frac{n_\uparrow - n_\downarrow}{n} \quad (1.6-100)$$

Here is the total density $n = n_\uparrow + n_\downarrow$, $2n_\uparrow = n(1 + \zeta)$, and $2n_\downarrow = n(1 - \zeta)$. With these equations (1.6-99) simplifies to

$$\epsilon_x^{unif}[n_\uparrow, n_\downarrow] = \epsilon_x^{unif}[n] + f(\zeta)[2^{1/3}\epsilon_x^{unif}[n] - \epsilon_x^{unit}[n]] \quad (1.6-101)$$

with $f(\zeta) = \frac{(1+\zeta)^{4/3} + (1-\zeta)^{4/3} - 2}{2^{4/3} - 2}$ the interpolation function that interpolates between $\zeta = 0$ (spin unpolarized) to $\zeta = 1$ (fully spin polarized). Similarly, the LSDA correlation can be expressed as

$$E_c[n_\uparrow, n_\downarrow] = \int d^3r n(\vec{r}) \epsilon_c^{unif}(r_s, \zeta) \quad (1.6-102)$$

Here ϵ_c^{unif} is known exactly only for the high-density limit ($r_s \rightarrow 0$)[56] and low-density limit ($r_s \rightarrow \infty$)[57]. Ceperley and Alder[58] calculated the correlation energy per electron at various points ($0 < r_s < \infty$) using the quantum Monte Carlo (QMC) calculation. Several parameterizations [51, 59, 60] have been proposed that interpolate between the Ceperley-Alder values and then extrapolate to the known high- and low-

density limits. In the Perdew-Zunger parameterization[51].

$$\epsilon_c^{PZ}[r_s, 0] = 0.0311 \ln r_s - 0.048 + 0.002r_s \ln r_s - 0.0116r_s \quad (1.6-103)$$

$$\epsilon_c^{PZ}[r_s, 1] = 0.01555 \ln r_s - 0.0269 + 0.0007r_s \ln r_s - 0.00486r_s \quad (1.6-104)$$

for $r_s \leq 1$, and

$$\epsilon_c^{PZ}[r_s, 0] = \frac{-0.1423}{(1 + 1.0529\sqrt{r_s} + 0.3334r_s)} \quad (1.6-105)$$

$$\epsilon_c^{PZ}[r_s, 1] = \frac{-0.0843}{(1 + 1.398\sqrt{r_s} + 0.2611r_s)} \quad (1.6-106)$$

for $r_s > 1$. For any ζ ,

$$\epsilon_c^{PZ}[r_s, \zeta] = \epsilon_c[r_s, 0] + f(\zeta)[\epsilon_c(\zeta, 1) - \epsilon_c[r_s, 0]] \quad (1.6-107)$$

By design LSDA/LDA is exact for the uniform electron gas and is expected to be accurate for very-slowly varying density. LSDA should be preferred over LDA if the system is in a spin-dependent potential or the system is spin-polarized such as open-shell atoms, magnetic materials. LSDA is more accurate than LDA because the spin-density approximation gets more input information than the spin un-polarized one. Although it is far from reality, its success is surprising. One of the reasons is the error cancellation between the exchange (which is not too negative) and correlation energy (which is too negative), which is bound to happen due to the sum rule. LSDA also satisfies other exact constraints on the exchange-correlation energy.

1.6.2 Generalized gradient approximation:

LSDA fails to capture the inhomogeneity in real systems as the local density at a point completely determines everything. In order to account for inhomogeneity, we need to consider the contribution of density from other points. In the semilocal approximation, we consider densities at two neighboring points, so we can define two inputs- density and its gradient at a point. The second order gradient expansion (GE2)[61] was an early attempt to improve upon the LSDA. Unfortunately, this works worse than LSDA. Since GE2 is an expansion to the 2^{nd} order, it cannot satisfy the exact constraint on $E_{xc}[n_{\uparrow}, n_{\downarrow}]$ that LSDA does. This led to the development of generalized gradient approximation (GGA)[62, 63, 64, 17, 65] in which the exchange-correlation energy is

$$E_{xc}^{GGA} = \int d^3r f(n_{\uparrow}, n_{\downarrow}, \nabla n_{\uparrow}, \nabla n_{\downarrow}) \quad (1.6-108)$$

It should be constructed in such a way that it recovers the 2^{nd} order gradient approximation for slowly-varying density and needs to satisfy new exact constraints of the exchange-correlation energy beside the ones LSDA satisfies. Here we briefly discuss the Perdew-Burke-Ernzerhof (PBE) [46] approximation for the exchange and correlation energy.

The exchange energy for the spin unpolarized case can be expressed as

$$E_x^{PBE}[n] = \int d^3r n(\vec{r}) \epsilon_x^{unif} F_x(s) \quad (1.6-109)$$

where ϵ_x^{unif} is the exchange energy per electron of the uniform electron gas. $F_x(s)$ is the enhancement factor. $s = |\nabla n|/[2(3\pi^2)^{1/3}n^{4/3}]$ is the dimensionless density gradient. The exchange energy for the spin polarized case is obtained by using the spin scaling relation. To construct E_x we require it to satisfy the following

I) uniform density scaling

II) uniform electron gas limit: $F_x(0) = 1$

III) LSDA linear response: as $F_x(s) \rightarrow 1 + \mu s^2$, $\mu = 0.21951$ as $s \rightarrow \infty$

IV) Lieb-Oxford lower bound: $F_x(s) \leq 1.804$ A function satisfying I, II, III, and IV can be chosen to be

$$F_x(s) = 1 + \kappa - \frac{\kappa}{1 + \mu s^2/\kappa} \quad (1.6-110)$$

where $\kappa = 0/804$ Similarly, the correlation energy can be expressed as

$$E_c^{PBE}[n_\uparrow, n_\downarrow] = \int d^3r n(\vec{r}) [\epsilon_c^{unif}(r_s, \zeta) + H(r_s, \zeta, t)] \quad (1.6-111)$$

where $t = |\nabla n|/2\phi k_s n$ is a dimensionless density gradient, k_s is the Thomas Fermi screening wave vector. $\phi(\zeta) = [(1 + \zeta)^{2/3} + (1 - \zeta)^{2/3}]/2$ is a spin scaling factor. Here $H(r_s, \zeta, t)$ has the following form

$$H(r_s, \zeta, t) = \gamma \phi^3 \ln \left[1 + \frac{\beta}{\gamma} t^2 \left(\frac{1 + At^2}{1 + At^2 + A^2 t^4} \right) \right] \quad (1.6-112)$$

with

$$A = \frac{\beta}{\gamma} [\exp(-\epsilon_c^{unif}/\gamma \phi^3) - 1]^{-1} \quad (1.6-113)$$

Here $\gamma = 0.031091$, $\beta = 0.066725$. $H(r_s, \zeta, t)$ is constructed to satisfy:

I) for slowly-varying density ($t \rightarrow 0$), $H \rightarrow \beta \phi^3 t^2$, which is the second-order gradient approximation for the slowly-varying limit.

II) for rapidly-varying density ($t \rightarrow \infty$), $H \rightarrow -\epsilon_c^{unif}$ to make the correlation energy vanish.

III) in the high-density limit ($r_s \rightarrow 0$), H cancels the logarithmic singularity of ϵ_c^{unif} , satisfying

$$\lim_{\gamma \rightarrow \infty} E[n_\gamma] = \text{constant}$$

1.6.3 Meta-generalized gradient approximation:

In meta-generalized approximation (meta-GGA), the exchange-correlation energy can be expressed as

$$E_{xc}^{MGGA}[n_{\uparrow}, n_{\downarrow}] = \int d^3r n(\vec{r}) \epsilon_{xc}(n_{\uparrow}, n_{\downarrow}, \nabla n_{\uparrow}, \nabla n_{\downarrow}, \tau_{\uparrow}, \tau_{\downarrow}) \quad (1.6-114)$$

where $\tau_{\sigma} = \frac{1}{2} \sum_i^{occu} |\nabla \psi_{i\sigma}|^2$ is the kinetic energy density of Kohn-Sham orbital of spin σ . Inclusion of τ_{σ} enables meta-GGA to recover the fourth-order gradient expansion in the slowly-varying density limit. Many meta-GGAs[66, 67, 68, 69, 70, 71, 72] have been developed, but our focus is on the recent meta-GGA “strongly constrained and appropriately normed” SCAN[72] functional. The τ dependence is made through a dimensionless variable $\alpha = \frac{\tau - \tau^w}{\tau^{unif}}$, where the Weizsäcker kinetic energy density $\tau^w = \frac{|\nabla n|^2}{8n}$, which is exact for single orbital and $\tau^{unif} = \frac{3}{10}(3\pi^2)^{2/3} n^{5/3}$ the Thomas-Fermi uniform density limit. So α can recognize different chemical bonding: $\alpha \approx 0$ (covalent single bond), $\alpha \approx 1$ (metallic bond), and $\alpha \gg 1$ (weak bonds).

The exchange energy for the spin unpolarized case is

$$E_x[n] = \int d^3r n(\vec{r}) \epsilon_x^{unif} F_x(s, \alpha) \quad (1.6-115)$$

Here the enhancement factor F_x is determined by interpolating between $\alpha = 0$ and $\alpha \approx 1$ and then extrapolating to $\alpha \rightarrow \infty$.

$$F_s(s, \alpha) = (h_x^1(s, \alpha) + f_x(\alpha)[h_x^0 - h_x^1(s, \alpha)])g_x(s) \quad (1.6-116)$$

where $h_x^0 = 1.174$, $g_x(s) = 1 - \exp[-a_1 s^{1/2}]$, $a_1 = 1.4979$. $f_x(\alpha) = \exp[-c_{1x}\alpha/(1 - \alpha)]\theta(1 - \alpha) - d_x \exp[c_{2x}/(1 - \alpha)]\theta(\alpha - 1)$ interpolates between $\alpha = 0$ and $\alpha = 1$. $c_{1x} = 0.667$, $c_{2x} = 0.8$, $d_x = 1.24$. For $\alpha \approx 1$, $F_x(s, \alpha) = h_x^1(s, \alpha)$. $h_x^1(s, \alpha)$ has the same functional form as the PBE enhancement factor but satisfies the fourth-order

gradient approximation for slowly-varying density.

$$h_x^1(s) = 1 + \kappa - \frac{\kappa}{1 + \mu s^2/\kappa} \quad (1.6-117)$$

with

$$x = \mu_{AK} s^2 [1 + (b_4 s^2 / \mu_{AK}) \exp(-|b_4| s^2 / \mu_{AK})] + [b_1 s^2 + b_2 (1 - \alpha) \exp(-b_3 (1 - \alpha)^2)]^2 \quad (1.6-118)$$

where $\mu_{AK} = 10/11$, $b_2 = (5913/405000)^{1/2}$, $b_1 = (511/13500)/2b_2$, $b_3 = 0.5$, $b_4 = \mu_{AK}/\kappa - 1606/18225 - b_1^2$, and $\kappa = 0.065$. SCAN satisfies a tighter bound $F_X \leq 1.174$ [73], whereas PBE, meta-GGA TPSS satisfy the Lieb-Oxford bound[54]. It does not have an order-of-limits problem as in TPSS[67]. The correlation energy is

$$E_c[n_\uparrow, n_\downarrow] = \int d^3r n(\vec{r}) [\epsilon_c^{unif}(r_s, \zeta, s, \alpha)] \quad (1.6-119)$$

where

$$\epsilon_c = \epsilon_c^1 + f_c^1(\alpha) [\epsilon_c^0 - \epsilon_c^1] \quad (1.6-120)$$

$$f_c(\alpha) = \exp[-c_{1c}\alpha/(1 - \alpha)]\theta(1 - \alpha) - d_c \exp[c_{2c}/(1 - \alpha)]\theta(\alpha - 1) \quad (1.6-121)$$

As for the exchange energy, it is determined by interpolating between $\alpha = 0$ and $\alpha \approx 1$ and then extrapolating to $\alpha \rightarrow \infty$. Here $c_{1c} = 0.64$, $c_{2c} = 1.5$, and $d_c = 0.7$.

The SCAN density functional has been tested for numerous properties and has been found to be superior to LSDA, GGAs, and other meta-GGAs, and in some cases as accurate as of the quantum Monte Carlo method and random phase approximation. It predicts accurate geometry and energetics, resolving the energy-geometry

dilemma of GGAs. Some of the successes of SCAN are for liquid water[74], metal surfaces[75], formation energies, liquid silicon[76], and others mentioned in ref[77]. Most notably, SCAN predicts accurate relative phase stability of the polymorphs of MnO₂[78] (a strongly correlated material), while PBE and even Hubbard-U correction fail to predict the ground-state structure. SCAN also gives accurate phase stability in 2d materials[79]. Another impressive success[80, 81] of SCAN is the accurate description of the structural, magnetic, electronic properties and the energetics of the insulating antiferromagnetic La₂CuO₄ and doped metallic La_{2-x}Sr_xCuO₄ phases; where LSDA, PBE, and the hybrid functional B3LYP do not give all these properties right. SCAN is reported to fail for some cases: vacancy formation energy[82], overmagnetisation[83, 84] in the transition metals.

1.7 Self-interaction error:

In the wave function theory, the exchange energy for orbitals $\psi_{i\sigma}$ is given by

$$E_x = -\frac{1}{2} \sum_{\sigma} \sum_{i,j} \int d^3r \int d^3r' \frac{\psi_{i\sigma}(\vec{r})\psi_{j\sigma}(\vec{r}')\psi_{j\sigma}(\vec{r})\psi_{i\sigma}(\vec{r}')}{|\vec{r} - \vec{r}'|} \quad (1.7-122)$$

Here the $i = j$ terms correspond to self-interaction. With $n_{i\sigma} = |\psi_{i\sigma}|^2$, the integral is simply the Coulomb interaction of $n_{i\sigma}$ with itself i.e. self Hartree energy $U[n_{i\sigma}]$. Thus the self-exchange and self-Hartree energy of all orbitals cancel each other, giving zero contribution to the total energy. This is also true in the density functional theory. Since, $\langle \hat{V}_{ee} \rangle = U[n] + E[n_{\uparrow}, n_{\downarrow}]$, clearly for single occupied orbital $E[n_{i\sigma}, 0] + U[n_{i\sigma}] = 0$. From this we find $E_c[n_{i\sigma} = 0]$, a constraint meta-GGA SCAN[72] satisfies. Since the exchange-correlation energy is approximated in the density functional theory perfect cancellation cannot be achieved, which leads to the self-interaction error (SIE).

Perdew and Zunger[51] in 1981 proposed the self-interaction correction (SIC) by subtracting the error ($\delta_{i\sigma} = E^{approx}[n_{i\sigma}, 0] + U[n_{i\sigma}] \neq 0$) on an orbital by orbital basis

from the total energy.

$$E_{xc}^{approx}[n_{\uparrow}, n_{\downarrow}] = E_{xc}^{approx}[n_{\uparrow}, n_{\downarrow}] - \sum_{i\sigma} (E^{approx}[n_{i\sigma}, 0] + U[n_{i\sigma}]) \quad (1.7-123)$$

which is not invariant under the unitary transformation between the occupied states. As the potential depends upon the orbital, DFT-SIC is treated under the generalized Kohn-Sham scheme[85]. The PZ-SIC theory works for atoms, small molecules. But when applied to solids the self-interaction correction vanishes. SIC varies like $v^{-\beta}$ [31], (V is volume of solid) when the Bloch function is used and so it vanishes when $V \rightarrow \infty$ leading to the size-consistency problem. This, however, can be removed if the total energy is minimized with respect to localized orbitals.

The localized orbitals can be obtained by a unitary transformation of the occupied Kohn-Sham orbitals. The Fermi-Lowdin orbital self-interaction correction (FLOSIC)[86, 87] method is an efficient way of obtaining the localized orbitals, which transforms the Kohn-Sham orbitals to the Fermi orbitals

$$F_{i\sigma} = \frac{\sum_{\alpha} \psi_{\alpha\sigma}^*(\vec{a}_{i\sigma}) \psi_{\alpha\sigma}(\vec{r})}{\sqrt{\sum_{\alpha} |\psi_{\alpha\sigma}(\vec{a}_{i\sigma})|^2}} \quad (1.7-124)$$

At $\vec{r} = \vec{a}_{i\sigma}$, $|F_{i\sigma}|^2 = \sum_{\alpha} n_{i\sigma}(\vec{a}_{i\sigma})$ showing that $F_{i\sigma}$ is a localized function. $\vec{a}_{i\sigma}$ is called a Fermi orbital descriptor (FOD). In the FLOSIC method, a set of orthonormal orbitals $\{\phi_{i\sigma}\}$ is constructed using Lowdins symmetric orthogonalization[88, 89] of the Fermi orbitals ($F_{i\sigma}$), and the energy is minimized with respect to FODs.

CHAPTER 2

ACCURATE CRITICAL PRESSURES FOR STRUCTURAL PHASE TRANSITIONS OF GROUP IV, III-V, AND II-VI COMPOUNDS FROM THE SCAN DENSITY FUNCTIONAL

Reprinted with permission from C Shahi, J Sun, JP Perdew. Accurate critical pressures for structural phase transitions of group IV, III-V, and II-VI compounds from the SCAN density functional, Phys. Rev. B 97, 094111. Copy-right (2018).

2.1 Abstract

Most of the group IV, III-V, and II-VI compounds crystallize in semiconductor structures under ambient conditions. Upon application of pressure, they undergo structural phase transitions to more closely packed structures, sometimes metallic phases. We have performed density functional calculations using projector augmented wave (PAW) pseudopotentials to determine the transition pressures for these transitions within the local density approximation (LDA), the Perdew-Burke-Ernzerhof (PBE) generalized gradient approximation (GGA), and the strongly constrained and appropriately normed (SCAN) meta-GGA. LDA underestimates the transition pressure for most of the studied materials. PBE under- or overestimates in many cases. SCAN typically corrects the errors of LDA and PBE for the transition pressure. The accuracy of SCAN is comparable to that of computationally expensive methods like

the hybrid functional HSE06, the random phase approximation (RPA), and quantum Monte Carlo (QMC), in cases where calculations with these methods have been reported, but at a more modest computational cost. The improvement from LDA to PBE to SCAN is especially clearcut and dramatic for covalent semiconductor-metal transitions, as for Si and Ge, where it reflects the increasing relative stabilization of the covalent semiconducting phases under increasing functional sophistication.

2.2 Introduction

The experimental study of pressure-induced structural phase transitions of group IV, III-V, and II-VI compounds began in the early 1960s. Much progress has been made with advances in measurement methods. However, it is quite challenging to find an accurate equilibrium transition pressure (the pressure at which both phases can coexist in equilibrium) experimentally. Hysteresis due to an energy barrier is common in a first-order phase transition, making it hard to locate the transition point. Also, the transition pressure may be sensitive to the measurement method, sample type, and non-hydrostatic stress condition.

The structural phase transition of solids also poses a considerable challenge to theoretical models. The high-pressure phases of these materials using density functional calculation within the local density approximation (LDA) have been reviewed by Mujica *et al.*[90]. LDA underestimates the transition pressure for the first transition of a series under increasing pressure. Most of the first transitions are reconstructive, and the initial phases are semiconducting. The semiconductor-metal (diamond \rightarrow β -tin) transition for Si is the most studied: Hennig *et al.*[91] have shown that LDA and GGA functionals underestimate the transition pressure. Older meta-GGAs predict a less accurate transition pressure than GGA does[92, 93]. However, the hybrid functional HSE06, the random phase approximation (RPA), and diffusion Monte Carlo (DMC) predict the transition pressure in agreement with experiment, but at an increased

computational cost. The recent meta-GGA SCAN[72], on the other hand, yields an accurate prediction for Si[77] at a GGA-like cost, suggesting that SCAN is a promising functional for the study of structural transition. In this paper, we calculate the transition pressure for group IV, III-V, and II-VI materials using SCAN as well as LDA and PBE.

The critical pressure of a structural phase transition is a sensitive test of an approximate density functional, because it depends upon a small change of total energy arising from a large change of electron density[92]. By contrast, the lattice constant for a given structure is relatively much more accurate, even in the simplest density functional approximation, because it depends upon a small change of energy arising from a small change of electron density[92].

In ground-state density functional theory (DFT)[31, 48], the density functional for the exchange-correlation energy E_{xc} is the only needed approximation. Jacob's ladder[94] is often used to order the approximate functionals, in which higher rungs are potentially more sophisticated and accurate. The first three rungs of approximations can be described by the formula

$$E_{xc}[n_{\uparrow}, n_{\downarrow}] = \int d^3r n(\vec{r}) \epsilon_{xc}(n_{\uparrow}, n_{\downarrow}, \nabla n_{\uparrow}, \nabla n_{\downarrow}, \tau_{\uparrow}, \tau_{\downarrow}) \quad (2.2-1)$$

Here $n = n_{\uparrow} + n_{\downarrow}$ is the total electron density. ∇n_{σ} is the spin-density gradient and $\tau_{\sigma} = \sum_i^{occ} \frac{1}{2} |\nabla \psi_{i,\sigma}|^2$ is the orbital kinetic density for Kohn-Sham orbitals $\psi_{i,\sigma}$ of spin σ .

Eq. (2.2-1) represents the local spin density approximation (LSDA)[31], the first rung of Jacob's ladder, if the spin densities n_{σ} are the only ingredients of the exchange-correlation energy per particle $\epsilon_{xc}(\vec{r})$. In this approximation, a general nonuniform electron gas is considered locally uniform. The exchange-correlation energy for a uniform gas is well known. Therefore the LSDA is exact for a uniform gas and accurate

for very slowly-varying spin densities. It is expected to work for simple metals, but it works better than it was expected to work for atoms and molecules, in which the electron density is far from homogeneous. Since LSDA overly favors homogeneity, it overestimates the cohesive energy of molecules and solids, and underestimates bond length and lattice constant.

The second rung of Jacob’s ladder is the generalized gradient approximation (GGA), in which spin densities and their gradients at a point are the ingredients of ε_{xc} . The Perdew-Burke-Ernzerhof (PBE) [65] is a popular GGA functional. It is constructed to satisfy 11 known exact constraints on the exchange-correlation energy functional. PBE favors inhomogeneity more than the LDA does. It underestimates the cohesive energy and overestimates the lattice constant of a solid.

The third rung of Jacob’s ladder is the meta-GGA. The “Strongly Constrained and Appropriately Normed” (SCAN)[72] functional is a new meta-GGA, designed to satisfy all 17 known exact constraints that a semilocal functional can. In SCAN, the exchange-correlation energy per particle ε_{xc} for a spin-unpolarized density depends on the orbital kinetic densities only via the dimensionless variable

$$\alpha = (\tau - \tau^w)/\tau^{\text{unif}}.$$

Here $\tau^w = |\nabla n|^2/8n$ is the von Weizsäcker kinetic energy density, which is exact for any system with a single orbital shape, and $\tau^{\text{unif}} = (3/10)(3\pi^2)^{2/3}n^{5/3}$ is the Thomas-Fermi uniform density limit. Without being fitted to any bonded system, SCAN accurately describes materials with different types of bonding: covalent (characterized by $\alpha \approx 0$ for single bonds), metallic ($\alpha \approx 1$) and weak ($\alpha \gg 1$).[71] At a computational cost at most only a few times greater than that of PBE, SCAN meets many condensed-matter challenges: ferroelectrics[95, 96], metal surfaces[75], formation energies[9], structure prediction[9], liquid water[74], and liquid silicon[76].

2.3 Computational Method

We performed density functional calculations for energy per unit cell as a function of cell volume with the VASP [97, 98] code (Vienna *ab initio* simulation package). VASP uses the projector augmented wave (PAW) method and a plane-wave basis set. Scalar relativistic effects are included via the PAW pseudopotential. For elements from the fourth row and further down the periodic table, semicore d electrons are considered as valence electrons, with the exception of Sb, Se, and Te, in which only outermost s and p electrons are considered as valence. Three levels of functional approximation were used: the Ceperley-Alder LDA [58] as parametrized by Perdew and Zunger [51], the Perdew-Burke-Ernzerhof (PBE) [65] GGA, and the SCAN [72] meta-GGA. The integration grids (k mesh) over the Brillouin zone were generated by the Γ -centered method. The total energy was converged to 1 meV per atom with respect to the energy cutoff and the k mesh. In the structural optimization, the forces on the atoms were below 0.01 eV \AA^{-1} . The kinetic energy cutoff for the plane wave expansion and the k -mesh size are provided in the Supplementary Information (see Appendix).

To calculate the transition pressure, we used the fact that the Gibbs free energies G (which reduce in our calculations to enthalpies at zero temperature) per formula unit of the two competing crystallographic phases with the same chemical formula must be equal at phase equilibrium under conditions of constant pressure and temperature. Our approach is formally equivalent to finding the equilibrium transition pressure as minus the slope of the common tangent to the binding energy curves of the two phases, but in practice our approach is numerically simpler and thus more accurate. Using the Murnaghan equation of state [99], enthalpy as a function of pressure can be expressed as

$$H(P) = E + PV = E_0 + \frac{B_0 V_0}{B'_0 - 1} \left[\left(1 + \frac{B'_0}{B_0} P \right)^{(B'_0 - 1)/B'_0} - 1 \right].$$

Here E_0 and V_0 are the equilibrium energy and volume per formula unit, while B_0 and B'_0 are the bulk modulus and pressure derivative of the bulk modulus at zero pressure. These parameters, extracted from our calculated energy as a function of cell volume for each considered solid phase and functional, are reported in the Supplementary Information, along with the fitting range for the equation of state.

2.4 Results and discussions

Our results are presented in Tables 2.1-2.3 and discussed below.

2.4.1 Si and Ge

Si and Ge crystallize in the tetrahedrally-bonded diamond structure at ambient conditions. The first high-pressure phase is a tetragonal β -tin phase. For these transitions, Gaál-Nagy *et al.* [100] have shown that the zero-point energy (ZPE) and the finite-temperature (300 K) phonon correction lower the transition pressure by 1.3 GPa.

Si undergoes this semiconductor-metal transition at 11.2-12.6 GPa [101]. With the ZPE and the finite-temperature correction [100] included, we find the transition pressure to be 5.8 GPa with LDA, 8.5 GPa with PBE, and 13.2 GPa with SCAN. LDA and PBE underestimate the transition pressure; this is in accord with previous studies [91, 93]. In fact, it was the serious underestimation [93, 92] by our earlier TPSS meta-GGA that provided the initial motivation to develop SCAN. The SCAN result is in good agreement with the experimental result. It agrees with the high-level approximations HSE06 (13.3 GPa) [92] and RPA (12.2 GPa) [92]. However, it is also important to compare the result with a more accurate method like quantum Monte Carlo (QMC). Our SCAN transition pressure is in perfect agreement with the DMC result of (14 ± 1) GPa [91]. This is because the SCAN energy difference

(417 meV/atom) is in agreement with the DMC result (424 ± 20 meV/atom). SCAN predicts an accurate energy difference of the two phases in Si because it can distinguish the covalent and metallic bonding of the low- and high-pressure phases and properly stabilize the covalent single bond.

The transition pressure for Ge is 10.6 GPa [102]. Taking ZPE and finite temperature correction[100] into account, LDA predicts a transition pressure of 5.9 GPa, PBE gives 7.5 GPa, and SCAN gives 10.1 GPa in excellent agreement with experimental results.

Table 2.1: The calculated equilibrium transition pressure (in GPa) for the group IV materials within the LDA, PBE and SCAN XC functionals. ZPE and vibrational effects are not included in the calculated value. The experimental pressure (in GPa) to the right of the vertical bar corresponds to the forward transition and the left one to the reverse transition.

	LDA	PBE	SCAN	Other works	Expt.
Si (diamond \rightarrow β -tin)	7.1	9.8	14.5	3.5 – 10[91], 12.2[92]	11.3 – 12.6[101]
Ge (diamond \rightarrow β -tin)	6.6	7.9	11.3	9.8[103]	10.6(5)[102]
Sn (β -tin \rightarrow bct)	10.3	5.4	16.2	19[104], 10.4[105]	9.5[106], 13[105], 15 – 20[107]
Pb (fcc \rightarrow hcp)	11.6	13.9	16	13[108]	14[109]
SiC (zb \rightarrow NaCl)	59.4	64.8	74	67[110]	35 100[111]

2.4.2 Sn

Tin crystallizes in the β phase (white tin) at normal temperature and pressure. On application of pressure, the β phase undergoes a transition to the body-centered tetragonal (bct) phase at about 9.5 GPa [106] at room temperature. At 0 K the transition pressure is estimated to be about 15-20 [107] or 13 GPa [105] from the measured equation of state. The calculation with LDA gives a pressure of 10.3 GPa,

close to the experimental pressure at room temperature. It also agrees with the pressure reported by Ref.[105]. However, the SCAN result (16.2 GPa) is in agreement with the experimental transition pressure of Ref. [107] at 0 K. PBE underestimates the transition pressure.

2.4.3 Pb

The tetrahedrally bonded structure is completely absent in Pb. It crystallizes in the fcc structure. It undergoes a transition to the hexagonal close-packed structure at 14 GPa [109]. LDA predicts a smaller transition pressure of 11.6 GPa, while PBE predicts 13.9 GPa, and SCAN predicts 16 GPa, in agreement with experimental results.

2.4.4 SiC

SiC undergoes a phase transition from the 3C-SiC polytype form to the NaCl (rocksalt) structure at about 100 GPa [111]. The high-pressure phase persists until 35 GPa under decompression, indicating a very large hysteresis. The predictions of LDA, PBE, and SCAN fall within the experimental error bar.

2.4.5 GaP

Gallium phosphide is a wide band-gap semiconductor. It crystallizes in the zincblende (zb) structure at ambient conditions. The high-pressure phase of GaP was initially reported to be the tetragonal β -Sn structure by x-ray diffraction experiments [112, 113]. However, Nemes *et al.* [114] showed that only a distorted Cmc₂m structure is compatible with the observed angle-dispersive x-ray (ADX) powder diffraction pattern and also with the Ruoff x-ray pattern [112], ruling out the existence of the β -tin structure. Mujica *et al.* [115] studied the high-pressure phases of GaP with a

density functional calculation within LDA. They found the coexistence pressure for the zincblende and $Cmcm$ phases as 17.7 GPa. Our calculation with LDA predicts a pressure of 18.1 GPa, low compared to the experimental value of 26 GPa [114]. PBE gives a better pressure of 20.7 GPa. SCAN predicts a transition pressure of 25.9 GPa, in excellent agreement with experimental results.

2.4.6 GaAs

GaAs is an important semiconductor for its technological uses in solar cells, semiconductor lasers, diodes, etc. At about 17 GPa, it was initially reported to undergo a phase transition from the zincblende structure to an orthorhombic structure with space group $Pmm2$ [116]. But, later the high-pressure phase was confined to be a structure having space group $Cmcm$ [117]. Theoretical study [118] on the stability of high-pressure phases of GaAs showed that the $Cmcm$ structure is indeed favored over other reported candidates like rocksalt, $Pmm2$ structure. Our calculations using LDA and PBE predict a lower pressure such as 12.4 and 14.1 GPa, respectively, low in comparison to experimental results. SCAN gives a transition pressure of 17.1 GPa, in agreement with the experimental result.

Although experiments and theoretical studies have shown that GaAs-II is the $Cmcm$ structure, a recent QMC study [119] has investigated the $zb \rightarrow NaCl$ transition. QMC predicts 17 GPa for this semiconductor-metal transition, so we have also made calculations for this transition. Both LDA (12.7 GPa) and PBE (14.6 GPa) underestimate the transition pressure, while the SCAN result (18.7 GPa) is in good agreement with the QMC value. Furthermore, our results for this transition pressure are higher than that for $zb \rightarrow Cmcm$, indicating that the $zb \rightarrow Cmcm$ transition is energetically favored over the $zb \rightarrow NaCl$ transition.

Table 2.2: The calculated equilibrium transition pressure (in GPa) for the group III-IV compounds within the LDA, PBE and SCAN XC functionals. ZPE and vibrational effects are not included in the calculated value. The experimental pressure (in GPa) to the right of the vertical bar corresponds to forward transition and the left one to reverse transition.

	LDA	PBE	SCAN	Other work	Expt.
GaP (zb→Cmcm)	18.1	20.7	25.9	17.7[115]	26[114]
GaAs (zb→Cmcm)	12.4	14.1	17.1	12.1[118]	11.2 17.3[117]
GaN (wur→NaCl)	42.3	46.2	42.1	42.5[120], 33.7[121]	30 47[122], 52.2[123], 37[124]
InN (wur→NaCl)	8.9	12.2	10.6	10[121]	12.1[123], 10[125]
AlN (wur→NaCl)	7.2	13.1	12.5	9.2[121]	0 14[126], 22[127], 20[128]
InP (zb→NaCl)	6.2	8.4	10.6	5.6[115], 7.4[129]	9.8(5)[90], 10.8(5)[130]
InAs (zb→NaCl)	4.2	6.0	7.5	3.9[115]	7.0[131],
AlP (zb→NiAs)	6.8	9.4	11.5	7.7[132]	4.8 14.2[133]
AlAs (zb→NiAs)	6.7	8.9	10.7	7[132]	2 12[134]
AlSb (zb→Cmcm)	3.7	5.1	6.6	4.7[132]	2.2 8.1[114]

2.4.7 GaN, InN, and AlN

GaN, AlN, and InN crystallize in the wurtzite structure at ambient conditions. However, they can also be modified into the zincblende structure using an epitaxial technique. The wurtzite phase has a wide band gap, so it is useful for optoelectronic devices that operate in high-frequency ranges. On application of pressure, the wurtzite phase undergoes a transition to the NaCl phase.

For AlN, the experimental phase transition has been reported to occur at 22.9 GPa by Ueno *et al.* [127], at 14 GPa by Xia *et al.*, [126] and at 20 GPa by Uehara *et al.* [128]. Xia *et al.* also observed that the high-pressure phase stays in the NaCl structure down to atmospheric pressure, indicating a large hysteresis. Our calculation with LDA gives a transition pressure of 7.2 GPa, PBE gives 13.1 GPa, and SCAN predicts 12.5 GPa. Taking the uncertainty due to the hysteresis into account, our results are close to the middle of the hysteresis cycle.

Different values for transition pressure have been reported for GaN as well. Xia *et al.* [124] using an EDX method reported 37 GPa, while Ueno *et al.* [123] (ADX method) found 52.2 GPa. Another experiment[122] reported a forward transition pressure of 47 GPa and 30 GPa upon decompression. Our calculation with LDA predicts a pressure of 42.3 GPa, PBE predicts 46.2 GPa, and SCAN predicts 42.1 GPa. All calculated pressures are in agreement with the experimental results within the reported experimental values 37 – 52.2 GPa. Interestingly, the LDA pressure is here similar to the SCAN, and RPA results (42.5 GPa) [120], and is higher than the LDA value reported by Serrano *et al.* [121].

For InN, Xia *et al.* [125] found the transition to occur at 10 GPa and the reverse transition at 5 GPa, while Ueno *et al.* [123] reported the transition pressure as 12.1 GPa. Our calculated transition pressures are 8.9 GPa (LDA), 12.2 GPa (PBE) and 10.6 GPa (SCAN), in reasonable agreement with the experimental result.

2.4.8 InP and InAs

InP and InAs crystallize in the zincblende structure at normal conditions. The first transition is from zincblende to the NaCl structure. The transition pressure for InP is 9.8 GPa [90], or 10.8 ± 0.05 GPa [130]. Our calculated pressures with LDA (6.2 GPa) and PBE (8.4 GPa) are smaller than the experimental results. SCAN predicts the transition pressure as 10.6 GPa, in good agreement with the experimental result.

The transition of InAs occurs at 7 GPa [131, 135]. LDA predicts the transition to occur at 4.2 GPa. The PBE prediction (6 GPa) is close to experiment, while the SCAN result (7.5 GPa) is in better agreement with the experimental result.

2.4.9 AlP and AlAs

AlP and AlAs crystallize in the zincblende structure at normal conditions. On application of pressure, they were found to transform to a metallic phase: the NiAs structure. The NiAs phase for AlAs was first predicted theoretically by Froyen *et al.* [136] before it was verified experimentally by Greene *et al.* [134].

For AlAs, the transition is found to occur at 12 GPa [134], while the reverse transition occurs at 2 GPa. Our calculated pressure with LDA, PBE, and SCAN are well within 2-12 GPa (Table 2.2).

The transition of AlP was reported to occur between 4.8 and 14.2 GPa [133]. The pressure with LDA is 6.8 GPa, small compared to the middle of the hysteresis interval (9.5 GPa). PBE and SCAN predict 9.4 and 11.5 GPa, respectively, and are in better agreement with experimental results.

2.4.10 AlSb

The low-pressure phase of AlSb is the zincblende structure. Different structures were assigned as the high-pressure phase until Nelmes *et al.* [114] identified it as an orthorhombic structure with space group $Cmcm$. A theoretical study of Mujica *et al.* [132] also shows that the transition to the $Cmcm$ structure is favored over the $zb \rightarrow NiAs$ transition, as in AlP and AlAs. The transition was reported to occur at 8.1 GPa [114] with a hysteresis [137]. Our calculated pressure for the $zb \rightarrow Cmcm$ transition with LDA is underestimated, while PBE and SCAN are in reasonable agreement with experimental results (Table 2.2).

2.4.11 ZnO

ZnO undergoes a transition from its low-pressure wurtzite structure to the semi-conducting NaCl structure at 9.8 GPa [138] or at 9.1 GPa [139], with a large hysteresis. Our LDA pressure (9.1 GPa) is higher than that reported by Jaffe *et al.* [140]. The LDA, PBE, and SCAN results are close to the onset of the transition on an increase of pressure. The LDA and SCAN pressures are also in agreement with the RPA result (9.18 GPa) [120].

2.4.12 ZnS

ZnS crystallizes in the zincblende structure at ambient pressure. On application of pressure, it transforms to the NaCl structure at 17.4 ± 1.2 GPa [141] or at 14.7 GPa [142]. However, a more recent experiment [143] reports the pressure as 16.9 GPa. The calculated pressures with LDA, PBE, and SCAN are within the experimental range 15 to 17.4 GPa.

2.4.13 ZnSe

ZnSe undergoes a phase transition from zincblende to the metallic NaCl structure at about 12-20 GPa [144]. Galit *et al.* [145] have reported that ZnSe undergoes a transition to a narrow-gap semiconducting phase [146], and to the metallic NaCl phase at 17 GPa. The low-pressure phase was recovered at 10.5 GPa under decompression. For the zb \rightarrow NaCl transition, our results with LDA (12.1 GPa), PBE (13.7 GPa), and SCAN (15.9 GPa) are in reasonable agreement with the experimental results.

2.4.14 ZnTe

Unlike ZnS and ZnSe, ZnTe undergoes a transition to the semiconducting trigonal cinnabar structure. The transition pressure is about 9.5 GPa [147]. Our calculations with LDA (8.7 GPa), PBE (9.7 GPa), and SCAN (10.5 GPa) are in agreement with the experimental results.

2.4.15 CdS and CdSe

Both CdS and CdSe have the wurtzite structure under normal conditions. They undergo a wurtzite to NaCl transition on the application of pressure 2-3 GPa. For CdS, the transition is reported to occur at 2.54 [154] or 3 GPa [155]. The transition pressure with LDA is 2.4 GPa, smaller than the experimental pressure. PBE predicts a higher transition pressure. SCAN is in excellent agreement with the experimental results.

For CdSe, the transition pressure is 2.72 GPa [156]. The calculated pressure with LDA is 2.3 GPa. PBE predicts a higher pressure, while the SCAN result (3.2 GPa)

Table 2.3: The calculated equilibrium transition pressure (in GPa) for the group II-VI materials within the LDA, PBE and SCAN XC functionals. ZPE and vibrational effects are not included in the calculated value. The experimental pressure (in GPa) to the right of the vertical bar corresponds to the forward transition and the left one to the reverse transition

	LDA	PBE	SCAN	Other work	Expt.
ZnO (wur→NaCl)	9.1	11.6	8.8	6.6[140], 9.3[140], 9.18[120]	1.9(2) 9.1(2)[139], 9.8[138]
ZnS (zb→NaCl)	15.2	16.8	18.3	14.35[148], 15.4[149], 17.2[150]	10 14.7[151], 17.4[141], 16.9[143]
ZnSe (zb→NaCl)	12.1	13.7	15.9	15.2[144, 145], 11[152], 14.7[150]	12 – 20[144, 145]
ZnTe (zb→cinn)	8.7	9.7	10.5	10.3[150]	8 9.5[147]
CdS (wur→NaCl)	2.4	4.4	2.9	3.1[153]	1.2 2.54[154], 3[155]
CdSe (wur→NaCl)	2.4	4.1	3.3	2.5[152]	1.7 2.72[156]
CdTe (zb→cinn)	3.8	4.8	4.2	2.5[152]	2.67 3.53[157], 3.8[158]
HgS (cinn→NaCl)	11.1	15.8	21.9	26.57[159]	20.5(7)[160]
HgSe (cinn→NaCl)	6.7	10.4	15.8	7[161], 11.5[161]	14.6(6)[162], 15.5[163]
HgTe (cinn→NaCl)	2.3	5.2	6.6	2.5[161], 6.5[161]	8[164, 163]

is in excellent agreement with the experimental results.

2.4.16 CdTe

Although there was an initial report of a $zb \rightarrow NaCl$ transition at 3.53 GPa [157], Nelmes *et al.* [165] found an intermediate trigonal cinnabar phase with a transition pressure at 3.5 GPa. Using the electrical resistivity method, a recent experiment reports the transition pressure as 3.8 GPa [158]. The calculated pressures with LDA, PBE, and SCAN are in reasonably good agreement with the experimental results.

2.4.17 HgS

HgS crystallizes in the cinnabar structure at normal conditions. On application of pressure, it undergoes a structural transition to the NaCl structure at 20.5 GPa [160]. Both LDA and PBE underestimate the transition pressure, while SCAN is in

excellent agreement with the experimental results.

2.4.18 HgSe and HgTe

A theoretical study[161] by Mujica *et al.* has shown that LDA and PBE work well for the first transition (zb to cinn), and underestimate pressure for the cinn to NaCl transition. Our LDA and PBE results (except PBE result for HgTe, which is smaller in our case) agree with their results. SCAN is in better agreement with the experimental results.

2.4.19 Overall Analysis

Figure 2.1 and Table 2.4 compare the predictions of the XC functionals LDA, PBE, and SCAN to experimental results. Except for a few materials, LDA underestimates the coexistence pressure, in agreement with the conclusions of Mujica *et al.* [90]. PBE improves upon the LDA prediction, but it still underestimates the pressure in many cases and overestimates in a few. On the other hand, SCAN predictions are in good agreement with the experimental transition pressures.

Table 2.4: The mean percentage error (MPE) and mean absolute percentage error (MAPE) for XC functionals LDA, PBE, and SCAN. The experimental reference value is \bar{P}_e , as defined in the caption of Fig. 1.

	LDA	PBE	SCAN
MPE	-30.92	-10.17	0.36
MAPE	31.14	24.54	11.78

The predictive power of density functionals in the present context depends upon how well they capture the energy difference of the two phases. The systematic underestimation by LDA can be understood by the fact that it favors homogeneity. Since the high-pressure phases are more closely packed structures, their electron density is

somewhat more homogeneous. As a result, LDA works better for the high-pressure phase than it does for the low-pressure phase, thereby underestimating the true energy difference. The better PBE results are due to an improved energy difference. PBE lowers the total energy of the more inhomogeneous phase more and thus increases the difference. The ability of SCAN to predict an accurate transition pressure is due to its better description of diverse kinds of bonding, including the covalent bonding in diamond-structure Si and Ge. It has been argued that the inaccurate prediction of transition pressure by semilocal functionals is due to their inaccurate description of the band gap. The HSE06 functional gives the correct transition pressure for the diamond to β -tin transition for silicon, and also gives an accurate band gap. However, our calculation shows that SCAN gives an accurate transition pressure although it only partly improves the band gap [96], calling the relevance of the gap into question.

It is important to remark that we have neglected the zero-point motion of ions and the effect of temperature in our calculations. Most of the experimental pressures are measured at room temperature, whereas the calculated pressures correspond to 0 K. This makes the comparison of the experiment and theory difficult. However, in the case of Si and Ge, inclusion of these effects makes the performance of SCAN even better. The temperature dependence [105, 107] in the case of Sn explains in part the apparent overestimation of the pressure within SCAN. We expect the agreement between experiment and the SCAN results to be good for other materials as well.

Hysteresis can also be a major issue in the comparison. The kinetic barrier between two coexisting phase often hinders the transition, leading to the hysteresis. This makes it hard to locate the true equilibrium transition point experimentally. The middle of the hysteresis cycle is sometimes taken as an estimate of the equilibrium transition pressure, and half the width of the cycle as its uncertainty.

Because of all these uncertainties, our fixed-nucleus equilibrium transition pressures can be more cleanly compared to those of a fifth-rung density functional, the

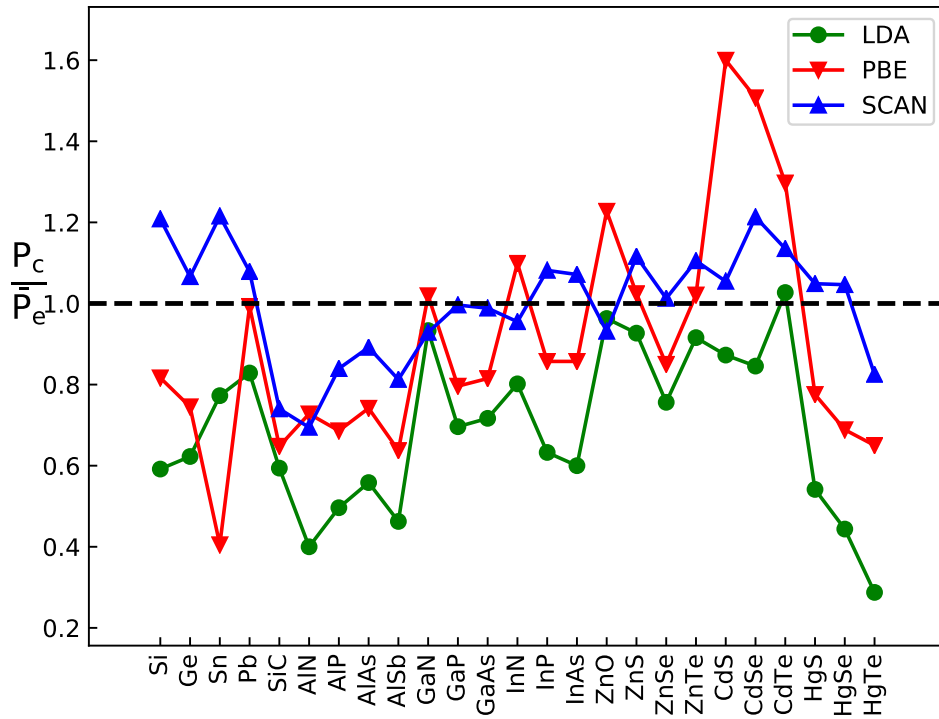


Figure 2.1: Ratio of the calculated transition pressure P_c and the experimental pressure \bar{P}_e . \bar{P}_e is the average of all experimental forward pressures (from Tables 2.1-2.3). An accurate functional might make this ratio less than or about equal to 1, in view of hysteresis, uncertainty, and vibrational effects in the experiments. Reverse pressures have been measured for only 13 out of the 25 materials.

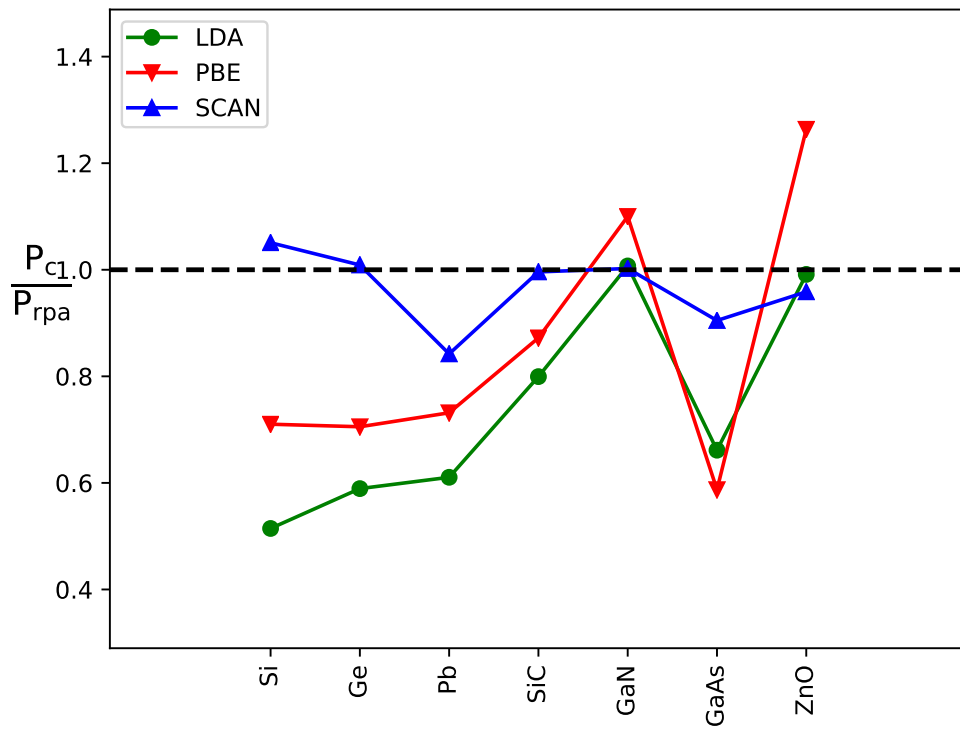


Figure 2.2: Comparison of the calculated transition pressure P_c with the RPA transition pressure P_{rpa} .

random phase approximation or RPA in a density functional context [166], also implemented for calculation of the equilibrium transition pressure at fixed nuclear positions. Figure 2 shows this comparison for our seven materials for which an RPA transition pressure is known [167, 120] and suggests an almost systematic improvement as we climb the ladder from LDA to PBE to SCAN to RPA. For isoelectronic energy differences [74, 167, 168, 169, 170] in condensed matter, for which RPA is typically accurate, SCAN results are often close to those of the expensive RPA. For the materials where QMC equilibrium transition pressures are known, SCAN is close to QMC (with a 6% difference for Si diamond \rightarrow β -tin and 10% for GaAs zb \rightarrow NaCl).

The clearest and most dramatic message from Fig. 2 is the great improvement from LDA to PBE to SCAN for the equilibrium transition pressures of the covalent semiconductor-metal transitions (e.g., Si and Ge), due to an increasing relative stabilization of the covalent semiconducting phase under increasing functional sophistication. Specifically, the PBE enhancement factor over LDA exchange increases above one as the magnitude of the local density gradient increases, stabilizing the more inhomogeneous phase. The SCAN enhancement factor over LDA exchange is greater than one even at bond centers where the density gradient is zero, so long as the variable α defined in Sec. I is close to zero there, and this further stabilizes covalent bonds. In contrast, “GGAs for solids”, such as AM05 [171] and PBEsol [172], yield better lattice constants and bulk moduli than LDA or PBE, and better surface energies [75] than PBE, but can be worse [91] than both for the transition pressure in Si.

PBE includes almost no van der Waals (vdW) attraction, AM05 and PBEsol provide an intermediate-range vdW correction to PBE, which as expected stabilizes preferentially the higher density phase and so reduces the transition pressure. While SCAN includes intermediate-range vdW [77, 75], it also includes other effects (i.e., recognizes different chemical environments characterized by different chemical bonds)

which raise the transition pressure in 19 of the 25 cases studied here.

Just as SCAN halves the PBE mean absolute error for the transition pressures in Table 2.4, it does the same [9, 173] for the formation energies of solids and for their predicted ground-state crystal structures. In a recent and very extensive test for main-group molecules [174] the non empirical SCAN outperformed all other tested meta-GGAs, including those heavily fitted to molecular data. Molecules have much in common with semiconductors.

2.5 Conclusions

We have investigated the performance of the nonempirical, general-purpose, semilocal density functionals LDA, PBE, and SCAN for the first structural phase transitions of 25 group IV, III-V, and II-VI compounds. LDA underestimates the transition pressures, while PBE can under- or overestimate. SCAN provides a systematic improvement over LDA and PBE, and its predictions are in reasonable agreement with experimental results. For those materials where a comparison can be made, SCAN yields transition pressures as good as computationally more expensive methods like the hybrid functional HSE06, RPA, and QMC. We conclude that SCAN is a usefully accurate and efficient method for predicting transition pressures in these and probably other solids. For tests on some other solids, see Ref.[167].

2.6 Acknowledgements

We thank Haowei Peng, Jefferson E. Bates, Christopher R. Spano, Yubo Zhang, Abhirup Patra, Niraj Nepal, Niladri Sengupta for their help during calculations. This work was supported by National Science Foundation under Grant No. DMR-1607868. This research was supported in part by the National Science Foundation through major research instrumentation Grant No. CNS-09-58854. J.S. acknowledges the

support from the Center for Computational Design of Functional Layered Materials, an Energy Frontier Research Center funded by the US Department of Energy (DOE), Office of Science, Basic Energy Sciences (BES) under Award No. DE-SC0012575. The figures were generated by MATPLOTLIB [175]. AFLOW software [176] was used to create the primitive cell.

C.S., J.S., and J.P.P. designed the project and wrote the paper, while C.S. performed all the calculations.

Supporting information

Following are the tables containing the fit parameters for the energy-volume curve using the Murnaghan equation of state, and the input parameters for energy calculation. For SCAN, we used more plane waves than we were probably needed. For the structures having free structural parameters, we carried out a full geometry optimization, that is, for a given volume, we found the cell shape and the atomic positions that minimize the energy. However, for LDA, PBE, and SCAN, we were able to optimize only the atomic positions for the Cmc₂m phase of AlSb and GaAs, employing the experimental orthorhombic cell shape, Ref.[112], with fixed axial ratios. For GaP, where the full geometry optimization was possible, we found that this partial optimization did not affect the calculated transition pressure. In the energy-volume calculation, the volume range we considered is $0.9 \lesssim V/V_0 \lesssim 1.1$. For Sn, we could find good fits only in the range $0.95 \lesssim V/V_0 \lesssim 1.06$.

Table 2.5: The calculated equilibrium energy E_0 (in eV) and volume V_0 (in \AA^3) per formula unit and the bulk modulus B_0 (in GPa) and its pressure derivative B'_0 for XC functionals SCAN, PBE, and LDA. The equilibrium energy of the low-pressure phase has been set to zero and that of the high-pressure phase to the energy difference. Only the structural change in E_0 from a PAW code is physically meaningful.

		SCAN				PBE				LDA			
		E_0	V_0	B_0	B'_0	E_0	V_0	B_0	B'_0	E_0	V_0	B_0	B'_0
Si	diamond	0.000	19.99	98.9	4.1	0.000	20.45	88.4	4.2	0.000	19.71	96.1	4.2
	β -tin	0.417	14.97	114.2	5.0	0.291	15.34	106.1	4.6	0.208	14.82	115.8	4.4
Ge	diamond	0.000	22.66	71.0	4.2	0.000	23.89	58.5	4.9	0.000	22.25	71.8	4.7
	β -tin	0.267	18.53	77.1	4.9	0.231	19.32	67.6	4.6	0.181	17.95	83.2	4.5
Sn	β -tin	0.000	27.44	51.4	6.1	0.000	28.4	47.6	4.9	0.000	26.19	59.9	4.7
	bct	0.109	27.07	46.7	3.2	0.022	27.81	45.7	4.6	0.040	25.62	57.0	4.8
Pb	fcc	0.000	30.68	45.5	4.6	0.000	32.01	39.7	4.7	0.000	29.13	52.1	4.8
	hcp	0.017	30.51	44.9	4.6	0.017	31.88	39.3	4.4	0.012	28.95	51.9	4.9
SiC	zb	0.000	20.6	225.4	3.9	0.000	20.99	211.8	3.9	0.000	20.31	228.1	3.9
	NaCl	1.639	16.28	266.0	5.0	1.485	16.71	242.9	3.8	1.340	16.12	263.2	4.2
AlN	wur	0.000	20.7	212.0	3.8	0.000	21.28	192.7	3.9	0.000	20.48	210.5	3.9
	NaCl	0.323	16.36	278.1	3.8	0.345	16.85	251.5	4.1	0.190	16.17	276.5	3.9
AlP	zb	0.000	40.83	91.3	4.0	0.000	41.73	82.4	4.2	0.000	40.14	89.9	4.1
	NiAs	0.600	31.72	113.8	4.2	0.501	32.46	103.7	4.3	0.357	31.2	113.3	4.2
AlAs	zb	0.000	45.55	75.8	4.2	0.000	46.97	66.7	4.3	0.000	44.67	75.1	4.2
	NiAs	0.595	35.93	91.8	4.4	0.497	37.13	82.0	4.4	0.370	35.26	92.9	4.3
AlSb	zb	0.000	58.8	56.2	4.4	0.000	60.53	49.3	4.5	0.000	57.33	56.5	4.4
	Cmcm	0.492	45.96	60.5	4.7	0.399	47.29	54.0	4.7	0.276	44.71	63.3	5.1
GaN	wur	0.000	22.94	198.8	3.7	0.000	23.47	169.5	4.4	0.000	22.18	200.8	4.3
	NaCl	0.931	18.82	252.5	3.6	0.963	19.47	207.5	4.7	0.877	18.35	248.0	4.6
GaP	zb	0.000	40.49	86.5	4.2	0.000	41.77	74.6	4.3	0.000	39.24	89.7	4.3
	Cmcm	0.982	33.33	99.7	4.1	0.813	34.37	86.9	4.7	0.694	32.26	104.1	4.6

Table 2.6: The calculated equilibrium energy E_0 (in eV) and volume V_0 (in \AA^3) per formula unit and the bulk modulus B_0 (in GPa) and its pressure derivative B'_0 for XC functionals SCAN, PBE, and LDA. The equilibrium energy of the low-pressure phase has been set to zero and that of the high-pressure phase to the energy difference. Only the structural change in E_0 from a PAW code is physically meaningful.

		SCAN				PBE				LDA			
		E_0	V_0	B_0	B'_0	E_0	V_0	B_0	B'_0	E_0	V_0	B_0	B'_0
GaAs	zb	0.000	45.58	70.7	4.1	0.000	47.52	59.0	4.5	0.000	44.11	74.2	4.5
	Cmcm	0.783	37.66	65.5	4.7	0.662	39.24	58.7	5.3	0.565	36.25	76.9	4.5
InN	wur	0.000	31.2	138.1	4.4	0.000	32.22	120.3	4.6	0.000	30.2	145.0	4.5
	NaCl	0.364	25.3	181.7	4.7	0.427	26.12	156.1	4.8	0.299	24.52	191.1	4.7
InP	zb	0.000	51.19	68.7	4.3	0.000	52.92	59.0	4.7	0.000	49.52	70.7	4.6
	NaCl	0.580	41.39	82.8	4.8	0.493	42.5	73.1	4.9	0.356	39.77	88.9	4.7
InAs	zb	0.000	56.8	56.7	4.8	0.000	59.25	48.1	4.8	0.000	54.86	59.8	4.7
	NaCl	0.468	45.87	70.2	4.9	0.401	47.59	60.6	4.8	0.268	44.04	76.1	4.8
ZnO	wur	0.000	23.63	150.3	4.8	0.000	24.86	128.0	4.4	0.000	22.86	160.2	4.5
	NaCl	0.221	19.39	195.7	4.9	0.296	20.43	165.0	4.5	0.216	18.85	206.5	4.5
ZnS	zb	0.000	38.74	79.1	5.3	0.000	40.47	68.9	4.4	0.000	37.32	85.9	4.4
	NaCl	0.659	32.22	99.3	3.4	0.637	33.32	85.9	4.5	0.547	30.76	107.0	4.4
ZnSe	zb	0.000	45	67.6	4.9	0.000	47.29	56.3	4.5	0.000	43.37	71.0	4.5
	NaCl	0.667	37.32	81.2	4.7	0.614	38.78	70.0	4.6	0.518	35.61	89.2	4.6
ZnTe	zb	0.000	56.26	50.3	4.5	0.000	59.1	43.0	4.6	0.000	54.09	55.1	4.6
	cinn	0.305	50.95	54.5	4.7	0.303	53.35	46.8	4.7	0.259	48.77	60.6	4.6
CdS	wur	0.000	50.64	60.7	4.4	0.000	52.38	52.8	4.6	0.000	48.15	67.3	4.6
	NaCl	0.181	40.61	83.3	4.4	0.273	41.72	71.7	4.7	0.141	38.4	92.0	4.7
CdSe	wur	0.000	57.52	51.6	4.5	0.000	59.86	44.3	4.7	0.000	54.7	57.2	4.6
	NaCl	0.224	45.96	69.7	4.8	0.294	47.46	59.8	4.8	0.160	43.43	78.2	4.8
CdTe	zb	0.000	69.79	40.4	4.6	0.000	72.69	34.9	4.7	0.000	66.2	45.8	4.7
	cinn	0.183	62.26	45.0	4.3	0.214	64.72	38.7	4.8	0.161	58.85	51.3	4.8
HgS	cinn	0.000	51.04	16.3	7.0	0.000	56.13	7.1	8.1	0.000	43.88	37.5	8.6
	NaCl	0.396	41.88	76.6	5.0	0.359	43.42	65.9	5.1	0.168	39.75	89.6	5.0
HgSe	cinn	0.000	56.7	14.4	7.4	0.000	59.85	7.2	10.2	0.000	48.54	40.2	6.4
	NaCl	0.354	46.87	66.5	5.0	0.262	48.92	56.7	5.2	0.109	44.6	78.8	5.1
HgTe	cinn	0.000	65.44	11.5	9.2	0.000	67.46	10.4	13.5	0.000	57.56	34.4	3.3
	NaCl	0.243	54.25	56.1	5.9	0.185	58.07	46.0	5.4	0.054	52.85	65.4	5.3

Table 2.7: The kinetic energy cutoff and the k-mesh size. The cutoffs used here for SCAN are un-necessarily large. VASP recommends setting the cutoff for the energy-volume calculation to 1.3 times the default cutoff. We have found the same SCAN transition pressure for Si with 440 eV as with 720 eV. For fine energy differences, we believe that 520 eV, as used in Ref.[9], should be safe.

		SCAN		PBE and LDA	
		k-mesh	encut(eV)	k-mesh	encut (eV)
Si	diamond	12x12x12	720	12x12x12	440
	β -tin	20x27x20	720	18x25x18	440
Ge	diamond	12x12x12	720	12x12x12	440
	β -tin	22x16x16	720	22x16x16	440
Sn	β -tin	16x16x30	560	16x16x30	440
	bct	16x16x19	560	16x16x19	440
Pb	fcc	20x20x20	600	20x20x20	440
	hcp	18x18x11	600	18x18x11	440
SiC	zb	6x6x6	720	6x6x6	600
	NaCl	11x11x11	720	11x11x11	600
AlN	wur	8x8x4	800	8x8x4	600
	NaCl	18x18x18	800	18x18x18	600
AlP	zb	12x12x12	800	12x12x12	480
	NiAs	16x16x10	800	16x16x10	480
AlAs	zb	14x14x14	720	14x14x14	440
	NiAs	16x16x10	720	16x16x10	440
AlSb	zb	14x14x14	600	8x8x8	440
	Cmcm	12x11x13	600	12x11x13	440
GaN	wur	10x10x6	640	10x10x6	640
	NaCl	16x16x16	640	16x16x16	640
GaP	zb	8x8x8	600	8x8x8	440
	Cmcm	12x12x12	600	12x12x12	440
GaAs	zb	8x8x8	600	8x8x8	440
	Cmcm	12x11x13	600	12x11x13	440

Table 2.8: The kinetic energy cutoff and the k-mesh size. The cutoffs used here for SCAN are un-necessarily large. VASP recommends setting the cutoff for the energy-volume calculation to 1.3 times the default cutoff. We have found the same SCAN transition pressure for InAs with 440 eV as with 700 eV. For fine energy differences, we believe that 520 eV, as used in Ref.[9], should be safe.

		SCAN		PBE and LDA	
		k-mesh	encut(eV)	k-mesh	encut (eV)
InN	wur	10x10x5	700	10x10x5	640
	NaCl	12x12x12	700	14x14x14	640
InP	zb	12x12x12	680	12x12x12	440
	NaCl	20x20x20	680	18x18x18	440
InAs	zb	12x12x12	700	12x12x12	440
	NaCl	18x18x18	700	18x18x18	440
ZnO	wur	10x10x6	680	10x10x6	680
	NaCl	16x16x16	680	16x16x16	680
ZnS	zb	12x12x12	720	12x12x12	600
	NaCl	16x16x16	720	16x16x16	600
ZnSe	zb	12x12x12	720	12x12x12	480
	NaCl	16x16x16	720	16x16x16	480
ZnTe	zb	12x12x12	720	12x12x12	480
	cinn	10x10x5	720	10x10x5	480
CdS	wur	10x10x6	720	10x10x6	520
	NaCl	14x14x14	720	14x14x14	520
CdSe	wur	10x10x6	720	10x10x6	480
	NaCl	16x16x16	720	16x16x16	480
CdTe	zb	12x12x12	720	12x12x12	480
	cinn	10x10x4	720	12x12x5	480
HgS	cinn	8x8x4	720	8x8x4	560
	NaCl	16x16x16	720	16x16x16	560
HgSe	cinn	8x8x4	600	8x8x4	440
	NaCl	20x20x20	600	20x20x20	440
HgTe	cinn	8x8x4	600	8x8x4	480
	NaCl	18x18x18	600	18x18x18	480

CHAPTER 3

STRETCHED OR NODDED ORBITAL DENSITIES AND SELF-INTERACTION CORRECTION IN DENSITY FUNCTIONAL THEORY

Reprinted with permission from C Shahi, P Bhattarai, K Wagle, B Santra, S Schwalbe, T Hahn, J Kortus, KA Jackson, JE Peralta, K Trepte, S Lehtola, NK Nepal, H Myneni, B Neupane, S Adhikari, A Ruzsinszky, Y Yamamoto, T Baruah, RR Zope, and JP Perdew. J. Chem. Phys. 150, 174102 Copy-right (2019).

3.1 Abstract

Semilocal approximations to the density functional for the exchange-correlation energy of a many-electron system necessarily fail for lobed one-electron densities, including not only the familiar stretched densities but also the less familiar but closely related noded ones. The Perdew-Zunger (PZ) self-interaction correction (SIC) to a semilocal approximation makes that approximation exact for all one-electron ground- or excited-state densities and accurate for stretched bonds. When the minimization of the PZ total energy is made over real localized orbitals, the orbital densities can be noded, leading to energy errors in many-electron systems. Minimization over complex localized orbitals yields nodeless orbital densities, which reduce but typically do not eliminate the SIC errors of atomization energies. Other errors of PZ

SIC remain, attributable to the loss of the exact constraints and appropriate norms that the semilocal approximations satisfy, suggesting the need for a generalized SIC. These conclusions are supported by calculations for one-electron densities and for many-electron molecules. While PZ SIC raises and improves the energy barriers of standard generalized gradient approximations (GGAs) and meta-GGAs, it reduces and often worsens the atomization energies of molecules. Thus, PZ SIC raises the energy more as the nodality of the valence localized orbitals increases from atoms to molecules to transition states. PZ SIC is applied here, in particular, to the strongly constrained and appropriately normed (SCAN) meta-GGA, for which the correlation part is already self-interaction-free. This property makes SCAN a natural first candidate for a generalized SIC.

3.2 Introduction: Semilocal Approximation and Self-Interaction Correction

Kohn-Sham density functional theory[31, 177] simplifies the many-electron ground-state problem of condensed-matter physics or quantum chemistry to a self-consistent one-electron form, in a way that is formally exact for the total energy and electron density. To make this theory tractable and widely useful, an approximation (typically a computationally efficient semilocal one) must be made to the exact density functional for the exchange-correlation energy, the many-body glue that binds atoms to form molecules and solids.

A semilocal approximation expresses this energy as a single integral over three-dimensional space of a function of various ingredients that are available from the solution of the self-consistent one-electron Schrödinger equation. The local spin density approximation (LSDA)[31, 60] uses only the local electron spin densities as ingredients, the generalized gradient approximation (GGA) adds their gradients, and the

meta-GGA further adds the positive spin-resolved orbital kinetic energy densities.

$$E_{xc}^{approx}[n_{\uparrow}, n_{\downarrow}] = \int d\mathbf{r} n(\mathbf{r}) \epsilon_{xc}^{approx}(n_{\uparrow}, n_{\downarrow}, \nabla n_{\uparrow}, \nabla n_{\downarrow}, \tau_{\uparrow}, \tau_{\downarrow}) \quad (3.2-1)$$

Square brackets in Eq. (3.2-1) indicate a functional, and round brackets indicate a function. The total electron density $n(r) = n_{\uparrow}(r) + n_{\downarrow}(r)$ is the sum of up- and down-spin contributions.

The integrand of Eq. (3.2-1) can be constructed empirically by fitting to molecular data or in a more first-principles way by satisfying known exact constraints and appropriate norms. Within a semilocal form, many but not all exact constraints or mathematical properties of the exact functional can be satisfied for all possible electron densities by the careful design of the integrand. The uniform electron gas [60] is an appropriate norm for the LSDA, for the Perdew-Burke-Ernzerhof (PBE) GGA [65] and for the strongly constrained and appropriately normed (SCAN) meta-GGA [72] that will be considered here. Free atoms (but not molecules) provide other appropriate norms for SCAN, which further satisfies all 17 known exact constraints that a semilocal form can satisfy. All three ingredients n_{σ} , $|\nabla n_{\sigma}|$, τ_{σ} in Eq. (3.2-1) are needed to recognize one- and two-electron regions for which there are special constraints (e.g., the correlation energy vanishes for any one-electron density). However, once a meta-GGA has been constructed, it is possible if desired to approximate n_{σ} in terms of n_{σ} , $|\nabla n_{\sigma}|$, $\nabla^2 n_{\sigma}$. [178].

Recent successes, e.g., Refs [77, 179, 180, 74, 9, 181], suggest that SCAN maybe approaching the limiting accuracy of semilocal functionals. It may be time to satisfy more exact constraints via fully non-local functionals. Semilocal spin-density functionals cannot be exact for all one-electron (fully spin-polarized) densities n , for which the exact spin-density functional for the exchange-correlation energy must ex-

actly cancel the fully nonlocal Hartree electrostatic energy

$$U[n] = \frac{1}{2} \int d\mathbf{r} n(\vec{r}) \int d\mathbf{r}' n(\vec{r}') / |\vec{r} - \vec{r}'| \quad (3.2-2)$$

For a one-electron density, all of the $U[n]$ term in the total energy is a spurious self-interaction. The residual self-interaction error of a semilocal functional for a one-electron density, due to an imperfect cancellation of $U[n]$ by the semilocal exchange-correlation energy, manifests in serious errors for stretched bonds that can arise in binding energy curves (e.g., for H_2^+ , [182, 183] as shown in Fig. 3.1), charge transfers, [184] energies of transition states for chemical reactions, [185] and in other ways.

In 1981, Perdew and Zunger [51] proposed a self-interaction correction (SIC) to any spin-density functional approximation

$$E_{xc}^{approx-SIC} = E_{xc}^{approx}[n_{\uparrow}, n_{\downarrow}] - \sum_{i\sigma}^{occup} \{U[n_{i\sigma}] + E_{xc}^{approx}[n_{i\sigma}, 0]\} \quad (3.2-3)$$

Here, $n_{i\sigma}(r)$ is the i th occupied orbital density of spin σ and, thus, a one-electron density. The resulting fully nonlocal functional is exact for any collection of separated one-electron densities, and the Perdew-Zunger (PZ) correction to the exact functional vanishes.

PZ SIC was an early attempt to improve approximate functionals via constraint satisfaction and was proposed without much concern that satisfying an additional constraint or norm (exactness for all one-electron densities) might violate preexisting constraints or norms (such as exactness for all uniform electron gases and 0% error for the exchange-correlation energies of neutral atoms in the limit of large atomic number [18]). A recent study [186] suggests that the SIC errors for these norms are not negligible.

When PZ SIC was proposed, LSDA was almost the only available density func-

tional approximation for exchange and correlation. LSDA is not very accurate for the compact one- and two-electron hydrogen and helium atoms, and those errors are corrected by PZ SIC. The later GGAs and meta-GGAs also largely correct those errors, but they continue to make self-interaction errors for electron transfer and for the lobed one-electron densities that will be discussed in Sec. 3.3.

The occupied orbital densities $n_{i\sigma}$ in Eq. (3.2-3) are not the squares of the occupied Kohn-Sham orbitals, which can be delocalized. To make SIC size-extensive, they should be the squares of unitarily equivalent occupied localized orbitals. This was discussed in Ref.[51], but implemented to minimize the SIC energy by Pederson, Heaton, and Lin,[187] enabling the first SIC calculations for molecules. The recently proposed Fermi-Lowdin orbitals,[86] which are guaranteed to be localized, correspond to a particular set of real unitary transformations. Without such a restriction on the unitary transformation, delocalized orbitals that violate size-extensivity can be obtained when the underlying functional has a positive self-interaction correction from any localized orbital. This is unlikely for atoms and molecules in LSDA-SIC, but it can happen for PBE-SIC or SCAN-SIC, where the underlying functional is more accurate for compact one-electron densities.

In the absence of an external magnetic field or a spin-orbit interaction, the Kohn-Sham orbitals are usually chosen to be real (although complex Kohn-Sham orbitals may bring some benefits for orbital functionals[188]). Thus, it was long assumed that the localized orbitals should also be real. Real orbitals that overlap one another must have nodes to ensure mutual orthogonality. Vydrov and Scuseria[189] showed that PZ SIC with real localized orbitals, applied to PBE, worsens the description of equilibrium (unstretched) bonds and that conclusion is supported by later studies.[190, 191, 192, 15] It has been suspected that noded localized orbitals limit the accuracy of PBE-SIC.[193] In 2011, Klmpfel, Klmpfel, and Jansson[16] found that complex localized orbitals with nodeless orbital densities improve the accura-

cy of PBE-SIC over real ones. (While the real and imaginary parts of an orbital may have nodal surfaces, these surfaces can be different, leading to nodeless orbital densities.[16, 194]) Complex localized orbitals have also been found[190] to reduce but not eliminate PZ SIC symmetry-breaking in molecules. One argument[16] for their better performance is that introducing complex localized orbitals increases variational freedom and produces lower and more realistic PBE-SIC total energies. References [190] and[16] found that complex orbitals yield lower energies than real ones for most systems. The problems that noded orbitals pose for semilocal functionals were also discussed in Refs.[193] and [194]. Hofmann, Klmpfel, Klmpfel, and Kmmel[194] say that The smoother orbital densities without nodal planes are much closer to the realm where (semi) local functionals are considered to be appropriate.

Here, we will argue that semilocal approximations must fail for noded orbital densities for the same fundamental reason and in the same way that they must fail for stretched orbital densities. Perhaps the best-known failures of semilocal functionals occur for stretched orbital densities. In applications to ground states, the stretched orbitals are problematic for semilocal functionals, while the noded orbitals are problematic only for SIC functionals.

PZ SIC with real localized orbitals does indeed correct errors for stretched bonds, as shown in Fig. 3.1, but when applied to a semilocal functional, it introduces other errors arising from the nodes of the orbital densities. The density-nodality error of PZ SIC is absent from uncorrected semilocal functionals applied to ground-state total densities, which are always nodeless for real systems. The most problematic ground states for the semilocal functionals are those of stretched radicals, such as H_2^+ , He^+ , and transition states of chemical reactions. Large errors in the total energies from semilocal approximations would also occur for strongly stretched H_2 and N_2 if spin symmetry were not allowed to break.

It is well-known that the exact Kohn-Sham theory is exact for ground-state en-

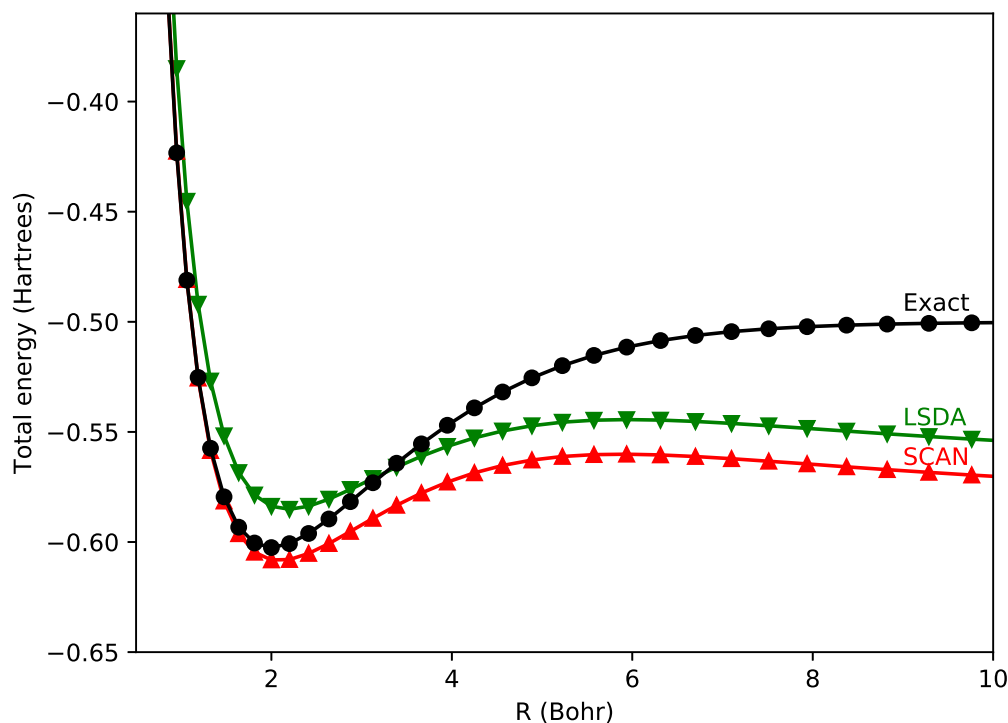


Figure 3.1: Binding energy curves: exact (or equivalently SIC), LSDA, and SCAN total energies as functions of bond length R , for the one-electron molecular ion H_2^+ , calculated from self-consistent densities with the PySCF code [1, 2] and the cc-pVQZ [3] Gaussian basis set. Note that SCAN (as well as PBE, not shown) is accurate for the compact one-electron densities of compressed or equilibrium bond length but makes the energy increasingly too negative as the bond is stretched. (Note further that, beyond one- and two-electron densities, SCAN and SIC make greater demands on the mesh for the integral of Eq. (3.2.1) than LSDA or PBE do. For example, in the FLOSIC [4] code, the volume per mesh point is 3.7 times smaller for SCAN than for LSDA or PBE.)

ergies and densities but not for most excited states of many-electron systems. The argument at the end of Sec. 3.3 shows that it is also exact for the excited states of one-electron systems.

3.3 Why semilocal approximations fail for lobed (e.g., stretched or noded) one-electron densities.

A formally exact expression for the exchange-correlation energy is[49, 47]

$$E_{xc}[n_{\uparrow}, n_{\downarrow}] = \frac{1}{2} \int d\mathbf{r} n(\vec{r}) \int d\mathbf{r}' n_{xc}([n_{\uparrow}, n_{\downarrow}], \vec{r}, \vec{r}') / |\vec{r} - \vec{r}'| \quad (3.3-4)$$

i.e., a Coulomb interaction between the electron density at a position \vec{r} and the density at \vec{r}' of the exchange-correlation hole surrounding an electron at \vec{r} . Around a given electron, one electron is missing from the rest of the density, leading to the sum rule[49, 47]

$$\int d\vec{r}' n_{xc}([n_{\uparrow}, n_{\downarrow}], \vec{r}, \vec{r}') = -1 \quad (3.3-5)$$

The hole density is thus typically negative, and the more negative it is close to its electron the more negative the exchange-correlation energy will be. Although we do not usually know the hole density exactly, its known exact properties can be used to understand the power and limitations of approximate density functionals[49, 47] and to provide an alternative and earlier construction[195] of the PBE GGA.[65]

Semilocal approximations either explicitly[195] or implicitly[196] model the hole density as a function of \mathbf{r}' that is localized (on a scale set by the local spatial variation of the electron density) around the electron position \mathbf{r} and that satisfies the sum rule of Eq. (3.3-5). This model is reasonably correct in many cases. A functional like PBE or SCAN can be accurate both for the extended densities in solids and for the compact densities of atoms or of molecules at equilibrium geometries, while LSDA

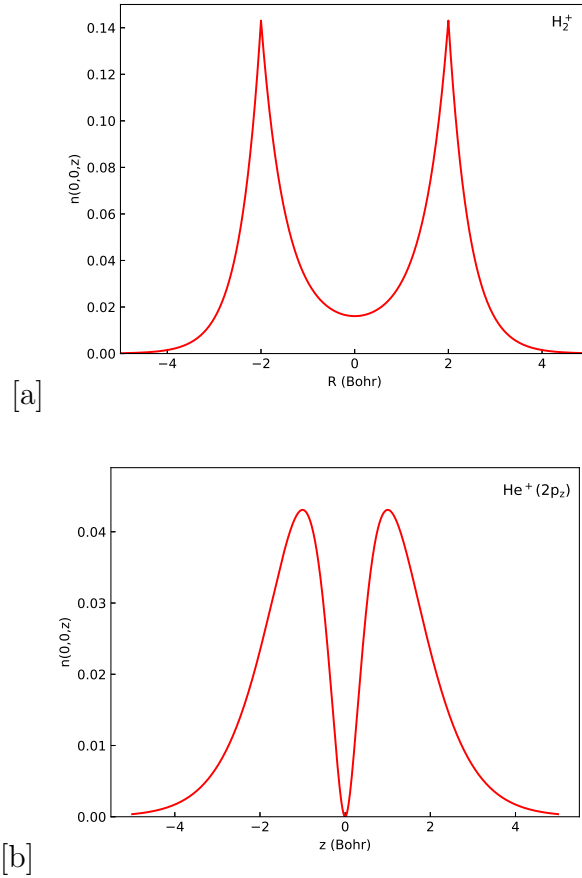


Figure 3.2: (a) Exact (Hartree-Fock or PZ SIC) nonrelativistic electron density (in atomic units) of the one-electron molecular ion H_2^+ in its ground state at stretched bond length $R = 4$ Bohrs, computed in the complete basis-set limit using the code HeIFEM.[5, 6] A similar density with slightly lower and more rounded nuclear cusps was obtained with the FLOSIC [4] all-electron Gaussian-type-orbital code using the NRLMOL default basis set.[7] (b) Electron density (in atomic units) of He^+ in its noded $2p_z$ excited state, computed using the exact nonrelativistic analytic expression. The one-electron density of (a) is stretched and that of (b) is noded, but both are similarly lobed.

is less accurate, especially for the compact densities. However, for any one-electron density n , the exact hole density is $-n(\mathbf{r}')$, independent of \mathbf{r} , making Eq. (3.2-3) reduce to

$$E_{xc}[n, 0] = -U[n] \quad (3.3-6)$$

or minus the Hartree electrostatic energy of the one-electron density. Unless the one-electron density is reasonably compact, a semilocal approximation cannot mimic the full nonlocality of Eq. (3.3-6) (Fig. 3.1). While LSDA cannot mimic Eq. (3.3-6), PBE and SCAN can do so for compact orbital densities (as in the small- R part of Fig. 3.1). However, if a one-electron density is separated into two equal lobes (as in the large- R part of Fig. 3.1 and in Fig. 3.2), then the exact hole density is shared equally between the lobes, while the semilocal hole density is concentrated on the lobe nearer to the electron, making the PBE or SCAN exchange-correlation energy too negative. In the limit of large separation between the lobes, the approximate hole is entirely on the lobe nearer the electron.

To illustrate this problem, Fig. 3.2 shows the electron density of the stretched one-electron ion H_2^+ . The exact exchange-correlation hole density for any electron position \mathbf{r} is $-n(\mathbf{r}')$, independent of \mathbf{r} , or Fig. 3.2 turned upside down. The LSDA hole density at \mathbf{r}' for electron position \mathbf{r} is a function of $|\mathbf{r} - \mathbf{r}'|$ that minimizes at the value $-n(\mathbf{r})$ when $\mathbf{r}' = \mathbf{r}$ and then rises to zero over a length scale roughly proportional to $n(\mathbf{r})^{-1/3}$. This qualitative failure of LSDA is shared by GGA and meta-GGA for stretched H_2^+ and other stretched radicals.

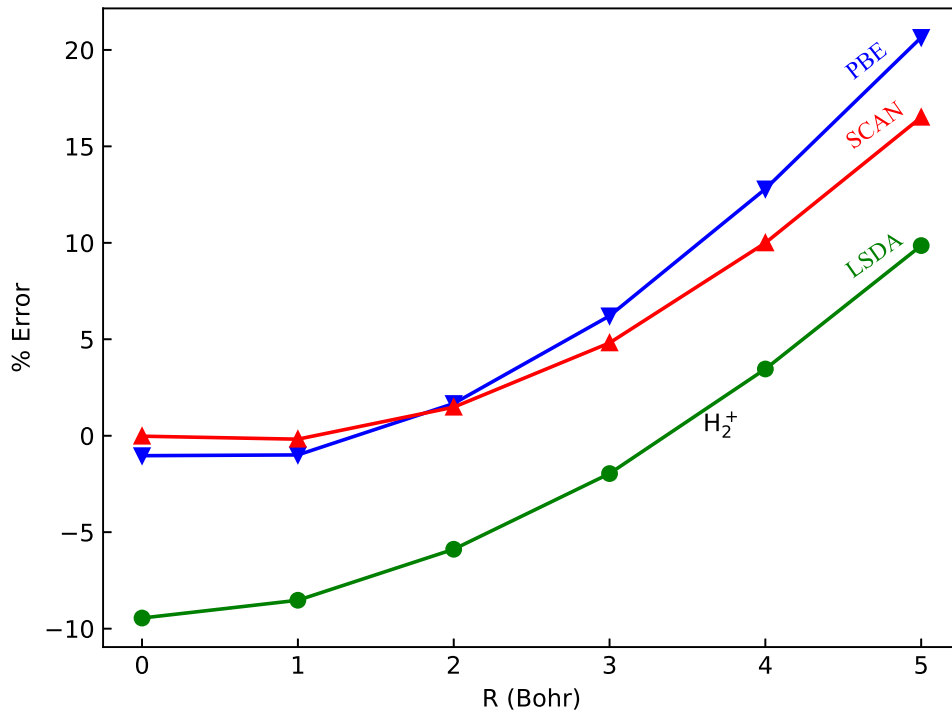


Figure 3.3: Relative error of LSDA, PBE, and SCAN for E_{xc} of H_2^+ , using exact (i.e., SIC) electron densities from the FLOSIC code,[4] as functions of bond length R . Note that at $R = 0$, the exchange-correlation energy is that of $He^+ 1s$. The equilibrium bond length is around 2 Bohrs (Fig. 3.1). The results for the nonzero bondlengths of H_2^+ correct erroneous results from Ref.[8]. For PBE and SCAN, the self-interaction error grows as the bond is stretched, but it grows more slowly in SCAN.

Table 3.1: Relative errors (%) of LSDA, PBE, and SCAN for E_{xc} of H_2^+ at $R = 4$ Bohrs and $\text{He}^+ 2p_z$, both using exact densities. The H_2^+ values from PySCF[1, 2] using the cc-pVQZ[3] Gaussian basis set correct erroneous values from Ref.[8]. Exact and approximate exchange (but not correlation) energies of the He^+ canonical orbitals scale up in proportion to the nuclear charge Z . Note the similarities in the numbers between the stretched H_2^+ and the noded $\text{He}^+ 2p_z$ densities. Note further that SCAN is better than PBE for these highly stretched or strongly noded one-electron densities. The bottom row shows the exact E_{xc} of Eq. (3.3-6), in Hartrees.

Approx.	Stretched H_2^+	$\text{He}^+ 2p_z$
LSDA(%)	3.6	3.4
PBE(%)	12.9	12.8
SCAN(%)	10.1	8.8
E_{xc}	-0.2285	-0.1957

Table 3.2: Relative errors of LSDA, PBE, and SCAN for E_{xc} of individual real Fermi-Löwdin orbitals in the Ne atom and the CH_4 molecule, calculated here using the corresponding SIC orbital densities from the FLOSIC[4] code. The exact entry $-U[n_{i\sigma}]$ is displayed for the SCAN-SIC orbital density. For the Ne atom, the core orbital is $1s$ and the valence orbitals are rotationally equivalent sp^3 hybrids. The purpose of this table is not to compare atoms with molecules but to show that the relative errors of PBE and SCAN for the valence orbitals are much smaller here than those in Table 3.1 because the real Fermi-Löwdin orbital densities are less severely noded than is the $2p_z$ orbital density. (As usual, PBE and SCAN are much more accurate than LSDA for the compact $1s$ core orbital densities.) The bottom row shows the exact E_{xc} of Eq. (3.3-6), in Hartrees. For CH_4 , we have employed the QCISD/MG3 equilibrium geometry[10] from the HTBH38/08 database.

Approx .	Ne core	Ne valence	CH_4 core	CH_4 valence
LSDA(%)	-12.5	-6.3	-11.6	-6.4
PBE(%)	-1.8	3.9	-1.5	1.2
SCAN(%)	0.2	3.2	0.2	1
Exact	-3.065	-0.589	-1.781	-0.345

From the very beginning of density-functional theory, it was known that the exact density functional for the exchange-correlation energy is nonlocal. For example, the exact exchange-correlation potential around an atom decays as $-1/r$ as $r \rightarrow \infty$, like a Coulomb potential. A more radical nonlocality, which does not decay to zero with increasing separation, was identified by Perdew, Parr, Levy, and Balduz,[197] who were motivated in part by PZ SIC. This radical nonlocality is associated with a noninteger average electron number on a separated subsystem. Stretched H_2^+ , with half an electron (and half an exact exchange-correlation hole) around each separated proton, was identified as an example by Zhang and Yang,[182] who found wrong dissociation limits with the BLYP, GGA and B3LYP hybrid functionals and made a quantitative model to explain this. It is clear from Ref.[182] that only a fully nonlocal functional such as Hartree-Fock or PZ SIC can account for the energies of such systems. No semilocal approximation can be correct for such systems, where the error of a semilocal approximation grows gradually with increasing separation as in Fig. 3.3. The errors that semilocal approximations make for noded orbital densities reflect the incipient division of one electron into fragments of non integer electron number.

Table 3.3: Mean error (ME) and mean absolute error (MAE) (kcal/mol) for LSDA,PBE, SCAN, LSDA-RSIC, PBE-RSIC, SCAN-RSIC, LSDA-CSIC, PBE-CSIC, and SCAN-CSIC for the molecular atomization energies of the small representative AE6 set. RSIC is SIC with real localized orbitals, and CSIC is SIC with complex localized orbitals. The AE6[10] set comprises the six molecules SiH₄, S₂, SiO, C₃H₄ (propyne), HCOCOH (glyoxal), and C₄H₈ (cyclobutane). All densities are self-consistent. We have used the Gaussian-type-orbital ERKALE code of Lehtola et al.[11, 2] with the cc-pVQZ[3] basis set, using fixed nuclear geometries at the QCISD/MG3 level (see <https://comp.chem.umn.edu/db/index.html>). A Lebedev grid of 50 radial and 194 angular points delivered good agreement with reference values.[12] See the supplementary material for further details. (1 Hartree = 627.5 kcal/mol = 27.21 eV.) Note that here PZ SIC worsens the atomization energies of SCAN, but less severely in CSIC than in RSIC.

AE6		
Approx.	ME	MAE
LSDA	77.3	77.3
LSDA-RSIC	57.1	60.0
LSDA-CSIC	62.6	62.6
PBE	12.5	15.6
PBE-RSIC	-14.4	17.8
PBE-CSIC	-8.6	10.0
SCAN	-2.2	4.4
SCAN-RSIC	-23.0	24.3
SCAN-CSIC	-16.9	17.1

GGAs and meta-GGAs can accurately describe compact one-electron densities such as the 1s density in H or He⁺. For example, the total energy of the hydrogen atom in Hartree is -0.479 (LSDA), -0.500 (PBE or SCAN), or -0.500 (exact). It is well known that stretched orbitals, as in the stretched one-electron molecular ion H₂⁺, are poorly described even by GGAs and meta-GGAs.[182] It is less well known (but see Ref.[8]) that noded orbitals, which are also lobed, encounter a similar self-interaction error. Figure 3.2 compares the densities of two different systems built up from one electron and two protons. The first is H₂⁺ in its 1σ even-parity ground state at the stretched bond length $R = 4$ Bohrs, with its density plotted along the bond axis. The second is the He⁺ atomic ion in its 2p_z excited state, with its density plotted along the z axis in Fig. 3.2. These systems are similarly lobed, and for both

of them, PBE or SCAN makes large and remarkably similar relative errors (Table 3.1). (The $2p_z$ state of He^+ is introduced because its density is strongly noded, in much the same way that the H_2^+ density in Fig. 3.2 is strongly stretched. A noded density is the limit of a sequence of un-noded ground-state densities, as discussed at the end of this section.)

Table 3.4: Same as Table 3.3, but for the barrier heights of the small representative BH6[10] set. There are forward and backward barriers for each of three reactions: (1) $\text{OH} + \text{CH}_4 \rightarrow \text{CH}_3 + \text{H}_2\text{O}$, (2) $\text{OH} + \text{H} \rightarrow \text{O} + \text{H}_2$, and (3) $\text{H} + \text{H}_2\text{S} \rightarrow \text{HS} + \text{H}_2$. Note that PZ SIC improves the barrier heights for all the semilocal functionals

BH6		
Approx.	ME	MAE
LSDA	-18.1	18.1
LSDA-RSIC	-5.1	5.1
LSDA-CSIC	-4.1	4.1
PBE	-9.6	9.6
PBE-RSIC	-0.2	4.1
PBE-CSIC	2.2	2.2
SCAN	-7.9	7.9
SCAN-RSIC	-1.2	2.7
SCAN-CSIC	-0.7	2.3

While a compact orbital density is clearly a single system with an integer (1) electron number, stretching or noding can be regarded as early steps in the formation of separate systems with a noninteger average electron number for which semilocal approximations always fail dramatically. Figure 3.3 shows that the PBE and SCAN errors almost go to zero as the bond length R of H_2^+ is reduced to zero. Similarly, the large nodality errors for the $2p_z$ orbital density are greatly reduced but not eliminated for typical real SIC localized orbitals of atoms and molecules (Table 3.2). The $2p_z$ orbital density is strongly noded, with a nodal plane through its center, but the real Fermi-Lwdin orbitals considered in Table 3.2 are more weakly noded, with nodal surfaces nearer their edges. Since ground-state densities are typically nodeless, can we even define the exact ground-state exchange-correlation energy of a noded

Table 3.5: Same as Table 3.3, but for the 55 molecular formation energies of the G2-1 data set,[13] using SCAN, SCAN-RSIC, and SCAN-CSIC. The formation energies are constructed in such a way that their MAEs are essentially those of the molecular atomization energies, and their MEs are essentially minus those of the atomization energies. We have used B3LYP geometries with zero-point expansion. Note that the FLOSIC method implemented in the PySCF code [1, 2] (PyFLOSIC[14]) agrees within 0.6 kcal/mol with these RSIC results from the ERKALE code.[11, 2] (See the supplementary material for details.) For LSDA, LSDA-RSIC, PBE, and PBE-RSIC, see Ref.[15].

G2-1		
Approx	ME	MAE
SCAN	1.7	4.1
SCAN-RSIC	14.2	16.0
SCAN-CSIC	8.9	10.2

density? We can do so by regarding a noded one-electron density as the limit of a sequence of nodeless one-electron ground-state densities. For example, the $2p_z$ orbital density in Fig. 3.2(b) varies like z^2 near the nodal plane $z = 0$ and can be obtained as the $a^2 \rightarrow 0$ limit of a sequence of one-electron densities that behave like $z^2 + a^2$ near $z = 0$. A similar limit can be defined for any noded one-electron density, and the sequence of unnoded densities will all be v -representable ground-state densities by inversion of the one-electron Schrödinger equation for the positive square root of the density to find the potential $v(\mathbf{r})$. The integral of Eq. (3.2-2) then tells us that, for a noded and for a nodeless one-electron density n , Eq. (3.4-6) is valid. In other words, the exact ground-state exchange-correlation functional for spin-polarized one-electron ground-state densities, Eq. (3.4-6), applied to a sequence of nodeless spin-polarized one-electron ground-state densities that lie within its domain of definition implies Eq. (3.4-6) even for noded spin-polarized one-electron densities. The exact exchange-correlation energy of a spin-polarized one-electron density is Eq. (3.3-6), which depends only on the amplitude and not on the phase of the one-electron wavefunction. Thus, as claimed in Ref.[51], the PZ correction on the extreme right of Eq. (3.2-3) does vanish when applied to the exact functional. Unfortunately, this

does not imply that the correction will be acceptably small when applied to a semilocal functional in a situation for which that functional is accurate, as discussed in Sec. 3.4. From the discussion of the previous paragraph, the exact Kohn-Sham theory is exact for the ground and excited states of any one-electron density although, of course, not for all excited states of many-electron systems, and PZ SIC is exact for all

3.4 Why complex localized orbitals work better than real ones in PZ SIC

GGA and meta-GGA functionals of the total density often work well, but not in regions where there are stretched orbitals. Our previous example was stretched H_+^2 , [182] but the same effect occurs for the stretched bonds between different open-shell atoms [184] and in the transition states [185] of chemical reactions, where again the semilocal exchange-correlation energy is too negative, making the energy barriers too low. A standard cure is the Perdew-Zunger (PZ) self-interaction correction (SIC) of Eq. (3.2-3). To work well, the PZ correction from each occupied localized orbital should be small (i.e., $E_{xc}^{approx}[n_{i\sigma}, 0]$ must nearly cancel $U[n_{i\sigma}]$), except when that orbital is stretched. But, as argued in Sec. 3.3, that cancellation will be less perfect when the SIC orbital density is noded (Tables 3.1 and 3.2) and even less perfect as the orbital density becomes more strongly noded. As the orbital density becomes more noded, its semilocal exchange-correlation energy becomes more negative and its PZ self-interaction correction of Eq. (3.2-3) becomes more positive, even when the orbital density is unstretched. Noded SIC orbitals can be avoided, even when the canonical or generalized Kohn-Sham orbitals are real, by making the unitary transformation matrix and the resulting localized SIC orbitals complex, as in Refs. [190] and [16]. Tables 3.3-3.5 confirm this expectation for the atomization energies of molecules in

the small representative set AE6,[10] for the barrier heights of chemical reactions in the small representative set BH6,[10] and for the 55 molecular formation energies of the G2-1 set.[13] For PBE and SCAN, the PZ self-interaction-corrected results are more accurate when complex SIC orbitals are used. These results for PBE-SIC are in agreement with those of earlier studies, [189, 191, 190, 192, 15] which also noted that only the real localized orbitals are noded. But the explanation in the previous paragraph for the better results from complex orbitals is ours. The SCAN and SCAN-SIC atomization energies of molecules (Tables 3.3 and 3.5) illustrate the magnitude of the problem that remains to be solved. Without fitting to any bonded system, SCAN yields errors much smaller than those of LSDA or PBE. But SCAN-SIC yields errors that are bigger than those of SCAN by a factor of four or five for real SIC orbitals and three or four for complex SIC orbitals. Table 3.3-3.5 also agree with earlier studies [189, 191, 190, 192, 15, 193, 16, 194] showing that PZ-SIC with real localized orbitals, applied to PBE (and in our study to SCAN), improves barriers but often worsens atomization energies. Use of complex orbitals solves only part of the problem by reducing but not eliminating the problematic lobed character of the orbital densities. (See Fig. 3.2 of Ref.[194].) The best SIC atomization energies in Table 3.3 are those of PBE-CSIC, as in Table I of Ref.[190]. Perhaps significantly, PBE-CSIC also yields the most accurate SIC total energies for large- Z atoms. PZ SIC imposes a new exact constraint (exactness for all one-electron densities) at the cost of other exact constraints or of appropriate norms such as exactness for the uniform electron gas and for large- Z atoms.[186] This in turn results in errors that do not fully cancel out in the energy differences between free atoms and molecules. Needed is a generalization of PZ SIC that treats occupied localized orbitals in the PZ way only when they do not overlap with other occupied localized orbitals but (unlike earlier attempts to scale down the self-interaction correction in many-electron regions [193]) retains the full Hartree part of the PZ SIC. Such a generalization is being attempted [198] to

make SIC exact for all large- Z atoms and other slowly varying densities. While this seems to be achievable, restoring some of the other exact constraints satisfied by the nonempirical semilocal functionals may be harder to achieve with a fully nonlocal approximation.

3.5 Discussions and Conclusions

PZ SIC applied to a semilocal functional like the PBE GGA or the SCAN meta-GGA removes troublesome self-interaction errors that manifest most strongly for stretched bonds. But it introduces other errors, which manifest significantly in the atomization energies of molecules. Some of these are orbital-density nodality errors that can be removed by replacing real localized orbitals by complex ones (Tables 3.33.5). Removing the nodes of the localized orbital densities reduces but does not eliminate their problematic lobed one-electron structure. Errors remain because the PZ-corrected functional for the total electron density violates (at least for real Fermi-Lwdin orbitals)[186] exact constraints or appropriate norms that are built into PBE and especially SCAN. Hopefully a generalized PZ SIC [198] will be able to recover some of these correct features of SCAN, thus providing a large self-interaction correction only where it is needed. SCAN, which is already self-correlation free, is a natural candidate for a generalized self-interaction correction. As a first step, we have presented here what may be the first results for the ungeneralized PZ SIC applied to SCAN. (For a recent alternative approach, see Ref.[199])

Table 3.6: Total PZ self-interaction corrections to the exchange-correlation energies of rare-gas atoms, in Hartrees. Shown is the orbital-density-dependent correction of Eq. (3.2-3) to the exchange-correlation energy in an energy-minimized SIC calculation, with real (RSIC) or complex (CSIC) orbitals, using the ERKALE code[11, 2] and the standard NRLMOL basis set.[7] Note that the CSIC values are lower than the RSIC values, as expected, and that the difference increases from LSDA to PBE to SCAN. The CSIC correction to PBE is relatively small, consistent with Ref.[16]. To set a scale, the last rows show the accurate total exchange-correlation energy from a self-consistent SCAN calculation and a nearly exact exchange-correlation energy (exchange from Ref.[17] and correlation from Ref. [18]).

Functional	Ne	Ar	Kr	Xe
LSDA-RSIC	-1.06	-2.61	-7.55	-13.74
LSDA-CSIC	-1.11	-2.75	-8.02	-14.57
PBE-RSIC	0.08	0.26	1.28	2.99
PBE-CSIC	-0.04	-0.08	-0.01	0.56
SCAN-RSIC	0.16	0.46	1.76	3.80
SCAN-CSIC	-0.20	-0.65	-3.54	-8.08
Total E_{xc} (SCAN)	-12.45	-30.99	-95.79	-181.99
Total E_{xc} (exact)	-12.50	-30.91	-95.74	-182.20

The PZ self-interaction correction does indeed vanish [51] when applied to the exact density functional for the exchange-correlation energy, but unfortunately this conclusion does not guarantee that, when applied to a good semilocal approximate functional, this correction will be acceptably small in situations where the semilocal functional is accurate. This is because the densities of occupied localized orbitals are typically more challenging to the semilocal functional than is the total electron density. To make PZ SIC exact for any collection of separated one-electron densities, the right orbitals for the PZ SIC must span the space of occupied generalized Kohn-Sham or canonical orbitals. Using the often-delocalized generalized Kohn-Sham orbitals themselves would lead to a well-known size-extensivity problem.[51] We have found here a second reason not to use canonical orbitals: They can be highly noded (e.g., the $2p_z$ orbital), with disastrous results for PZ SIC applied to semilocal functionals beyond LSDA(Table 3.1). A better choice is to use real localized orbitals that are

more-weakly noded, i.e., noded near the edges but not near the center, such as the real Fermi-Lwdin orbitals.[86] Still better for the correction of semilocal functionals are complex localized orbitals with nodeless orbital densities.[16] Complex Fermi-Lwdin orbitals are possible [200] and also presumably guarantee the size-extensivity of SIC. A good semilocal functional like PBE or SCAN will, by our analysis of Sec. 3.3, produce a positive PZ self-interaction correction in Eq. (3.2-3) from any highly stretched or strongly noded localized orbital. As shown in Table 3.6, even the total self-interaction corrections to the exchange-correlation energies for atoms, using the weakly noded real Fermi-Lwdin orbitals, tend to be positive for these functionals. Thus, the strong nodality of some Kohn-Sham orbitals in atoms and small molecules drives the energy-minimizing localized orbitals away from the highly noded Kohn-Sham orbitals and toward the more weakly noded Fermi-Lwdin orbitals. But, even so, the PBE-SIC and SCAN-SIC exchange-correlation energies with real SIC orbitals are not negative enough and are much less accurate than those of SCAN (Table 3.6). PZ SIC reduces atomization energies of molecules (often by too much) and raises energy barriers to chemical reactions. We can now propose a tentative explanation for this although the explanation is restricted to the case of real localized SIC orbitals. In the ground state, real localized SIC orbitals that overlap must be noded to achieve orthogonality. As we pass from separated atoms to the molecules they form or from separated molecules to the transition states they form, the valence orbitals acquire more orbitals with which they overlap and, hence, become more noded. As the valence orbitals become more noded, their PZ self-interaction correction of Eq. (3.2-3) becomes more positive or less negative. Thus, PZ SIC raises the energy of a molecule relative to the energy of its separated atoms and raises the energy of a transition state relative to its separated molecules. PZ SIC also raises the energy of the transition state relative to its separated molecules through bond stretching. The correlation energy as defined in the exact Kohn-Sham theory is numerically close to its quantum-chemistry

definition,[201] the deviation of the total energy from the Hartree-Fock value. In this sense, the transition states of chemical reactions are more strongly correlated than are the ground states of molecules in equilibrium since the Hartree-Fock energy barriers to chemical reactions are seriously too high. The barriers from semilocal functionals are seriously too low, suggesting that in this sense they “over-correlate” for stretched radicals, but the barriers are rather accurate when a self-interaction correction is applied. This and other results (e.g., Refs. [180] and [202]) suggest that properly self-interaction-corrected semilocal functionals might usefully describe the energetics of strongly correlated systems. By properly self-interaction-corrected, we mean exact for all one-electron densities and reasonably accurate even for the fractional electron number, as in PZ SIC, but roughly as accurate as SCAN for atomization energies and equilibrium bondlengths (an accuracy that arises from the satisfaction of exact constraints and appropriate norms, with no fitting to bonded systems). The SCAN and SCAN-SIC results in Tables 3.3, 3.5, and 3.6 show how far we still are from this goal. Hybrid functionals, [202] which mix an empirical fraction of exact exchange with a complementary fraction of semilocal exchange, go only part of the way toward this goal by reducing but not eliminating the self-interaction error.

It is not only atomization energies but also equilibrium bond lengths that are worsened by PZ SIC. For small molecules, LSDA-SIC bond lengths are shorter and less accurate than those of LSDA, and PBE-SIC bond lengths are shorter and less accurate than those of PBE, whether real [193] or complex [203] SIC orbitals are used. In addition, PZ SIC breaks molecular symmetries.[190] We plan to return to these problems in future work.

A by-product of this work is the observation that the exact Kohn-Sham theory, with the standard exact ground-state exchange-correlation energy functional, is exact for all excited states of one-electron systems, as well as for all ground-states, and that the Perdew-Zunger self-interaction correction[51] (PZ SIC) perfectly imitates

the exact Kohn-Sham theory in this special case of one-electron densities. For a many-electron excited state, of course, there is no exact Kohn-Sham theory, but removing the self-interaction error from an approximate functional could improve the approximate description of an excited state.

Supporting information

3.6 Computational details: ERKALE and PySCF/PyFLOSIC

All calculations were performed on a single node with a maximum number of 20 cores per node using OMP parallelization. Local density approximation (LDA) calculations were performed using Slater exchange[37, 204] and the Perdew-Wang parametrization for the correlation part of LDA[60]. For ERKALE this corresponds to the method tag `ldax-ldacpw` and for PySCF/PyFLOSIC this corresponds to the xc tag `LDA, PW`. The Perdew-Burke-Ernzerhof (PBE)[65] functional was used for all generalized gradient approximation (GGA) calculations. Corresponding in ERKALE to the method tag `ggaxpbe-ggacpbe` and for PySCF/PyFLOSIC this corresponds to the xc tag `PBE, PBE`. The meta-GGA level calculations were performed with the Strongly Constrained and Appropriately Normed Semilocal (SCAN)[72] density functional. The method tag in ERKALE is `mggaxscan-mggacscan` and the corresponding xc tag in PySCF/PyFLOSIC is `SCAN, SCAN`. ERKALE, PySCF as well as PyFLOSIC use exchange-correlation functional implementations from the `libxc` library[205, 2]. All calculations were carried out spin-polarized.

Table 3.7: Total energies (in Hartree) using ERKALE[11] and the cc-pVQZ basis set. ALebedev-Lakov grid of 50 radial and 194 angular points was used.

system	LDA	PBE DFT	SCAN
H	-0.47859	-0.49985	-0.50009
C	-37.46715	-37.79717	-37.84053
O	-74.52547	-75.01166	-75.07061
Si	-288.20827	-289.2296	-289.40198
S	-396.73079	-397.94764	-398.12341
SiH4	-290.67681	-291.72818	-291.91578
S2	-793.67521	-796.07666	-796.41953
SiO	-363.09132	-364.55317	-364.76823
C3H4 (pro)	-115.59414	-116.54123	-116.63468
HCOCOH	-226.14357	-227.67639	-227.82873
C4H8 (cyc)	-155.77684	-157.05072	-157.18675
RSIC			
H	-0.49995	-0.49995	-0.49995
C	-37.95657	-37.81608	-37.81287
O	-75.28478	-75.00298	-74.99451
Si	-290.00832	-289.10282	-289.13592
S	-398.92955	-397.77087	-397.77295
SiH4	-292.58917	-291.62084	-291.65542
S2	-798.03765	-795.69429	-795.70365
SiO	-365.58544	-364.34963	-364.37859
C3H4 (pro)	-117.11192	-116.54241	-116.50946
HCOCOH	-228.5889	-227.59352	-227.54715
C4H8 (cyc)	-157.91682	-157.10669	-157.04691
CSIC			
H	-0.49995	-0.49995	-0.49995
C	-37.95938	-37.82574	-37.86991
O	-75.30689	-75.04877	-75.17169
Si	-290.09779	-289.31177	-289.80893
S	-399.04308	-398.04137	-398.64414
SiH4	-292.67712	-291.82746	-292.30878
S2	-798.27273	-796.24194	-797.45143
SiO	-365.7153	-364.63463	-365.27073
C3H4 (pro)	-117.14618	-116.60448	-116.71258
HCOCOH	-228.65109	-227.7299	-228.05876
C4H8 (cyc)	-157.91743	-157.10757	-157.23111

3.7 Atomization energies: AE6 benchmark

The total energies, using LDA, PBE and SCAN exchange-correlation functional and considering density functional theory (DFT), self-interaction correction with real localized orbitals (RSIC), as well as self-interaction correction with complex localized orbitals (CSIC) for all systems which are part of the AE6 set[10], are reported in table 3.7. The AE6 and BH6 calculations were performed on fixed nuclei geometries at the QCISD/MG3 level (see <https://comp.chem.umn.edu/db/index.html>). The AE6 set is a subset of the MGAE109/11 set including the molecules SiH₄ (¹A₁, 2S + 1 = 1), S₂ (³Σ_g, 2S + 1 = 3), SiO (¹Σ, 2S + 1 = 1), C₃H₄ (propyne) (¹A, 2S + 1 = 1), HCOCOH (ethandial) (¹A_g, 2S + 1 = 1), C₄H₈ (cyclobutane) (¹A₁, 2S + 1 = 1) as well as the corresponding atoms (H, C, O, S, Si). A Lebedev-Lakovgrid of 50 radial and 194 angular points delivered a good agreement with reference values[193, 12]

3.8 Barrier heights: BH6 benchmark

The BH6 set[10] is a subset of the HTBH38/08 benchmark set including the reactions 7 and 8 (forward and reverse, see Eq. (3.8-7)), 23 and 24 (forward and reverse, see Eq. (3.8-8)) and 25 and 26 (forward and reverse, see Eq. (3.8-9)). The numbering is adapted from the original HTBH38/08 benchmark set.



Overall, this set includes the molecules OH, H₂, HS, H₂S, H₂O, CH₃, CH₄, transition state molecule 4 (TS-4), transition state molecule 12 (TS-12), transition state molecule 13 (TS-13) and the atoms H and O. Total energies for the BH6 test set using

the same approximations as before are reported in table 3.8.

3.9 Enthalpies of formation: G2-1 benchmark

The total energies for all systems within the G2-1 set (molecular geometries taken from Ref.13), using LDA, PBE and SCAN and considering DFT, RSIC as well as CSIC, are given in tables 3.9 and 3.10 for ERKALE. Values using SCAN and SCAN-FLOSIC obtained from PyFLOSIC[1, 14] are given in tables 3.11 and 3.12. For the FLOSIC calculations, the Fermi-orbital descriptors (FOD) were optimized until the absolute value of the maximum forcecomponent of the FOD forces was less than 0.0001 eV/ Å. Further, analysis of errors in the calculated enthalpies of formation with respect to reference values according to the G2-1 theory for SCAN and SCAN-FLOSIC [1, 14] are presented in table . The FLOSIC results from PyFLOSIC agree within 0.6 kcal/mole with the RSIC results from the ERKALE code.

Table 3.8: BH6: Total energies (in Hartree) using ERKALE[11] and the cc-pVQZ basis set. A Lebedev-Lakov grid of 50 radial and 194 angular points was used.

system	LDA	PBE	SCAN
	DFT		
H	-0.47859	-0.49985	-0.50009
O	-74.52547	-75.01166	-75.07061
OH	-75.20086	-75.68576	-75.74254
CH ₄	-40.11828	-40.46654	-40.50614
CH ₃	-39.44319	-39.79102	-39.83672
H ₂ O	-75.90533	-76.38298	-76.43408
H ₂	-1.1372	-1.16655	-1.17175
H ₂ S	-398.01582	-399.23653	-399.41236
HS	-397.36615	-398.58718	-398.76443
TS-4	-115.34601	-116.16091	-116.25216
TS-12	-75.68261	-76.18017	-76.23862
TS-13	-398.50509	-399.73834	-399.91683
	RSIC		
H	-0.49995	-0.49995	-0.49995
O	-75.28476	-75.00298	-74.99451
OH	-75.96903	-75.66086	-75.65566
CH ₄	-40.70187	-40.4788	-40.46965
CH ₃	-39.9952	-39.79589	-39.79627
H ₂ O	-76.67922	-76.33767	-76.3332
H ₂	-1.18244	-1.16375	-1.16921
H ₂ S	-400.25836	-399.05694	-399.05985
HS	-399.58953	-398.41138	-398.41405
TS-4	-116.66436	-116.12013	-116.11021
TS-12	-76.45352	-76.1403	-76.14013
TS-13	-400.7557	-399.55016	-399.55732
	CSIC		
H	-0.49995	-0.49995	-0.49995
O	-75.30689	-75.04877	-75.17156
OH	-75.98736	-75.70162	-75.8483
CH ₄	-40.70197	-40.47888	-40.51754
CH ₃	-40.00012	-39.80858	-39.85626
H ₂ O	-76.69873	-76.38597	-76.53688
H ₂	-1.18244	-1.16375	-1.16921
H ₂ S	-400.36543	-399.31648	-399.92715
HS	-399.69892	-398.67327	-399.27934
TS-4	-116.68119	-116.16142	-116.36193
TS-12	-76.47407	-76.18387	-76.32345
TS-13	-400.86347	-399.80905	-400.42341

Table 3.9: ERKALE G2-1 (atoms): Total energies (in Hartree) using ERKALE [11] and the cc-pVQZ basis set. A Lebedev-Lakov grid of 50 radial and 194 angular points was used.

system	SCAN	SCAN-RSIC	SCAN-CSIC
H	-0.50009	-0.49995	-0.49995
Li	-7.47954	-7.47404	-7.47405
Be	-14.64931	-14.64248	-14.64255
C	-37.8403	-37.81279	-37.86987
N	-54.59017	-54.53536	-54.64587
O	-75.07032	-74.99452	-75.17174
F	-99.75162	-99.64211	-99.91109
Na	-162.28732	-162.10953	-162.54036
Si	-289.40198	-289.1359	-289.80652
P	-341.29923	-340.98864	-341.75834
S	-398.12348	-397.7729	-398.64409
Cl	-460.20766	-459.80929	-460.79425

Table 3.10: ERKALE G2-1 (molecules): Total energies (in Hartree) using ERKALE[11] and the cc-pVQZ basis set. A Lebedev-Lakov grid of 50 radial and 194 angular points was used.

system	SCAN	SCAN-RSIC	SCAN-CSIC	system	SCAN	SCAN-RSIC	SCAN-CSIC
LiH	-8.06819	-8.06029	-8.0603	CO	-113.31215	-113.16418	-113.4278
BeH	-15.24634	-15.23814	-15.23938	HCO	-113.8575	-113.71021	-113.969
CH	-38.46891	-38.44258	-38.49448	H ₂ CO	-114.50184	-114.36039	-114.61484
CH ₂ (1A1)	-39.11677	-39.10432	-39.15795	CH ₃ OH	-115.72407	-115.59084	-115.82263
CH ₂ (3B1)	-39.1536	-39.11632	-39.18229	N ₂	-109.51574	-109.37298	-109.60702
CH ₃	-39.83672	-39.79623	-39.861	N ₂ H ₄	-111.86298	-111.73363	-111.96711
CH ₄	-40.50649	-40.46973	-40.52024	NO	-129.89743	-129.7351	-130.03101
NH	-55.22398	-55.16685	-55.2768	O ₂	-150.33987	-150.13361	-150.49095
NH ₂	-55.88037	-55.81916	-55.94023	H ₂ O ₂	-151.56525	-151.36977	-151.73764
NH ₃	-56.55405	-56.48603	-56.61528	F ₂	-199.56508	-199.30723	-199.8229
OH	-75.7425	-75.65552	-75.84793	CO ₂	-188.60479	-188.32197	-188.83331
H ₂ O	-76.43397	-76.33244	-76.54384	Na ₂	-324.59651	-324.24125	-325.0965
HF	-100.4702	-100.33675	-100.63154	Si ₂	-578.9188	-578.38347	-579.73561
SiH ₂ (1A1)	-290.63829	-290.37417	-291.03317	P ₂	-682.7785	-682.14502	-683.69877
SiH ₂ (3B1)	-290.62115	-290.35362	-291.02105	S ₂	-796.41925	-795.70242	-797.45594
SiH ₃	-291.26785	-291.00511	-291.6647	Cl ₂	-920.50744	-919.70533	-921.66446
SiH ₄	-291.91554	-291.65479	-292.3045	NaCl	-622.65044	-622.05966	-623.49203
PH ₂	-342.54952	-342.24556	-342.99893	SiO	-364.7674	-364.37587	-365.27134
PH ₃	-343.18549	-342.88109	-343.6234	CS	-436.22492	-435.80952	-436.76515
SH ₂	-399.41233	-399.05955	-399.9254	SO	-473.39966	-472.93255	-473.99918
HCl	-460.87725	-460.47349	-461.45914	ClO	-535.38709	-534.89324	-536.0453
Li ₂	-14.98872	-14.97845	-14.97847	ClF	-560.05722	-559.52512	-560.76643
LiF	-107.44523	-107.29345	-107.60289	Si ₂ H ₆	-582.65451	-582.13151	-583.44042
C ₂ H ₂	-77.31438	-77.2251	-77.38162	CH ₃ Cl	-500.1771	-499.74106	-500.76166
C ₂ H ₄	-78.57151	-78.49394	-78.61961	CH ₃ SH	-438.71603	-438.33004	-439.23822
C ₂ H ₆	-79.81108	-79.74027	-79.83013	HOCl	-536.03841	-535.53857	-536.70838
CN	-92.70664	-92.58232	-92.7962	SO ₂	-548.66813	-548.07673	-549.3715
HCN	-93.41088	-93.29225	-93.49073				

Table 3.11: pyFLOSIC G2-1 (atoms): Total energies (in Hartree) using PyFLOSIC [14] and the DFO [7] basis set. A PySCF/PyFLOSIC grid level of 7 was used (e.g. corresponds for the H atom to Lebedev-Lakov grid of 90 radial and 974 angular points)[19].

System	SCAN	SCAN-FLOSIC
H	-0.50011	-0.49988
Li	-7.47988	-7.47378
Be	-14.64952	-14.64176
C	-37.83856	-37.80659
N	-54.58841	-54.53052
O	-75.07058	-74.99035
F	-99.74426	-99.63064
Na	-162.27505	-162.0891
Si	-289.39344	-289.11897
P	-341.29397	-340.97475
S	-398.15291	-397.79362
Cl	-460.18914	-459.78084

Table 3.12: pyFLOSIC G2-1 (molecules): Total energies (in Hartree) using PyFLOSIC[14] and theDFO[7] basis set. A PySCF/PyFLOSIC grid level of 7 was used (e.g. corresponds for the H atom to Lebedev-Lakov grid of 90 radial and 974 angular points)[19].

System	SCAN	SCAN-FLOSIC	System	SCAN	SCAN-FLOSIC
LiH	-8.06761	-8.05907	CO	-113.31087	-113.15211
BeH	-15.2421	-15.23297	HCO	-113.85646	-113.69796
CH	-38.46912	-38.43479	H ₂ CO	-114.50211	-114.34917
CH ₂ (1A1)	-39.11876	-39.08194	CH ₃ OH	-115.72601	-115.5803
CH ₂ (3B1)	-39.13581	-39.09544	N ₂	-109.52219	-109.36733
CH ₃	-39.83687	-39.79351	N ₂ H ₄	-111.87087	-111.7287
CH ₄	-40.50792	-40.46723	NO	-129.89669	-129.72141
NH	-55.22352	-55.16281	O ₂	-150.34064	-150.11991
NH ₂	-55.88263	-55.81727	H ₂ O ₂	-151.56598	-151.35539
NH ₃	-56.55907	-56.48471	F ₂	-199.54676	-199.27571
OH	-75.74378	-75.64378	CO ₂	-188.59934	-188.28968
H ₂ O	-76.43559	-76.32648	Na ₂	-324.57219	-324.20035
HF	-100.46273	-100.3219	Si ₂	-578.90948	-578.35181
SiH ₂ (1A1)	-290.6309	-290.35962	P ₂	-682.76082	-682.1084
SiH ₂ (3B1)	-290.60043	-290.32413	S ₂	-796.47575	-795.74073
SiH ₃	-291.26026	-290.98849	Cl ₂	-920.46828	-919.64885
SiH ₄	-291.90828	-291.63792	NaCl	-622.61932	-622.01155
PH ₂	-342.54215	-342.23006	SiO	-364.75804	-364.34988
PH ₃	-343.17745	-342.8643	CS	-436.25725	-435.82862
PH ₂	-399.44448	-399.08433	SO	-473.42657	-472.94262
HCl	-460.85885	-460.44613	ClO	-535.36599	-534.85702
Li ₂	-14.98842	-14.97714	ClF	-560.02812	-559.4801
LiF	-107.43674	-107.27834	Si ₂ H ₆	-582.63895	-582.09499
C ₂ H ₂	-77.31604	-77.21936	CH ₃ Cl	-500.15939	-499.71358
C ₂ H ₄	-78.57423	-78.48841	CH ₃ SH	-438.74913	-438.34517
C ₂ H ₆	-79.81479	-79.73502	HOCl	-536.01934	-535.50284
CN	-92.70739	-92.57365	SO ₂	-548.68746	-548.06606
HCN	-93.41478	-93.28655			

Table 3.13: Errors of enthalpies of formation with respect to reference values [20] in kcal/mol for FLOSIC and DFT with the SCAN functional for the full G2-1 set calculated with PyFLOSIC [14] using the DFO [7] basis set. A PySCF/PyFLOSIC grid level of 7 was used (e.g. corresponds for the H atom to Lebedev-Lakov grid of 90 radial and 974 angular points)[19]

System	Error	SCAN-DFT	SCAN-FLOSIC
		G2 procedure using HF ZPE	
2[0]*G2-1	MAE [kcal/mol]	3.42	16.49
	ME [kcal/mol]	1.19	15.1
		G2 procedure using B3LYP ZPE	
2[0]*G2-1	MAE [kcal/mol]	3.39	16.63
	ME [kcal/mol]	1.4	15.31

CHAPTER 4

SUMMARY AND CONCLUSIONS

In this thesis, we validated the meta-generalized gradient approximation SCAN for the pressure-induced structural phase transition of solids and the self-interaction corrected SCAN for the atomization energies and barrier heights of the chemical reactions. In the first chapter, we touched upon the wavefunction theory and its difficulties and the resulting necessity for the density functional theory. Then we went somewhat deeper into the modern density functional theory, discussing the Hohenberg-Kohn theorems and the Kohn-Sham self-consistent method. We discussed the exchange-correlation energy and some of its properties and the need for its approximation. We gave a brief description of the LSDA, PBE, and SCAN density functionals. Finally, we introduced the basics of the self-interaction error and its correction.

In chapter 2, we assessed the performance of LDA, PBE, and SCAN for the pressure-induced structural phase transitions of solids from group IV, III-V, and II-VI. This is a tough test for an approximate density functional, as it must capture a small change in energy that arises from a large change in electron density. We found that LDA underestimates the structural energy differences and thus the transition pressures of most of the systems we studied. PBE under- or overestimates the pressures in many cases. SCAN can recognize different chemical bonding (or chemical environments), making it an ideal density functional for the study of phase transitions. SCAN pressures are in good agreement with experimental results. The experimental results often have uncertainty due to the hysteresis, non-hydrostatic stress condition, measurement methods, sample types, etc., so it is instructive to compare the com-

puted pressure with higher-level calculations like quantum Monte Carlo (QMC) and random phase approximation (RPA). QMC is often regarded as a near-exact method. RPA, on the fifth rung of Jacob’s ladder, is often more accurate than the semilocal density functionals. For Si (diamond \rightarrow β -tin transition) and GaAs (Zincblende \rightarrow NaCl transition), SCAN pressures are in excellent agreement with QMC, which is remarkable. For Si (diamond \rightarrow β -tin), Ge (diamond \rightarrow β -tin), Pb (fcc \rightarrow hcp), SiC (Zincblende \rightarrow NaCl transition), GaAs (zincblende \rightarrow Cmc m), GaN (wurtzite \rightarrow NaCl) and ZnO (wurtzite \rightarrow NaCl), the agreement of our calculated pressures with the random phase approximation (RPA) values increase from LDA to PBE to SCAN. The accurate prediction of critical pressures from SCAN comes from proper stabilization of both the competing phases.

In chapter 3, we assessed the performance of the Perdew-Zunger self-interaction correction (PZ SIC) for the barrier heights of chemical reactions of the test set BH6, atomization energies of the test set AE6, and formation energies of the G2-1 test set. PZ SIC improves the barrier heights of chemical reaction, while it worsens the atomization energies when real orbitals are used to minimize the PZ energy. We calculated the self-interaction errors (SIE) that LSDA, PBE, and SCAN make for stretched bonds (example: stretched one-electron orbital density in H_2^+) and for noded orbitals (example: excited state $2p_z$ orbital density in He^+ ion). The former is known as the cause of the underestimation of the barrier heights of chemical reactions by semilocal density functionals while the latter we identify as the cause of the errors in the atomization energies mentioned above.

For the H_2^+ molecule at zero bond length $R = 0$, SCAN is exact by construction, whereas LSDA makes significant SIE (Fig. 5). We found that the SIE grows faster for PBE than for SCAN as we stretch the molecule. For $He^+(2p_z)$, LSDA, PBE, and SCAN make similar SIE as they make for H_2^+ at $R = 4$ bohrs. We further evaluated the SIE for the core ($1s$) and valence (sp^3 hybrids) orbitals of Ne and CH_4 molecules using

the Fermi-Löwdinorbital SIC densities. LSDA makes significant SIE for core electrons, showing its failure for the compact $1s$ density. For valence orbitals, PBE and SCAN SIEs are reduced compared to that of LSDA for the noded $2p_z$ orbital in excited He^+ . PBE and SCAN are very accurate for compact one-electron densities. As we stretch and thus lobe a one-electron density, the approximate exchange-correlation hole of a semilocal functional for that one-electron density must live on the lobe nearer to its electron, making the semilocal exchange-correlation energy too negative compared to that of the more spread-out exact exchange-correlation hole. For the same reason, a semilocal functional must make exchange-correction energy too negative for any stretched or noded one-electron density.

PZ SIC applied to SCAN raises the energies of separate atoms (by 0.35 Hartrees relative to the SCAN values for Si and O atoms at large separation), and it raises the energies of molecules by even more (by 0.40 Hartrees relative to SCAN values for the SiO molecule at equilibrium) when atoms combine to form molecules. As atoms come close to each other, the valence orbitals overlap, acquiring more nodes and leading to more negative SCAN exchange-correlation energy for each orbital density (from the above discussion) and hence more PZ SIC correction for the molecule. This explains why the atomization energies of the representative test set AE6 and the formation energy of the G2-1 set are worsened by the PZ-corrected semilocal density functionals when real orbitals are used to minimize the PZ energy, and why complex orbitals reduce the error in the PZ-SIC atomization energy. The remaining error is attributed to the fact that PZ SIC violates the exactness of SCAN for slowly-varying densities. By the same token, PZ SIC raises the energy of the transition states (via stretched bonds and nodality of real orbitals) relative to the separated molecules, yielding improved barrier heights. We found that PZ SIC barrier heights are greatly improved for the representative test set BH6 when we go from LSDA to PBE to SCAN.

BIBLIOGRAPHY

- [1] Qiming Sun, Timothy C Berkelbach, Nick S Blunt, George H Booth, Sheng Guo, Zhendong Li, Junzi Liu, James D McClain, Elvira R Sayfutyarova, Sandeep Sharma, et al. Pyscf: the python-based simulations of chemistry framework. *Wiley Interdisciplinary Reviews: Computational Molecular Science*, 8(1):e1340, 2018.
- [2] Susi Lehtola, Conrad Steigemann, Micael JT Oliveira, and Miguel AL Marques. Recent developments in libxc: comprehensive library of functionals for density functional theory. *SoftwareX*, 7:1–5, 2018.
- [3] Thom H Dunning Jr. Gaussian basis sets for use in correlated molecular calculations. i. the atoms boron through neon and hydrogen. *The Journal of chemical physics*, 90(2):1007–1023, 1989.
- [4] T. Baruah developed by R.R. Zope and based on the NRLMOL code of M.R. Pederson. K.A. Jackson. Flosic 0.1.2,.
- [5] Susi Lehtola. Fully numerical hartree-fock and density functional calculations. ii. diatomic molecules. *International Journal of Quantum Chemistry*, 119(19):e25944, 2019.
- [6] Susi Lehtola. Heifem finite element methods for electronic structure calculations on small systems.
- [7] Dirk Porezag and Mark R Pederson. Optimization of gaussian basis sets for density-functional calculations. *Physical Review A*, 60(4):2840, 1999.
- [8] Jianwei Sun, John P Perdew, Zenghui Yang, and Haowei Peng. Communication: Near-locality of exchange and correlation density functionals for 1-and 2-electron systems, 2016.
- [9] Yubo Zhang, Daniil A Kitchaev, Julia Yang, Tina Chen, Stephen T Dacek, Rafael A Sarmiento-Pérez, Maguel AL Marques, Haowei Peng, Gerbrand Ceder, John P Perdew, et al. Efficient first-principles prediction of solid stability: Towards chemical accuracy. *npj Computational Materials*, 4(1):9, 2018.
- [10] Benjamin J Lynch and Donald G Truhlar. Small representative benchmarks for thermochemical calculations. *The Journal of Physical Chemistry A*, 107(42):8996–8999, 2003.

- [11] Jussi Lehtola, Mikko Hakala, Arto Sakko, and Keijo Hämäläinen. Erkalea flexible program package for x-ray properties of atoms and molecules. *Journal of computational chemistry*, 33(18):1572–1585, 2012.
- [12] Oleg A Vydrov. *Correcting the self-interaction error of approximate density functionals*. PhD thesis, 2007.
- [13] Larry A Curtiss, Krishnan Raghavachari, Paul C Redfern, and John A Pople. Assessment of gaussian-2 and density functional theories for the computation of enthalpies of formation. *The Journal of Chemical Physics*, 106(3):1063–1079, 1997.
- [14] T. Hahn developed by S. Schwalbe, L. Fiedler and J. Kortus. Pyflosic, flo-sic implementation based on the pyscf code.
- [15] Sebastian Schwalbe, Torsten Hahn, Simon Liebing, Kai Trepte, and Jens Kortus. Fermi-löwdin orbital self-interaction corrected density functional theory: Ionization potentials and enthalpies of formation. *Journal of computational chemistry*, 39(29):2463–2471, 2018.
- [16] Simon Klüpfel, Peter Klüpfel, and Hannes Jónsson. Importance of complex orbitals in calculating the self-interaction-corrected ground state of atoms. *Physical Review A*, 84(5):050501, 2011.
- [17] Axel D Becke. Density-functional exchange-energy approximation with correct asymptotic behavior. *Physical review A*, 38(6):3098, 1988.
- [18] Kieron Burke, Antonio Cancio, Tim Gould, and Stefano Pittalis. Locality of correlation in density functional theory. *The Journal of chemical physics*, 145(5):054112, 2016.
- [19] Note that the default grid level in pyscf and pyflosic is not the same for all atoms, but changes from the lowest one for the h atom to better meshes for heavier elements.
- [20] R. D. Johnson. Computational chemistry comparison and benchmark database. *NIST standard reference database*, 101, 2016.
- [21] E. Schrödinger. Quantisierung als eigenwertproblem. *Annalen der physik*, pages 385–437, 1926.
- [22] Max Born and Robert Oppenheimer. Zur quantentheorie der molekeln. *Annalen der physik*, 389(20):457–484, 1927.
- [23] Douglas R Hartree. The wave mechanics of an atom with a non-coulomb central field. part i. theory and methods. In *Mathematical Proceedings of the Cambridge Philosophical Society*, volume 24, pages 89–110. Cambridge University Press, 1928.

- [24] Vladimir Fock. Näherungsmethode zur lösung des quantenmechanischen mehrkörperproblems. *Zeitschrift für Physik*, 61(1-2):126–148, 1930.
- [25] A. Szabo and N. S. Ostlund. *Modern quantum chemistry: introduction to advanced electronic-structure theory*. 2012.
- [26] Jorge Kohanoff. *Electronic Structure Calculations for Solids and Molecules: Theory and Computational methods*. 2006.
- [27] Rodney J Bartlett. Coupled-cluster approach to molecular structure and spectra: a step toward predictive quantum chemistry. *The Journal of Physical Chemistry*, 93(5):1697–1708, 1989.
- [28] Chr Møller and Milton S Plesset. Note on an approximation treatment for many-electron systems. *Physical review*, 46(7):618, 1934.
- [29] Walter Kohn. Nobel lecture: Electronic structure of matterwave functions and density functionals. *Reviews of Modern Physics*, 71(5):1253, 1999.
- [30] Pierre Hohenberg and Walter Kohn. Inhomogeneous electron gas. *Physical review*, 136(3B):B864, 1964.
- [31] Walter Kohn and Lu Jeu Sham. Self-consistent equations including exchange and correlation effects. *Physical review*, 140(4A):A1133, 1965.
- [32] Robert G. Parr and Yang. Weitao. *Density Functional Theory of Atoms and Molecules: Theory and Computational methods*. 1989.
- [33] Llewellyn H Thomas. The calculation of atomic fields. In *Mathematical Proceedings of the Cambridge Philosophical Society*, volume 23, pages 542–548. Cambridge University Press, 1927.
- [34] Enrico Fermi. Un metodo statistico per la determinazione di alcune priorietà dellatome. *Rend. Accad. Naz. Lincei*, 6(602-607):32, 1927.
- [35] Edward Teller. On the stability of molecules in the thomas-fermi theory. *Reviews of Modern Physics*, 34(4):627, 1962.
- [36] P Csavinsky. Approximate analytical solutions of the thomas-fermi-dirac and thomas-fermi-dirac-gombás equations. *The Journal of Chemical Physics*, 50(6):2476–2485, 1969.
- [37] Paul AM Dirac. Note on exchange phenomena in the thomas atom. In *Mathematical Proceedings of the Cambridge Philosophical Society*, volume 26, pages 376–385. Cambridge University Press, 1930.
- [38] Eugene Wigner. Effects of the electron interaction on the energy levels of electrons in metals. *Transactions of the Faraday Society*, 34:678–685, 1938.

- [39] CF v Weizsäcker. Zur theorie der kernmassen. *Zeitschrift für Physik A Hadrons and Nuclei*, 96(7):431–458, 1935.
- [40] H Englisch and R Englisch. Hohenberg-kohn theorem and non-v-representable densities. *Physica A: Statistical Mechanics and its Applications*, 121(1-2):253–268, 1983.
- [41] Mel Levy. Electron densities in search of hamiltonians. *Physical Review A*, 26(3):1200, 1982.
- [42] E. H. Lieb. Physics as natural philosophy: Essays in honor of laszlo tizsa on his 75th birthday, 1982.
- [43] Mel Levy. Universal variational functionals of electron densities, first-order density matrices, and natural spin-orbitals and solution of the v-representability problem. *Proceedings of the National Academy of Sciences*, 76(12):6062–6065, 1979.
- [44] Elliot H Lieb. Variational principle for many-fermion systems. *Physical Review Letters*, 46(7):457, 1981.
- [45] Thomas L Gilbert. Hohenberg-kohn theorem for nonlocal external potentials. *Physical Review B*, 12(6):2111, 1975.
- [46] David C Langreth and John P Perdew. Exchange-correlation energy of a metallic surface: Wave-vector analysis. *Physical Review B*, 15(6):2884, 1977.
- [47] David C Langreth and John P Perdew. The exchange-correlation energy of a metallic surface. *Solid State Communications*, 17(11):1425–1429, 1975.
- [48] J. P. Perdew and K. Kurth. *A Primer in Density Functional Theory: Theory and Computational methods*. 2002.
- [49] Olle Gunnarsson and Bengt I Lundqvist. Exchange and correlation in atoms, molecules, and solids by the spin-density-functional formalism. *Physical Review B*, 13(10):4274, 1976.
- [50] J Harris and RO Jones. The surface energy of a bounded electron gas. *Journal of Physics F: Metal Physics*, 4(8):1170, 1974.
- [51] John P Perdew and Alex Zunger. Self-interaction correction to density-functional approximations for many-electron systems. *Physical Review B*, 23(10):5048, 1981.
- [52] Mel Levy and John P Perdew. Hellmann-feynman, virial, and scaling requisites for the exact universal density functionals. shape of the correlation potential and diamagnetic susceptibility for atoms. *Physical Review A*, 32(4):2010, 1985.
- [53] GL Oliver and JP Perdew. Spin-density gradient expansion for the kinetic energy. *Physical Review A*, 20(2):397, 1979.

- [54] Elliott H Lieb and Stephen Oxford. Improved lower bound on the indirect coulomb energy. *International Journal of Quantum Chemistry*, 19(3):427–439, 1981.
- [55] Mel Levy. Density-functional exchange correlation through coordinate scaling in adiabatic connection and correlation hole. *Physical Review A*, 43(9):4637, 1991.
- [56] Murray Gell-Mann and Keith A Brueckner. Correlation energy of an electron gas at high density. *Physical Review*, 106(2):364, 1957.
- [57] Rosemary A Coldwell-Horsfall and Alexei A Maradudin. Zero-point energy of an electron lattice. *Journal of Mathematical Physics*, 1(5):395–404, 1960.
- [58] David M Ceperley and BJ Alder. Ground state of the electron gas by a stochastic method. *Physical Review Letters*, 45(7):566, 1980.
- [59] Seymour H Vosko, Leslie Wilk, and Marwan Nusair. Accurate spin-dependent electron liquid correlation energies for local spin density calculations: a critical analysis. *Canadian Journal of physics*, 58(8):1200–1211, 1980.
- [60] John P Perdew and Yue Wang. Accurate and simple analytic representation of the electron-gas correlation energy. *Physical Review B*, 45(23):13244, 1992.
- [61] KEITH A BRUECKNER et al. Correlation energy of an electron gas with a slowly varying high density. *Physical Review*, 165(1):18, 1968.
- [62] David C Langreth and MJ Mehl. Beyond the local-density approximation in calculations of ground-state electronic properties. *Physical Review B*, 28(4):1809, 1983.
- [63] John P Perdew and Wang Yue. Accurate and simple density functional for the electronic exchange energy: Generalized gradient approximation. *Physical review B*, 33(12):8800, 1986.
- [64] Axel D Becke. Density functional calculations of molecular bond energies. *The Journal of Chemical Physics*, 84(8):4524–4529, 1986.
- [65] John P Perdew, Kieron Burke, and Matthias Ernzerhof. Generalized gradient approximation made simple. *Physical review letters*, 77(18):3865, 1996.
- [66] John P Perdew, Stefan Kurth, Aleš Zupan, and Peter Blaha. Accurate density functional with correct formal properties: A step beyond the generalized gradient approximation. *Physical review letters*, 82(12):2544, 1999.
- [67] Jianmin Tao, John P Perdew, Viktor N Staroverov, and Gustavo E Scuseria. Climbing the density functional ladder: Nonempirical meta-generalized gradient approximation designed for molecules and solids. *Physical Review Letters*, 91(14):146401, 2003.

- [68] John P Perdew, Jianmin Tao, Viktor N Staroverov, and Gustavo E Scuseria. Meta-generalized gradient approximation: Explanation of a realistic nonempirical density functional. *The Journal of chemical physics*, 120(15):6898–6911, 2004.
- [69] Adrienn Ruzsinszky, Jianwei Sun, Bing Xiao, and Gbor I. Csonka. A meta-gga made free of the order of limits anomaly. *Journal of Chemical Theory and Computation*, 8(6):2078–2087, 2012. PMID: 26593840.
- [70] Jianwei Sun, Bing Xiao, and Adrienn Ruzsinszky. Communication: Effect of the orbital-overlap dependence in the meta generalized gradient approximation, 2012.
- [71] Jianwei Sun, Robin Haunschild, Bing Xiao, Ireneusz W Bulik, Gustavo E Scuseria, and John P Perdew. Semilocal and hybrid meta-generalized gradient approximations based on the understanding of the kinetic-energy-density dependence. *The Journal of chemical physics*, 138(4):044113, 2013.
- [72] Jianwei Sun, Adrienn Ruzsinszky, and John P Perdew. Strongly constrained and appropriately normed semilocal density functional. *Physical review letters*, 115(3):036402, 2015.
- [73] Jianwei Sun, John P Perdew, and Adrienn Ruzsinszky. Semilocal density functional obeying a strongly tightened bound for exchange. *Proceedings of the National Academy of Sciences*, 112(3):685–689, 2015.
- [74] Mohan Chen, Hsin-Yu Ko, Richard C. Remsing, Marcos F. Calegari Andrade, Biswajit Santra, Zhaoru Sun, Annabella Selloni, Roberto Car, Michael L. Klein, John P. Perdew, and Xifan Wu. Ab initio theory and modeling of water. *Proc. Natl. Acad. Sci. U.S.A.*, 114(41):10846–10851, 2017.
- [75] Abhirup Patra, Jefferson E Bates, Jianwei Sun, and John P Perdew. Pnas plus significance statements. *Proc. Natl. Acad. Sci. U.S.A.*, 114(44):11577–11581, 2017.
- [76] Richard C. Remsing, Michael L. Klein, and Jianwei Sun. Dependence of the structure and dynamics of liquid silicon on the choice of density functional approximation. *Phys. Rev. B*, 96:024203, Jul 2017.
- [77] J. Sun, R. C. Remsing, Y. Zhang, Z. Sun, A. Ruzsinszky, H. Peng, Zeng-Hui Yang, A. Paul, U. Waghmare, X. Wu, M. L. Klein, and J. P. Perdew. *Nature Chemistry*, 2016.
- [78] Daniil A. Kitchaev, Haowei Peng, Yun Liu, Jianwei Sun, John P. Perdew, and Gerbrand Ceder. Energetics of mno_2 polymorphs in density functional theory. *Phys. Rev. B*, 93:045132, Jan 2016.

- [79] Niraj K. Nepal, Liping Yu, Qimin Yan, and Adrienn Ruzsinszky. First-principles study of mechanical and electronic properties of bent monolayer transition metal dichalcogenides. *Phys. Rev. Materials*, 3:073601, Jul 2019.
- [80] James W Furness, Yubo Zhang, Christopher Lane, Ioana Gianina Buda, Bernardo Barbiellini, Robert S Markiewicz, Arun Bansil, and Jianwei Sun. An accurate first-principles treatment of doping-dependent electronic structure of high-temperature cuprate superconductors. *Communications Physics*, 1(1):11, 2018.
- [81] Christopher Lane, James W. Furness, Ioana Gianina Buda, Yubo Zhang, Robert S. Markiewicz, Bernardo Barbiellini, Jianwei Sun, and Arun Bansil. Antiferromagnetic ground state of La_2CuO_4 : A parameter-free ab initio description. *Phys. Rev. B*, 98:125140, Sep 2018.
- [82] Subrata Jana, Abhilash Patra, and Prasanjit Samal. Assessing the performance of the tao-mo semilocal density functional in the projector-augmented-wave method. *The Journal of Chemical Physics*, 149(4):044120, 2018.
- [83] Marcus Ekholm, Davide Gambino, H Johan M Jönsson, Ferenc Tasnádi, Björn Alling, and Igor A Abrikosov. Assessing the scan functional for itinerant electron ferromagnets. *Physical Review B*, 98(9):094413, 2018.
- [84] Daniel Mejía-Rodríguez and S. B. Trickey. Analysis of over-magnetization of elemental transition metal solids from the scan density functional. *Phys. Rev. B*, 100:041113, Jul 2019.
- [85] A Seidl, A Görling, P Vogl, JA Majewski, and M Levy. Generalized kohn-sham schemes and the band-gap problem. *Physical Review B*, 53(7):3764, 1996.
- [86] Mark R Pederson, Adrienn Ruzsinszky, and John P Perdew. Communication: Self-interaction correction with unitary invariance in density functional theory, 2014.
- [87] Zeng-hui Yang, Mark R Pederson, and John P Perdew. Full self-consistency in the fermi-orbital self-interaction correction. *Physical Review A*, 95(5):052505, 2017.
- [88] Per-Olov Löwdin. The normal constants of motion in quantum mechanics treated by projection technique. *Reviews of Modern Physics*, 34(3):520, 1962.
- [89] Mark R Pederson, Richard A Heaton, and Chun C Lin. Density-functional theory with self-interaction correction: Application to the lithium molecule. *The Journal of chemical physics*, 82(6):2688–2699, 1985.
- [90] A. Mujica, Angel Rubio, A. Muñoz, and R. J. Needs. *Rev. Mod. Phys.*, 75, 2003.
- [91] R. G. Hennig, A. Wadehra, K. P. Driver, W. D. Parker, C. J. Umrigar, and J. W. Wilkins. *Phys. Rev. B*, 82:014101, 2010.

- [92] B. Xiao, J. Sun, Adrienn Ruzsinszky, Jing Feng, Robin Haunschuld, Gustavo E. Scuseria, and John P. Perdew. *Phys. Rev. B*, 88:184103, 2013.
- [93] E. R. Batista, J. Heyd, R. G. Hennig, B. P. Uberuaga, R. L. Martin, G. E. Scuseria, C. J. Umrigar, and J. W. Wilkins. *Phys. Rev. B*, 74:121102, 2006.
- [94] J. P. Perdew and K. Schmidt. in *Density Functional Theory and its Application to Materials*. Number 577 in AIP Conf. Proc. AIP, Melville, NY, 2001.
- [95] A. Paul, J. Sun, J. P. Perdew, and U. V. Waghmare. Accuracy of first-principles interatomic interactions and predictions of ferroelectric phase transitions in perovskite oxides: Energy functional and effective hamiltonian. *Phys. Rev. B*, 95:054111, Feb 2017.
- [96] Zeng-Hui Yang, H. Peng, J. Sun, and J. P. Perdew. *Phys. Rev. B*, 93:205205, 2016.
- [97] G. Kresse and J. Furthmüller. *Phys. Rev. B*, 54:11169–11186, 1996.
- [98] G. Kresse and D. Joubert. *Phys. Rev. B*, 59:1758–1775, 1999.
- [99] FD Murnaghan. *Proc. Natl. Acad. Sci. U.S.A.*, 30(9):244–247, 1944.
- [100] K. Gaál-Nagy, A. Bauer, M. Schmitt, K. Karch, P. Pavone, and D. Strauch. Temperature and dynamical effects on the high-pressure cubic-diamond -tin phase transition in si and ge. *physica status solidi (b)*, 211(1):275–280, 1999.
- [101] J. Z. Hu, L. D. Merkle, C. S. Menoni, and I. L. Spain. *Phys. Rev. B*, 34:4679–4684, 1986.
- [102] Carmen S. Menoni, J. Z. Hu, and I. L. Spain. *Phys. Rev. B*, 34:362–368, 1986.
- [103] N. Moll, M. Bockstedte, M. Fuchs, E. Pehlke, and M. Scheffler. *Phys. Rev. B*, 52:2550–2556, 1995.
- [104] B. H. Cheong and K. J. Chang. *Phys. Rev. B*, 44:4103–4108, 1991.
- [105] N. E. Christensen and M. Methfessel. *Phys. Rev. B*, 48:5797–5807, 1993.
- [106] H. Olijnyk and W. Holzapfel. *J. Phys. Colloq.*, 45:C8–153, 1984.
- [107] Jennifer L. Corkill, Alberto García, and Marvin L. Cohen. Theoretical study of high-pressure phases of tin. *Phys. Rev. B*, 43:9251–9254, Apr 1991.
- [108] A. Y. Liu, A. García, M. L. Cohen, B. K. Godwal, and R. Jeanloz. Theory of high-pressure phases of pb. *Phys. Rev. B*, 43:1795–1798, 1991.
- [109] H.K. Mao, Y. Wu, J.F. Shu, J.Z. Hu, R.J. Hemley, and D.E. Cox. *Solid State Commun.*, 74(9):1027 – 1029, 1990.

- [110] K. Karch, F. Bechstedt, P. Pavone, and D. Strauch. *Phys. Rev. B*, 53:13400–13413, 1996.
- [111] M. Yoshida, A. Onodera, M. Ueno, K. Takemura, and O. Shimomura. *Phys. Rev. B*, 48:10587–10590, 1993.
- [112] M Baublitz Jr. and A. L. Ruoff. *J. Appl. Phys.*, 53(9):6179–6185, 1982.
- [113] J. Z. Hu, D. R. Black, and I. L. Spain. *Solid State Commun.*, 51(5):285 – 287, 1984.
- [114] R. J. Nelmes, M. I. McMahon, and S. A. Belmonte. *Phys. Rev. Lett.*, 79:3668–3671, 1997.
- [115] A. Mujica and R. J. Needs. *Phys. Rev. B*, 55:9659–9670, 1997.
- [116] Samuel T. Weir, Yogesh K. Vohra, Craig A. Vanderborgh, and Arthur L. Ruoff. *Phys. Rev. B*, 39:1280–1285, 1989.
- [117] M. I. McMahon and R. J. Nelmes. *Phys. Rev. Lett.*, 78:3697–3700, 1997.
- [118] Andrs Mujica and R J Needs. *J. Phys. Condens. Matter*, 8(15):L237, 1996.
- [119] C. N. M. Ouma, M. Z. Mapelu, N. W. Makau, G. O. Amolo, and Ryo Maezono. Quantum monte carlo study of pressure-induced $b3 - b1$ phase transition in gaas. *Phys. Rev. B*, 86:104115, Sep 2012.
- [120] H. Peng and S. Lany. *Phys. Rev. B*, 87:174113, 2013.
- [121] J. Serrano, A. Rubio, E. Hernández, A. Muñoz, and A. Mujica. *Phys. Rev. B*, 62:16612–16623, 2000.
- [122] P. Perlin, C. Jauberthie-Carillon, J. P. Itié, A. San Miguel, I. Grzegory, and A. Polian. *Phys. Rev. B*, 45:83–89, 1992.
- [123] M. Ueno, M. Yoshida, A. Onodera, O. Shimomura, and K. Takemura. *Phys. Rev. B*, 49:14–21, 1994.
- [124] H. Xia, Q. Xia, and A. L. Ruoff. *Phys. Rev. B*, 47:12925–12928, 1993.
- [125] Q. Xia, H. Xia, and A. L. Ruoff. *J. Phys. Condens. Matter*, 08(05):345–350, 1994.
- [126] Q. Xia, H. Xia, and A. L. Ruoff. *J. Appl. Phys.*, 73(12):8198–8200, 1993.
- [127] M. Ueno, A. Onodera, O. Shimomura, and K. Takemura. *Phys. Rev. B*, 45:10123–10126, 1992.
- [128] S. Uehara, T. Masamoto, Akifumi Onodera, Masaki Ueno, O. Shimomura, and K. Takemura. *J. Phys. Chem. Solids*, 58(12):2093 – 2099, 1997.

- [129] O. Arbouche, B. Belgoumène, B. Soudini, Y. Azzaz, H. Bendaoud, and K. Amara. *Comput. Mater. Sci.*, 47(3):685 – 692, 2010.
- [130] Carmen S. Menoni and Ian L. Spain. *Phys. Rev. B*, 35:7520–7525, 1987.
- [131] R. J. Nelmes, M. I. McMahon, N. G. Wright, D. R. Allan, H. Liu, and J. S. Loveday. *J. Phys. Chem. Solids*, 56(3):539 – 543, 1995.
- [132] A. Mujica, P. Rodríguez-Hernández, S. Radescu, R. J. Needs, and A. Muñoz. *Physica Status Solidi (b)*, 211(1):39–43, 1999.
- [133] R. G. Greene, H. Luo, and A. L. Ruoff. *J. Appl. Phys.*, 76(11):7296–7299, 1994.
- [134] R. G. Greene, H. Luo, T. Li, and A. L. Ruoff. *Phys. Rev. Lett.*, 72:2045–2048, 1994.
- [135] Y. K. Vohra, S. T. Weir, and A. L. Ruoff. *Phys. Rev. B*, 31:7344–7348, 1985.
- [136] S. Froyen and M. L. Cohen. *Phys. Rev. B*, 28:3258–3265, 1983.
- [137] R. G. Greene, H. Luo, K. Ghandehari, and A. L. Ruoff. *J. Phys. Chem. Solids*, 56(3):517 – 520, 1995.
- [138] F. Decremps, J. Zhang, and R. C. Liebermann. *EPL (Europhysics Letters)*, 51(3):268, 2000.
- [139] Serge Desgreniers. *Phys. Rev. B*, 58:14102–14105, 1998.
- [140] J. E. Jaffe, J. A. Snyder, Z. Lin, and A. C. Hess. *Phys. Rev. B*, 62:1660–1665, 2000.
- [141] W. H. Gust. *J. Appl. Phys.*, 53(7):4843–4846, 1982.
- [142] Y. Zhou, A. J. Campbell, and D. L. Heinz. *J. Phys. Chem. Solids*, 52(6):821 – 825, 1991.
- [143] Jun Yang, Feng Zhu, Qian Zhang, Ye Wu, Xiang Wu, Shan Qin, Jun-Cai Dong, and Dong-Liang Chen. In situ xafs investigation on zincblende zns up to 31.7 gpa. *Chin. Phys. Lett.*, 30(4):046101, 2013.
- [144] Valeri I. Smelyansky and John S. Tse. Theoretical study on the high-pressure phase transformation in znse. *Phys. Rev. B*, 52:4658–4661, Aug 1995.
- [145] Galit Itkin, Giovanni R. Hearne, Eran Sterer, Moshe P. Pasternak, and Walter Potzel. *Phys. Rev. B*, 51:3195–3197, 1995.
- [146] S. Cui, H. Hu, W. Feng, X. Chen, and Z. Feng. *J. Alloys Compd.*, 472(1):294 – 298, 2009.
- [147] A. San-Miguel, A. Polian, M. Gauthier, and J. P. Itié. *Phys. Rev. B*, 48:8683–8693, 1993.

- [148] A. Qteish, M. Abu-Jafar, and A. Nazzal. *J. Phys. Condens. Matter*, 10(23):5069, 1998.
- [149] Xiang-Rong Chen, Xiao-Feng Li, Ling-Cang Cai, and Jun Zhu. Pressure induced phase transition in zns. *Solid State Commun.*, 139(5):246–249, 2006.
- [150] Jia Jin Tan, Guang Fu Ji, Xiang Rong Chen, and Qing Quan Gou. Phase transition and phonon spectrum of zinc-blende structure znx (x= s, se, te). *Communications in Theoretical Physics*, 53(6):1160, 2010.
- [151] H. Karzel, W. Potzel, M. Köfferlein, W. Schiessl, M. Steiner, U. Hiller, G. M. Kalvius, D. W. Mitchell, T. P. Das, P. Blaha, K. Schwarz, and M. P. Pasternak. *Phys. Rev. B*, 53:11425–11438, 1996.
- [152] M. Côté, O. Zakharov, A. Rubio, and M. L. Cohen. *Phys. Rev. B*, 55:13025–13031, 1997.
- [153] M. D. Knudson, Y. M. Gupta, and A. B. Kunz. *Phys. Rev. B*, 59:11704–11715, 1999.
- [154] H. Sowa. *Solid State Sci*, 7(1):73 – 78, 2005.
- [155] Y. Li, X. Zhang, H. Li, X. Li, C. Lin, W. Xiao, and J. Liu. *J. Appl. Phys.*, 113(8):083509, 2013.
- [156] H. Sowa. *Solid State Sci*, 7(11):1384 – 1389, 2005.
- [157] A. N. Mariano and E. P. Warekois. . *Science*, 142:672–673, 1963.
- [158] C. He, C X Gao, B G Liu, M. Li, X W Huang, A M Hao, C L Yu, D M Zhang, Y Wang, H W Liu, Y Z Ma, and Z T Zou. *J. Phys. Condens. Matter*, 19(42):425223, 2007.
- [159] S. R. Sun and Y. H. Dong. *Phys. Rev. B*, 72:174101, 2005.
- [160] R. J. Nelmes and M.I. McMahon. *in Semiconductors and Semimetals*. Academic Press, New York, 1998.
- [161] S. Radescu, A. Mujica, J. López-Solano, and R. J. Needs. Theoretical study of pressure-driven phase transitions in hgse and hgte. *Phys. Rev. B*, 83:094107, 2011.
- [162] M. I. McMahon, R. J. Nelmes, H. Liu, and S. A. Belmonte. *Phys. Rev. Lett.*, 77:1781–1784, 1996.
- [163] A. Ohtani, T. Seike, M. Motobayashi, and A. Onodera. *J. Phys. Chem. Solids*, 43(7):627 – 632, 1982.
- [164] A. San-Miguel, N. G. Wright, M. I. McMahon, and R. J. Nelmes. *Phys. Rev. B*, 51:8731–8736, 1995.

- [165] R. J. Nelmes, M. I. McMahon, N. G. Wright, and D. R. Allan. *Phys. Rev. B*, 48:1314–1317, 1993.
- [166] D. C. Langreth and J. P. Perdew. Theory of nonuniform electronic systems. i. analysis of the gradient approximation and a generalization that works. *Phys. Rev. B*, 21:5469–5493, Jun 1980.
- [167] Niladri Sengupta, Jefferson E. Bates, and Adrienn Ruzsinszky. From semilocal density functionals to random phase approximation renormalized perturbation theory: A methodological assessment of structural phase transitions. *Phys. Rev. B*, 97:235136, Jun 2018.
- [168] Menno Bokdam, Jonathan Lahnsteiner, Benjamin Ramberger, Tobias Schäfer, and Georg Kresse. Assessing density functionals using many body theory for hybrid perovskites. *Phys. Rev. Lett.*, 119:145501, Oct 2017.
- [169] Niraj K. Nepal, Adrienn Ruzsinszky, and Jefferson E. Bates. Rocksalt or cesium chloride: Investigating the relative stability of the cesium halide structures with random phase approximation based methods. *Phys. Rev. B*, 97:115140, Mar 2018.
- [170] Haowei Peng, Zeng-Hui Yang, John P. Perdew, and Jianwei Sun. Versatile van der waals density functional based on a meta-generalized gradient approximation. *Phys. Rev. X*, 6:041005, Oct 2016.
- [171] R. Armiento and A. E. Mattsson. Functional designed to include surface effects in self-consistent density functional theory. *Phys. Rev. B*, 72:085108, Aug 2005.
- [172] John P. Perdew, Adrienn Ruzsinszky, Gábor I. Csonka, Oleg A. Vydrov, Gustavo E. Scuseria, Lucian A. Constantin, Xiaolan Zhou, and Kieron Burke. Restoring the density-gradient expansion for exchange in solids and surfaces. *Phys. Rev. Lett.*, 100:136406, Apr 2008.
- [173] Yoyo Hinuma, Hiroyuki Hayashi, Yu Kumagai, Isao Tanaka, and Fumiyasu Oba. Comparison of approximations in density functional theory calculations: Energetics and structure of binary oxides. *Phys. Rev. B*, 96:094102, Sep 2017.
- [174] Lars Goerigk, Andreas Hansen, Christoph Alexander Bauer, Stephan Ehrlich, Asim Najibi, and Stefan Grimme. A look at the density functional theory zoo with the advanced gmtkn55 database for general main group thermochemistry, kinetics and noncovalent interactions. *Phys. Chem. Chem. Phys., early edition*. doi:10.1039/C7CP04913G, 2017.
- [175] J. D. Hunter. Matplotlib: A 2d graphics environment. *Computing In Science & Engineering*, 9(3):90–95, 2007.
- [176] Stefano Curtarolo, Wahyu Setyawan, Gus LW Hart, Michal Jahnatek, Roman V Chepulskii, Richard H Taylor, Shidong Wang, Junkai Xue, Kesong Yang, Ohad

- Levy, et al. Aflow: an automatic framework for high-throughput materials discovery. *Computational Materials Science*, 58:218–226, 2012.
- [177] Robert O Jones. Density functional theory: Its origins, rise to prominence, and future. *Reviews of modern physics*, 87(3):897, 2015.
- [178] Daniel Mejia-Rodriguez and SB Trickey. Deorbitalized meta-gga exchange-correlation functionals in solids. *Physical Review B*, 98(11):115161, 2018.
- [179] Yubo Zhang, Jianwei Sun, John P Perdew, and Xifan Wu. Comparative first-principles studies of prototypical ferroelectric materials by lda, gga, and scan meta-gga. *Physical Review B*, 96(3):035143, 2017.
- [180] Haowei Peng and John P Perdew. Synergy of van der waals and self-interaction corrections in transition metal monoxides. *Physical Review B*, 96(10):100101, 2017.
- [181] Chandra Shahi, Jianwei Sun, and John P Perdew. Accurate critical pressures for structural phase transitions of group iv, iii-v, and ii-vi compounds from the scan density functional. *Physical Review B*, 97(9):094111, 2018.
- [182] Yingkai Zhang and Weitao Yang. A challenge for density functionals: Self-interaction error increases for systems with a noninteger number of electrons. *The Journal of chemical physics*, 109(7):2604–2608, 1998.
- [183] Adrienn Ruzsinszky, John P Perdew, and Gabor I Csonka. Binding energy curves from nonempirical density functionals. i. covalent bonds in closed-shell and radical molecules. *The Journal of Physical Chemistry A*, 109(48):11006–11014, 2005.
- [184] Adrienn Ruzsinszky, John P Perdew, Gábor I Csonka, Oleg A Vydrov, and Gustavo E Scuseria. Spurious fractional charge on dissociated atoms: Pervasive and resilient self-interaction error of common density functionals. *The Journal of chemical physics*, 125(19):194112, 2006.
- [185] Serguei Patchkovskii and Tom Ziegler. Improving difficult reaction barriers with self-interaction corrected density functional theory. *The Journal of Chemical Physics*, 116(18):7806–7813, 2002.
- [186] Biswajit Santra and John P Perdew. Perdew-zunger self-interaction correction: How wrong for uniform densities and large-z atoms? *The Journal of chemical physics*, 150(17):174106, 2019.
- [187] Mark R Pederson, Richard A Heaton, and Chun C Lin. Local-density hartree-fock theory of electronic states of molecules with self-interaction correction. *The Journal of chemical physics*, 80(5):1972–1975, 1984.

- [188] Wuming Zhu, Liang Zhang, and SB Trickey. Random phase approximation with second-order screened exchange for current-carrying atomic states. *The Journal of chemical physics*, 145(22):224106, 2016.
- [189] Oleg A Vydrov and Gustavo E Scuseria. Effect of the perdew–zunger self-interaction correction on the thermochemical performance of approximate density functionals. *The Journal of chemical physics*, 121(17):8187–8193, 2004.
- [190] Susi Lehtola, Elvar O Jonsson, and Hannes Jonsson. Effect of complex-valued optimal orbitals on atomization energies with the perdew–zunger self-interaction correction to density functional theory. *Journal of chemical theory and computation*, 12(9):4296–4302, 2016.
- [191] Susi Lehtola, Martin Head-Gordon, and Hannes Jónsson. Complex orbitals, multiple local minima, and symmetry breaking in perdew–zunger self-interaction corrected density functional theory calculations. *Journal of chemical theory and computation*, 12(7):3195–3207, 2016.
- [192] Giovanni Borghi, Andrea Ferretti, Ngoc Linh Nguyen, Ismaila Dabo, and Nicola Marzari. Koopmans-compliant functionals and their performance against reference molecular data. *Physical Review B*, 90(7):075135, 2014.
- [193] Oleg A Vydrov, Gustavo E Scuseria, John P Perdew, Adrienn Ruzsinszky, and Gábor I Csonka. Scaling down the perdew-zunger self-interaction correction in many-electron regions. *The Journal of chemical physics*, 124(9):094108, 2006.
- [194] D Hofmann, S Klüpfel, P Klüpfel, and S Kümmel. Using complex degrees of freedom in the kohn-sham self-interaction correction. *Physical Review A*, 85(6):062514, 2012.
- [195] John P Perdew, Kieron Burke, and Yue Wang. Generalized gradient approximation for the exchange-correlation hole of a many-electron system. *Physical Review B*, 54(23):16533, 1996.
- [196] Lucian A Constantin, Eduardo Fabiano, and Fabio Della Sala. Construction of a general semilocal exchange-correlation hole model: Application to nonempirical meta-gga functionals. *Physical Review B*, 88(12):125112, 2013.
- [197] John P. Perdew, Robert G. Parr, Mel Levy, and Jose L. Balduz. Density-functional theory for fractional particle number: Derivative discontinuities of the energy. *Phys. Rev. Lett.*, 49:1691–1694, Dec 1982.
- [198] Santra B. Perdew, J. P. and T. Hahn. Work in progress. *The Journal of Chemical Physics*, 106(3):1063–1079, 1997.
- [199] Chen Li, Xiao Zheng, Neil Qiang Su, and Weitao Yang. Localized orbital scaling correction for systematic elimination of delocalization error in density functional approximations. *National Science Review*, 5(2):203–215, 2017.

- [200] M. R. Pederson. Private communication. 106(3):1063–1079, 1997.
- [201] Per-Olov Löwdin. Quantum theory of many-particle systems. iii. extension of the hartree-fock scheme to include degenerate systems and correlation effects. *Phys. Rev.*, 97:1509–1520, Mar 1955.
- [202] Ionut D Prodan, Gustavo E Scuseria, and Richard L Martin. Covalency in the actinide dioxides: Systematic study of the electronic properties using screened hybrid density functional theory. *Physical Review B*, 76(3):033101, 2007.
- [203] Simon Klüpfel, Peter Klüpfel, and Hannes Jónsson. The effect of the perdew-zunger self-interaction correction to density functionals on the energetics of small molecules. *The Journal of chemical physics*, 137(12):124102, 2012.
- [204] F. Bloch. *Zeitschrift für Physik*. volume 57, page 545. Cambridge University Press, 1929.
- [205] Miguel AL Marques, Micael JT Oliveira, and Tobias Burnus. Libxc: A library of exchange and correlation functionals for density functional theory. *Computer physics communications*, 183(10):2272–2281, 2012.

APPENDIX

LIST OF PUBLICATIONS

- *Origin of the size-dependence of the equilibrium van der Waals binding between nanostructures.* Jianmin Tao, John P. Perdew, Hong Tang, and **Chandra Shahi**, J. Chem. Phys. 148, 074110 (2018)
- *Accurate critical pressures for structural phase transitions of group IV, III-V, and II-VI compounds from the SCAN density functional.* **Chandra Shahi**, Jianwei Sun, and John P. Perdew, Phys. Rev. B. 97, 094111 (2018)
- *How accurate are the parametrized correlation energies of the uniform electron gas?* Puskar Bhattarai, Ahirup Patra, **Chandra Shahi**, and John P. Perdew, Phys. Rev. B. 97, 195128 (2018)
- *Stretched or noded orbital densities and self-interaction correction in density functional theory,* **Chandra Shahi**, Puskar Bhattarai, Kamal Wagle, Biswajit Santra, Sebastian Schwalbe, Torsten Hahn, Jens Kortus, Koblar A. Jackson, Juan E. Peralta, Kai Trepte, Susi Lehtola, Niraj K. Nepal, Hemanadhan Myneni, Bimal Neupane, Santosh Adhikari, Adrienn Ruzsinszky, Yoh Yamamoto, Tunna Baruah, Rajendra R. Zope, and John P. Perdew, J. Chem. Phys. 150, 174102 (2019)
- *Self-interaction-free electric dipole polarizabilities for atoms and their ions using the Fermi-Löwdin self-interaction correction.,* Kushantha P. K. Withanage,

Sharmin Akter, **Chandra Shahi**, Rajendra P. Joshi, Carlos Diaz, Yoh Yamamoto, Rajendra Zope, Tunna Baruah, John P. Perdew, Juan E. Peralta, and Koblar A. Jackson